Quantum pre-geometry models for Quantum Gravity

by

Francesco Caravelli

A thesis

presented to the University of Waterloo

in fulfillment of the

thesis requirement for the degree of

Doctor of Philosophy

in

Physics

Waterloo, Ontario, Canada, 2012

Author's Declaration

I hereby declare that I am the sole author of this thesis. This is a true copy of the thesis, including any required final revisions, as accepted by my examiners. I understand that my thesis may be made electronically available to the public.

Abstract

In this thesis we review the status of an approach to Quantum Gravity through lattice toy models, Quantum Graphity. In particular, we describe the two toy models introduced in the literature and describe with a certain level of details the results obtained so far. We emphasize the connection between Quantum Graphity and emergent gravity, and the relation with Variable Speed of Light theories.

ACKNOWLEDGEMENTS

A long list of sincere thanks has to be given here. First of all, to my supervisors, Fotini Markopoulou and Lee Smolin, for the continuous and discrete support during the PhD. Then, a sincere thanks goes to the people I have closely collaborated with (and friends), Leonardo Modesto, Alioscia Hamma and Simone Severini, Arnau Riera, Dario Benedetti, Daniele Oriti, Lorenzo Sindoni, Razvan Gurau, Olaf Dreyer, Emanuele Alesci, Isabeau Prémont-Schwarz, Sylvain Carrozza and Cosimo Bambi. A particular thanks goes also to my family (Mamma, Papá e le sorelline), for continuous support, moral and economical. Then a long list of friends goes here. Having shared a double life between Waterloo (Canada) and Berlin (Germany), a list of people from all over the world follows! In Waterloo, I have to thank my buddy Cozmin(/Cozster Cosniverse Cosferatu) Ududec and my dear friend Mitzy Herrera, Owen Cherry (on top), Cohl Fur(e)y, Coco Escobedo, John Daly and Jessica Phillips, Jonathan Hackett and Sonia Markes . In Berlin I have to thank my russian friend Sasha Latnikova, die kleine Marina Zygelman, Anja Rogacheva, Sara Pernbrunner, Cosimo Restuccia, Ivano Pallante, to my not-girlfriend Elena Bruno, to the si-culo Marco Scalisi for many discussions about all-but-physics, to the puzzling and misterious friend Carlos Guedes and to *la francesina* Estelle de Tournadre in the good and the

bad (and the bad and the sad).

I thank in particular Isabeau, who kindly gave me his thesis in order to use his Latex style.

Research at Perimeter Institute is supported by the Government of Canada through Industry Canada and by the Province of Ontario through the Ministry of Research & Innovation. Part of this research has been also funded by the Templeton Foundation. Part of the numerical work was made possible by the facilities of the Shared Hierarchical Academic Research Computing Network (SHARCNET:www.sharcnet.ca). Also, hospitality at the Santa Fe Institute and the Albert Einstein Institute of Berlin have been much appreciated.

Dedication

Ancora

alla mia famiglia e ai miei amici,

a qualcun altro che dimentico,

e a qualcun altro che non voglio ricordare

(Again

to my family and my friends,

to somebody else I forgot,

and to somebody I do not want to remember)

CONTENTS

"You can know the name of a bird in all the languages of the world, but when you're finished, you'll know absolutely nothing whatever about the bird. So let's look at the bird and see what it's doing - that's what counts. I learned very early the difference between knowing the name of something and knowing something."

Richard Feynman

"Phantasie / Vorstellungskraft ist wichtiger als Wissen, denn Wissen ist begrenzt."

(Imagination is more important than knowledge, because knowledge is limited.)

Albert Einstein

"Ero giovanissimo, avevo l'illusione che l'intelligenza umana potesse arrivare a tutto. E perció m'ero ingolfato negli studi oltremisura."

(I was young, I had the illusion that human intelligence could get anywhere. For this reason I focused on studies beyond measure.)

Enrico Fermi

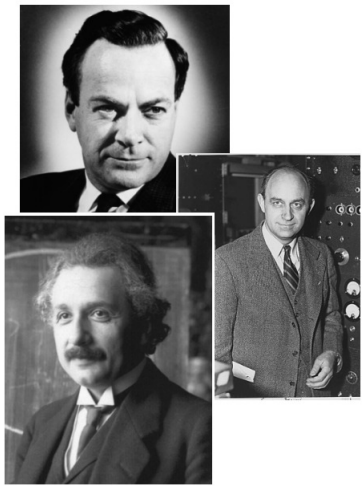

Thanks.

Chapter 1

Introduction

General Relativity is one of the most intriguing physical theories, since it deals with the nature of space and time, and our perception of reality. Using the Planck constant $\hbar$, the Newton constant G and the speed of light c, we can build a constant with the dimension of an energy. This is the Planck energy, given by:

$$E_p = \sqrt{\frac{\hbar c^5}{G}} \approx 10^{19} GeV.$$

When a gravitational process has an energy of the order of the Planck energy, using the intuition we gained by quantizing the other three known forces, we expect another theory, a Quantum Theory of Gravity, to replace General Relativity. As we will discuss later in detail, this process of quantization is very troublesome. So far, no fully satisfactory quantization of General Relativity exists.

What is a Quantum Theory of Gravity? A quantum theory of gravity is a theory which describes gravitational phenomena up to the Planck scale and such that in the

limit $\hbar \to 0$, reduces to a gravitational theory, and that at energies much smaller then the Planck energy, reduces to Einstein's General Relativity. Given this, it is rather complicated to describe a theory which do not exist yet. It is true that there are many proposals, but many of these are yet not fully convincing, or cannot predict a valuable and testable phenomenon[45].

Quantum mechanics is one of the milestones of the physics of the last century. It describes the physics of elementary particles and of atoms and molecules and has been tested extensively. General relativity is the other milestone of the past century. It describes the physics of spacetime and it works very well in describing the motion of celestial bodies in our solar system, in galaxies and in our Universe. However, when we put the two together and when we try to quantize gravity as it has been done for other forces, many obstructions appear.

In spite of progresses in several directions, finding this new theory has proven a challenging problem for several decades. In particular, there are several approaches proposing a quantization of gravity [33, 1, 120, 148].

In particular, Loop Quantum Gravity[33] (LQG) is a promising quantization of General Relativity. It establishes that spacetime is a foam, in which atoms of space are constructed on Wilson gauge lines, or *spin networks*. Many results have been obtained, as the spectrum of the area and volume operators [47] and the Bekenstein-Hawking Area-Entropy law[46]. The theory can be formulated both in the covariant and canonical form.

Causal Dynamical Triangulations[1] (CDT) instead is a discrete formulation of the Feynman's Path Integral. It is formulated on simplices which have a built-in direction of

time. Many results point in the direction that the resulting space-time is four dimensional and that the expansion of the Universe in CDT is very similar to a de Sitter cosmological model [50].

Causal sets [120] is another proposal for a quantization of gravity. It is based on the fact that a spacetime, i.e. the metric, can be eventually be described by its causal structure, together with a local notion of volume (put in mathematical terms, the local conformal factor). Thus, spacetime reduces to a directed graph in which loops are absent, and with the number of nodes representing the volume density. These graphs are sprinkled on a (given) metric and then the evolution of fields on these graphs is studied. The major achievement of the approach is the prediction of the order of magnitude of the cosmological constant[51].

String theory [148] is at the moment the most prominent of the proposals. The theory, initially born as a theory of strong interaction, slowly became a proposal for a unification of all forces, together with gravity. The fundamental objects are supersymmetric strings, whose excitations are expected to describe nature. Major achievement of the approach is the Bekenstein-Hawking entropy[52].

Current research is also paying substantial attention to the numerous theoretical indications that gravity may only be emergent[163, 63, 48], meaning that it is a collective, or thermodynamical, description of microscopic physics in which we do not encounter geometric or gravitational degree of freedom. For instance, the thermodynamics of black holes is an intriguing puzzle which pushes towards this direction. An analogy to illustrate this point of view is fluid dynamics and the transition from thermodynamics to

the kinetic theory. What we currently know is the low energy theory, the analogue of fluid dynamics. We are looking for the microscopic theory, the analogue of the quantum molecular dynamics. Just as there are no waves in the molecular theory, we may not find geometric degree of freedom in the fundamental theory. Not surprisingly, this significant shift in perspective opens up new routes that may take us out of the old problems.

From Aristotle to the most prominent physicists nowadays, the concept of emergence changed over the centuries. The emergent approach is concerned with the study of the macroscopic properties of systems with many bodies. Sometimes, these properties can be tracked down to the properties of the elementary constituents. In recent years, though, there has been a flourishing of novel quantum systems, which show behaviors of the whole system that have no explanation in terms of the constituting particles. These behaviors are instead a collective phenomenon due to interactions between the constituents. When the interaction between the particles cannot be ignored, like in systems of strongly interacting electrons, we see many novel and beautiful properties: gauge fields can emerge as a collective phenomenon, strange quantum phase transitions happen, unusual forms of superconductivity and magnetism appear, novel orders of the matter based on topological properties of the system and featuring exotic statistics are found[100].

Nevertheless, the word "emergent" does not lack of ambiguities. For instance, in string theory, the metric is an *emergent* object. There, the evidence for emergent gravity is, for instance, in the form of a spin-2 field, an effective metric, or the anti-de Sitter/conformal field theory (AdS/CFT) duality [57]. The emergent viewpoint we take

amounts to treating quantum gravity as a problem in statistical physics. For instance, the Navier-Stokes equation describes the physics of a huge number of particles. Are the Einstein equations the analogue of the Navier-Stoke equation for molecules? This question is today a fairly established field of research [36]. Still, the complexity of the physics of fluids is absolutely astonishing [1].

In this thesis we will see how pre-geometric models for gravity are interesting testgrounds for many questions which are at the boundary between Quantum Gravity and Emergent Gravity. A related issue which we will be discussing is the notion of locality. There are a number of indications that forcing for a local theory of gravity may not be correct (a thorough investigation of this question can be found in [79]). Non-locality, in fact, cures naturally the divergences appearing in Quantum Gravity[114]. Problems with Unitarity appear, and only recently this issue has been tackled again[118]. Moreover, a renormalization group approach to gravity points in the direction that a renormalizable theory of gravity has to be non-local[61].

For the purposes of the present thesis, it is important to note that there are two possible types of non-locality which contribute in different ways. One, violation of *microlocality*, disappears when the cut-off is taken to zero, while the other, violation of *macrolocality*, or *disordered locality*, does not [15]. Violations of macrolocality amount to the presence of paths through spacetime disallowed in a Lorentzian topology. These are easily described in lattice-type approaches, as non local-links in the graph. GR allows for such paths and,

[1] A funny anecdote involves Heisenberg. It seems that at the end of his PhD, he had been asked from his advisor whether he would be interested in studying fluids. He answered that the physics of fluid is too complicated and that he would rather choose a simpler topic, as particle physics, at that time a new field.

in principle, they should be taken into account in a full quantum theory of gravity. In particular, we will see that one of the models we will discuss[80] possesses an emergent notion of locality and that this is connected to Variable Speed of Light theories[164].

A powerful set of methods in statistical physics involve the use of lattice-based models, such as the Ising or Heisenberg model for ferromagnetism, the Hubbard model for the conductor/insulator transition, etc. Such methods have been introduced in quantum gravity. This thesis is focused on discussing lattice toy models to describe phenomena typical of GR.

It is natural for the lattice of system to play the role of (a primitive form of) geometry. The choice of graphs as the primitive objects describing geometry is choice due to their simplicity. General Relativity is a background independent theory, which means that a physical system is equivalent to another one if they are connected by a diffeomorphism. For instance, a quantity which is invariant under the action of a diffeomorphism is the relation between events in space and time. Thus, if two points in space and time are directly connected or not is an invariant under a diffeomorphism. This notion is easily implementable in a graph, as there this relation is encoded in the presence of an edge between two points of the graph or not. Then, choosing a graph, a discrete label for the points of spacetime, instead of a continuum of labels, is a mere simplification. These concepts are widespread also in other approaches to Quantum Gravity [33, 120, 1]. In our approach, we will have a continuous label for time, and a discrete label for the points in space.

Another important fact to consider is that the geometry of spacetime in GR is fully

dynamical. By analogy, we expect that the use of a fixed lattice is inappropriate and one instead needs models on a *dynamical* lattice. While for this reason desirable, dynamical lattices raise difficult technical problems that have not been previously addressed in the field of statistical physics. In this thesis we will address a systemic study of many problems related to having a dynamical lattice. In particular, we will discuss two Quantum Graphity models, one introduced in [80] and one introduced in [111]. The former was specifically introduced to understand the possibility that Universe might condensate, at early times, into a lattice which is local. The latter, instead, has been introduced in order to understand whether an interaction geometry-matter can drive this condensation. The two are just toy models, but given their simplicity, very precise questions can be asked and in some cases answered as well.

The techniques used in the thesis are those of many-body theory and quantum information. The questions we will ask, however, will be those of a general relativist. For instance: how is Lorentz symmetry emergent? How can be a black hole described in a graph-theoretic approach? How can be curvature emergent?

The thesis is divided into three parts. The first part, in particular Section 2, is devoted to understanding the problems existing with General Relativity, and the problems arising from its quantization treating the metric as a field. We will motivate with specific models, in Section 3, modifications of GR, our approach and in order to better understand the results. In the second part instead, we will introduce the Quantum Graphity models and study them. In section 4, we will describe the first Quantum Graphity model and study its mean field theory. The model is statistical and is aimed at describing a Quantum Graph

at a particular temperature, T. A Hamiltonian associated to graph-theoretic quantities is assumed to be the energy. As we will see, the model is related to the String-Net condensation introduced by Levin and Wen [44]. We will understand why a "space-condensation scenario" is related to the Variable Speed of Light theories introduced in Section 3. The Lieb-Robinson bounds will be the guiding techniques. Part of this section is based on Phys.Rev. D84 (2011) 024002. Section 5 is devoted to the analysis of the second Quantum Graphity model. This model introduces explicit degrees of freedom on the nodes of the graph. A detailed analysis of the quantum and classical model will be presented. This section is based on Phys.Rev. D81 (2010) 104032. The third part, Section 6, is instead focused on emergence. In particular, we will see how to describe trapped surfaces in graph models. Also, we will show how the quantum hopping of a particle on the graph, is related to the equation of motion of a scalar particle in *curved* space. We will also show two scenarios to give mass to the emergent scalar particle. This section is instead based on Phys.Rev. D85 (2012) 044046 and arXiv:1201.3206[2]. Conclusions follow.

[2]This paper was recently accepted in Phys. Rev. D.

Part I

General Relativity: a troubled son

Chapter 2

General Relativity and its problems

2.1 General Relativity

We briefly recall some known facts about Einstein general theory of gravitation. The equations which changed the way we look at the world take a seemingly simple form:

$$G^{\mu\nu} = \frac{8\pi G}{c^4} T^{\mu\nu}, \tag{2.1}$$

where $G_{\mu\nu}$ is the so called *Einstein tensor* and is given by:

$$G_{\mu\nu} = R_{\mu\nu} - \frac{1}{2} g_{\mu\nu} R, \tag{2.2}$$

and where $R_{\mu\nu}$ is the so called *Ricci tensor* and R is the *Ricci scalar*. The tensor $g_{\mu\nu}$, the most important object, is the metric and fully describes, if invertible, the space-time itself. The tensor $R_{\mu\nu}$ and the scalar R are related to the *Riemann tensor* $R^{\rho}{}_{\mu\sigma\nu}$ by subsequent

contractions, for the Ricci tensor the first higher index with the second lower index and the Ricci scalar by contractions of the two remaining indices. While the Ricci tensor comes for free putting equal the two indices, for the contraction of the two Ricci tensor indices we need to use the *inverse* metric $g^{\mu\nu}$, defined by $g^{\rho\sigma}g_{\sigma\nu} = \delta^{\rho}_{\nu}$. The metric tensor contains the informations about how we parametrize the manifold and the information on the distance between two points on it. In particular we have that the infinitesimal distance between two points is encoded in the line element,

$$ds^2 = g_{\mu\nu}dx^{\mu}dx^{\nu}. \tag{2.3}$$

The *covariant derivative* are the following differential operators:

$$\begin{aligned} D_{\alpha}u^{\beta} &= \partial_{\alpha}u^{\beta} + \Gamma^{\beta}_{\alpha\sigma}u^{\sigma}, \\ D_{\alpha}u_{\beta} &= \partial_{\alpha}u_{\beta} - \Gamma^{\sigma}_{\alpha\beta}u_{\sigma}, \end{aligned} \tag{2.4}$$

where the symbols $\Gamma^{\sigma}_{\alpha\beta}$ are called, if we impose zero torsion and metric compatibility, *Christoffel symbols*. The Christoffel symbols hold the information about the movements of a test particle on the manifold. These symbols are symmetric under the exchange of the two lower indices. It is important to stress that they do not transforms as tensors but as a covariant plus an affine transformation. The relation between the Christoffel symbols

and the metric is given by the following equation,

$$\Gamma^{\mu}_{\sigma\rho} = \frac{1}{2} g^{\mu\sigma}(\partial_\rho g_{\mu\nu} + \partial_\nu g_{\mu\rho} - \partial_\mu g_{\nu\rho}). \tag{2.5}$$

This ensures the metric compatibility, $D_\rho g_{\alpha\beta} = 0$. We recall also that through a diffeomorphism we can set the Christoffel symbols zero on a particular point[1]. This is the mathematical expression of the Equivalence principle, ensuring that locally observers observe a Minkowski space. In this sense, general relativity is described by a quasi-Riemannian geometry. Let me recall briefly the meaning attributed to the Riemann tensor of the Einstein equations. The information within this tensor is the change due to the curvature of a vector along a closed path. To figure out in a simple and standard way this fact, let us consider a sphere, we fix two poles, say north and south, and put a vector on one of the two poles. Then, we drag the vector along a short closed path, modifying the direction of the vector such that it is always parallel to itself. The curvature of the surface of the sphere affects the direction of the vector. This is expressed by the following formula:

$$\begin{aligned} &[D_\mu, D_\nu]A_\rho = R^{\sigma}{}_{\mu\nu\rho} A_\sigma, \\ &[D_\mu, D_\nu]A^\rho = -R^{\rho}{}_{\sigma\mu\nu} A^\sigma. \end{aligned} \tag{2.6}$$

[1]It is important to say that this is strongly local. The Christoffel symbols, once fixed to zero on a point, cannot be zero in a *neighborhood* of that point.

We can calculate in an explicit way this tensor from the definition above. We would find, lowering its indices:

$$R_{\mu\nu\rho\sigma} = \frac{1}{2}(\partial_\nu\partial_\rho g_{\mu\sigma} + \partial_\mu\partial_\sigma g_{\nu\rho} - \partial_\nu\partial_\sigma g_{\mu\rho} - \partial_\nu\partial_\rho g_{\nu\sigma}) + g_{\alpha\beta}(\Gamma^\alpha_{\nu\rho}\Gamma^\beta_{\mu\sigma} - \Gamma^\alpha_{\nu\sigma}\Gamma^\beta_{\mu\rho}). \tag{2.7}$$

From the above relation we get the following identity[2]:

$$R_{\mu\nu\rho\sigma} = -R_{\nu\nu\rho\sigma} = -R_{\mu\nu\sigma\rho} = R_{\rho\nu\mu\sigma}, \tag{2.8}$$

which implies that the tensor is somehow redundant. We recall the *Bianchi identity* as well, which comes from the fact that we are describing the geometry with a redundant formalism:

$$D_\sigma R_{\lambda\mu\nu\rho} + D_\rho R_{\lambda\mu\sigma\nu} + D_\nu R_{\lambda\mu\rho\sigma} = 0. \tag{2.9}$$

Using the identities written above we can contract some indices and we get:

$$D_\rho R^\rho_\sigma = \frac{1}{2} D_\sigma R. \tag{2.10}$$

It is a well known theorem that, if the Riemann tensor is zero, the spacetime is flat. The Ricci scalar is also invariant under diffeomorphism. This means that if we find R zero in a reference frame then we will find it zero in any other reference that can be reached trough a diffeomorphism or a Lorentz boost. The last notion we want to introduce is the so called

[2]However this symmetry is a general property of the Riemann tensor.

geodesic equation. This equation tells how a point particle moves in a gravitational field in general relativity. If we define the covariant differential:

$$D\xi^\mu = d\xi^\mu + \Gamma^\mu_{\nu\rho} dx^\nu \xi^\rho, \tag{2.11}$$

where ξ^μ is the coordinate of a test point particle, and u^μ its velocity. This particle will follow the path given by the solution of:

$$\frac{D^2\xi^\mu}{d\tau^2} = R^\mu{}_{\nu\rho\sigma} u^\nu u^\rho \xi^\sigma. \tag{2.12}$$

or the one of the *geodesic* equation:

$$\frac{Du^\mu}{d\tau} + \Gamma^\mu_{\nu\rho} u^\nu u^\rho = 0. \tag{2.13}$$

The exact solution is quite simple in case of zero curvature and is a straight line line along the spacetime, so we re-obtained the first Newton law. We want to stress that the name *general relativity* may be misleading. General relativity is less *relative* than *special relativity*. In fact [138], a space-time with a bump (a mass or anyway a little curvature somewhere) is different from one completely flat, and there is no way to restore flatness on the whole spacetime with a diffeomorphism.

2.1.1 Conceptual problems of GR

We cannot introduce a quantum gravity model without a discussion on the fundamental and technical problems of General Relativity [156, 157, 144] and the standard approach to quantize it. In the next two paragraphs we discuss the properties of spacetime in the presence of matter.

2.1.2 Breakdown of General Relativity: singularities

A singularity in General Relativity is a point of the space-time in which some diffeomorphism invariant quantity goes to infinity. This strange behavior is non physical and in a full gravitational theory should be avoided. One's hope is that a Quantum Theory of Gravity might be curing these features. Many solutions of the Einstein equations possess this sort of singularity, as for instance the Friedmann-Robertson-Lemaitre-Walker metric (FRLW), the Schwarzschild solution and many others.

From the mathematical point of view, a metric is *singular* if it is *timelike* or *null geodetic* incomplete[3].

We now recall some important theorems related to geodetical incompleteness[157][156][155]. First of all, we define a closed trapped surface $\mathcal{F}$. A closed trapped surface is a C^2 space-like closed two-surface such that the families of null geodesics orthogonal to $\mathcal{F}$ are only converging in $\mathcal{F}$ [4].

[3] Timelike geodetic incompleteness means that there are particles which after a certain amount of proper time stop to exist. This happens if the curvature become infinity.

[4] This is the mathematical analog of *event horizon* as in the Schwarzschild or Kerr black hole.

Theorem. A spacetime is not null geodesically complete if:

1. $R_{ab}K^aK^b \geq 0$ for every non-spacelike four-vector $\vec{K}$;

2. there is a non-compact Cauchy surface in the manifold or the Cauchy surface is compact but there is an observer who can not fall in the horizon requested by 3);

3. there is a closed trapped surface in the manifold.

Condition $1)$ is true for some physical spacetime[5]. This assumption is true, for instance, for pressureless perfect fluids. The first part of condition 2) is only technical and related to the proof of the theorem and so of scarce physical interest, but the second part is strongly physical. On the other hand condition 3) is the condition to have an event horizon in spacetime. This requirement on the Cauchy surface makes the theorem very weak if we expect it to have physical consequences. On the other hand the following theorem holds:

Theorem. A spacetime is not timelike and null geodesically complete if:

1. $R_{ab}K^aK^b \geq 0$ for every non-spacelike 4-vector K_μ;

2. The universe is spatially closed[6];

3. The universe is contracting or expanding[7].

These are now physical assumptions and apply, for instance, to the current cosmological model we have, the FRLW cosmology.

[5]When the *strong energy condition* holds, which is, for any observer with an energy greater than or equal to zero.

[6]i.e. there exists a compact spacelike three-surface.

[7]i.e. the normals to a spatial surface are everywhere converging or diverging from it.

In our past or in our future there was o there will be a singularity, as predicted by the FRLW cosmology. These singularities are known respectively as the *Big Bang* and the *Big Crunch*. General relativity predicts its own breakdown in our cosmological model. This is one of the main reasons why we search for a theory of quantum gravity, or quantum cosmology.

2.2 Why quantizing gravity?

The question we pose here is: why do we need a quantum theory of gravity[117, 143]? Here we will give many perspectives on this issue.

First of all, one might think that it is mostly for an aesthetical reason: we already quantized the Strong and the Electroweak forces, and a unified family quantum picture with Gravity standing in front might be desiderable. However, as we argued before, general relativity poses many questions related to its validity at certain scales. At the present time, it is not completely understood if a semiclassical treatment of general relativity makes really sense[150, 151]. Of course, this affects our comprehension of phenomena like the Hawking and Unruh effects. Some answers to this questions are offered in the context of analogue models [163].

The problem is that gravity and quantum mechanics are very different (and maybe incompatible) theories. In particular one might argue, for instance, that by probing very small scales, the energy involved might create a black hole[115, 116]. The creation of black hole would thus render the measure impossible. A modified Heisenberg uncertainty re-

lation is needed in this case, thus changing the structure of quantum mechanics[68]. Also, one might think that gravity might be induced by quantum fluctuations[145, 146] or by holography[63]. Somebody argues that geometry should not be quantized at all[152], while the matter field should. Thus, the Einstein equations should be replaced by $G_{\mu\nu} = \langle T_{\mu\nu} \rangle$, where on the right hand side we have a quantum average.

String Theory [148], the most prominent and widespread theory of high energy physics, treats all the fields and gravity as an emergent feature. The excitations of supersymmetric strings in more dimensions are related to gravity and particles, and gravity (the metric) is also there an emergent phenomenon.

Given the plethora of approaches and ideas, it is worthwhile to stress that there is no true explanation for the conviction that gravity must be quantized. Due to the lack of experiments, many of these approaches cannot be tested and remain only a valid theoretical possibility. At the moment, we have many circumstantial theoretical evidences and no smoking gun experimental proof that a quantum theory of gravity, valid up to the Planck scale, is needed. Indeed, the thermodynamical aspects of gravity [48] are puzzling enough to be suspicious about gravity being a fundamental force.

So, why quantizing gravity? In principle, an optimistic theoretical physicist thinks that having a consistent theory of quantum gravity might solve all these problems in one shot. As we discussed in the previous section, General Relativity as a classical theory is far from being complete. For instance, no solution of the Einstein's equations which could model a rotating black hole, and which is physical in the whole spacetime in vacuum, is known. In fact, the Kerr metric suffers of violations of causality close the the singularity

at the core of the hole, where quantum gravity effects are expected to contribute. As we said, also our current cosmological model requires additional fields. For instance, an inflaton field has to be introduced in order to solve several cosmological puzzles, as the horizon problem, the structure of the Universe, baryogenesis and the current value of the cosmological constant[58]. Moreover, general relativity alone cannot explain the velocity profile of galaxies and nor the anomalous acceleration of the Universe. This implies that an invisible type of matter, dark matter, and an invisible type of energy, dark energy, are filling the Universe [59]. Given that General Relativity has been tested only in weak field regime [60], there is room both for modifications of gravity [106] in order to account of these mismatches, or just to believe in the additional fields. A quantum theory of gravity, for instance, could clarify what are the corrections to Einstein's General Relativity and if they contribute to these puzzling features.

In this thesis we will pursue the road (through toy models) in which gravity does not have to be quantized in a strict sense, but that it is an emergent phenomenon. We will motivate this assumption in Chapter III.

In the next section we will show what goes wrong with the standard quantum field theoretic approach to quantizing gravity.

2.3 First attempt of quantization

2.3.1 QFT: linearized theory and divergences

In the Quantum Field theoretic approach to gravity, a key role is given to the concept of *graviton*. A graviton has, in the framework of quantum gravity, the same role which the photon possesses in quantum electrodynamics: it is the gauge particle of the gravitational force. In order to see how the graviton appears, we consider the Einstein-Hilbert action with no cosmological constant:

$$S = \frac{2}{8\pi G}\int d^4x\sqrt{-g}R. \tag{2.14}$$

We then expand the metric around a background field:

$$g_{\mu\nu} = \bar{g}_{\mu\nu} + sh_{\mu\nu}, \tag{2.15}$$

where $s = \sqrt{8\pi G}$. The Einstein-Hilbert action can be expanded as[159]:

$$\frac{2}{s^2}\sqrt{g}R = \sqrt{\bar{g}}[\frac{2}{s^2}\bar{R} + \mathcal{L}_g^1 + \mathcal{L}_g^2 + \cdots] \tag{2.16}$$

$$\mathcal{L}_g^1 = \frac{h_{\mu\nu}}{s}[\bar{g}^{\mu\nu}\bar{R} - 2\bar{R}^{\mu\nu}] \tag{2.17}$$

$$
\begin{aligned}
\mathcal{L}_g^2 &= \frac{1}{2}\bar{D}_\alpha h_{\mu\nu}\bar{D}^\alpha h^{\mu\nu} - \frac{1}{2}\bar{D}_\alpha h\bar{D}^\alpha h \\
&+ \bar{D}_\alpha h\bar{D}_\beta h^{\alpha\beta} - \bar{D}_\alpha h_{\mu\nu}\bar{D}^\nu h^{\mu\alpha} + \bar{R}(\frac{1}{2}h^2 - \frac{1}{2}h_{\mu\nu}h^{\mu\nu}) \\
&+ \bar{R}^{\mu\nu}(2h^\lambda{}_\mu h_{\nu\alpha} - hh_{\mu\nu})
\end{aligned} \tag{2.18}
$$

This method is particularly useful because, thanks to it, it is possible to maintain the covariance of the theory explicitly. At this point the theory needs to be gauge fixed. This can be done, in the path integral approach, by means of a Fadeev-Popov procedure. A constrain that can be imposed is[133]:

$$
G^\alpha = \sqrt{\sqrt{g}}(\bar{D}^\nu h_{\mu\nu} - \frac{1}{2}\bar{D}_\mu h^\sigma{}_\sigma)t^{\nu\alpha}, \tag{2.19}
$$

with $\bar{g}^{\mu\nu} = \eta_{\alpha\beta}t^{\mu\alpha}t^{\nu\beta}$. The gauge fixing Lagrangian is:

$$
\mathcal{L}_{gf} = \sqrt{\bar{g}}(\bar{D}^\nu h_{\mu\nu} - \bar{D}_\mu h^\lambda{}_\lambda)(\bar{D}_\sigma h^{\mu\sigma} - \frac{1}{2}\bar{D}^\mu h^\lambda{}_\lambda), \tag{2.20}
$$

and the Ghosts Lagrangian is chosen to be:

$$
\mathcal{L}_{gh} = \sqrt{\bar{g}}\eta^{*\mu}[\bar{D}_\lambda D^\lambda \bar{g}_{\mu\nu} - R_{\mu\nu}]\eta^\nu, \tag{2.21}
$$

so the theory can be gauge fixed, and as usual this gives rise to a ghost field (2.21). Now we can see why, for instance, the graviton is a spin two particle, when expanded over a

Minkowski background:

$$g_{\mu\nu} = \eta_{\mu\nu} + f_{\mu\nu}, \tag{2.22}$$

where we assumed that $f_{\mu\nu}$ is a small perturbation of the background Minkowski metric, so that indices are raised and lowered using the latter metric. Using the de Donder gauge[8], we obtain:

$$\partial^{\nu} f_{\mu\nu} = \frac{1}{2} f^{\nu}{}_{\nu,\mu} \tag{2.23}$$

the linearized Einstein equations become:

$$\Box f_{\mu\nu} = -16\pi(T_{\mu\nu} - \frac{1}{2}\eta_{\mu\nu}T) \tag{2.24}$$

where $T_{\mu\nu}$ is the stress-energy tensor. If we change the variables through the transformation

$$\bar{f}_{\mu\nu} = f_{\mu\nu} - \frac{1}{2}\eta_{\mu\nu} f^{\rho}{}_{\rho}, \tag{2.25}$$

the Einstein equations become:

$$\Box \bar{f}_{\mu\nu} = -16\pi T_{\mu\nu}. \tag{2.26}$$

[8]The reason for using the de Donder gauge instead of others gauge is that the use of the transverse-traceless gauge renders the formalism straightforward.

This is analogue to the case of electromagnetism, where we have a gauge vector which satisfies a similar equation. In the vacuum case, the stress-energy tensor is zero and the solution is quite easy to find,

$$f_{\mu\nu} = e_{\mu\nu} e^{i\vec{k}\cdot\vec{x}} + e^{*}_{\mu\nu} e^{-i\vec{k}\cdot\vec{x}}, \tag{2.27}$$

with $k^2 = 0$ and $k^\mu e_{\mu\nu} = \frac{1}{2} k_\mu e^\rho{}_\rho$ because of the de Donder gauge. Now we note that under a gauge transformation of the form

$$x^\mu \to x^\mu + \xi^\mu, \tag{2.28}$$

$f_{\mu\nu}$ transforms as

$$f_{\mu\nu} \to f_{\mu\nu} - \xi_{(\mu,\nu)}. \tag{2.29}$$

Under this gauge transformation the de Donder condition transforms as well,

$$dD[f_{\mu\nu}] = 0 \to dD[f_{\mu\nu}] = -\Box\xi_\mu, \tag{2.30}$$

showing the ambiguity of the coordinates. We can fix this ambiguity by taking $\Box\xi_\mu = 0$; this means that ξ_μ must be a planar wave. We started from 10 degrees of freedom, and after having gauge fixed 4 degrees by means of a de Donder gauge and 4 degrees by fixing

the coordinates, we have two degrees left [9]. Another way to proceed is using the so called Transverse-Traceless gauge. We impose the following on $f_{\mu\nu}$:

$$k^\mu f_{\mu\nu} = f^\mu{}_\mu = 0 \tag{2.31}$$

So we can, thanks to this gauge do the following transformation:

$$f_{\mu\nu} \to f_{\mu\nu} + k_\mu q_\nu + k_\nu q_\mu \tag{2.32}$$

where $\xi_\mu = 2Re[q_\mu e^{i\vec{k}\cdot\vec{x}}]$. So we can choose q_μ such that the elements $f_{0\nu} = 0$. The result is that the tensor $f_{\mu\nu}$ is:

$$f_{\mu\nu} = \begin{pmatrix} 0 & 0 & 0 & 0 \\ 0 & 0 & 0 & 0 \\ 0 & 0 & f_{22} & f_{23} \\ 0 & 0 & f_{23} & -f_{22} \end{pmatrix}$$

[9] The same calculation can be done in 3d: we have 6 degrees for the metric tensors, and 3 degrees must be fixed in the coordinates and 3 with the gauge fixing. We have no degrees left, so the theory is topological.

If the wave is along the x-axis. This tensor can be written in terms of the so called *polarization tensors*:

$$\mathbf{e}_+ = \begin{pmatrix} 0 & 0 & 0 & 0 \\ 0 & 0 & 0 & 0 \\ 0 & 0 & 1 & 0 \\ 0 & 0 & 0 & -1 \end{pmatrix} = \mathbf{e}_y \otimes \mathbf{e}_y - \mathbf{e}_z \otimes \mathbf{e}_z$$

$$\mathbf{e}_x = \begin{pmatrix} 0 & 0 & 0 & 0 \\ 0 & 0 & 0 & 0 \\ 0 & 0 & 0 & 1 \\ 0 & 0 & 1 & 0 \end{pmatrix} = \mathbf{e}_z \otimes \mathbf{e}_y + \mathbf{e}_y \otimes \mathbf{e}_z$$

Where $\mathbf{e}_y, \mathbf{e}_z$ are the unit vectors along y and z. It is clear from the above expressions that under a counterclockwise rotation around x that:

$$\begin{aligned} \mathbf{e}'_+ &= \mathbf{e}_+ \cos(2\theta) + \mathbf{e}_x \sin(2\theta) \\ \mathbf{e}'_x &= \mathbf{e}_+ \cos(2\theta) - \mathbf{e}_x \sin(2\theta) \end{aligned} \tag{2.33}$$

So, if we call $\mathbf{e}_R = \frac{\mathbf{e}_+ + i\mathbf{e}_x}{\sqrt{2}}$ and $\mathbf{e}_L = \frac{\mathbf{e}_+ - i\mathbf{e}_x}{\sqrt{2}}$ they transform as $\mathbf{e}'_R = e^{2i\theta}\mathbf{e}_R$ and $\mathbf{e}'_L = e^{-2i\theta}\mathbf{e}_L$. We recognize in $\mathbf{e}_R$ and $\mathbf{e}_L$ the polarization tensors for states of *helicity* $+2$ and -2. In order to quantize the linearized theory using the path integral, we need a Lagrangian and we need to express the gravitons as representations of the Poincaré group. It is well known what is the Lie algebra of the Poincaré group and it is well known from Weyl how to

proceed: find a representation of the little group and then extend it trough the symmetry. For a massless particle, the little group is the invariance group of the euclidean geometry. It happens that these states can be reduced to the eigenvalues of the operator $\vec{J}_3 \cdot \vec{k}$, which is proportional to the *helicity* of the particle. In this case, the helicity is ± 2 and so the states can be represented as the helicity eigenvalue of the J_3 operator. The Lagrangian for the linearized theory on the Minkowski background, has been introduced by Pauli and Fierz:

$$\mathcal{L} = \frac{1}{64\pi G}(f^{\mu\nu,\sigma} f_{\mu\nu,\sigma} - f^{\mu\nu,\sigma} f_{\sigma\nu,\mu} - f^{\nu\mu,\sigma} f_{\sigma\mu,\nu} - f^{\mu}{}_{\mu,\nu} f^{\rho}{}_{\rho}{}^{,\nu} + 2 f^{\rho\nu}{}_{,\nu} f^{\sigma}{}_{\sigma,\rho}) + \frac{1}{2} T_{\mu\nu} f^{\mu\nu} \tag{2.34}$$

The Euler-Lagrange equations for the Pauli-Fierz Lagrangian, give:

$$f_{\mu\nu,\sigma}{}^{\sigma} - f_{\sigma\nu,\nu}{}^{\sigma} - f_{\sigma\nu,\mu}{}^{\sigma} + f^{\rho}{}_{\rho,\mu\nu} + \eta_{\mu\nu}(f^{\alpha\beta}{}_{,\alpha\beta} - f^{\rho}{}_{\rho,\sigma}{}^{\sigma}) = -16\pi G T_{\mu\nu} \tag{2.35}$$

By means of a trace, we find the equation:

$$(f^{\alpha\beta}{}_{,\alpha\beta} - f^{\rho}{}_{\rho,\sigma}{}^{\sigma}) = 8\pi G T \tag{2.36}$$

and thus:

$$\Box f_{\mu\nu} - f_{\sigma\mu,\nu}{}^{\sigma} - f_{\sigma\nu,\mu}{}^{\sigma} + f^{\rho}{}_{\rho\mu\nu} = -16\pi G(T_{\mu\nu} - \frac{1}{2}\eta_{\mu\nu} T) \tag{2.37}$$

In the linearized theory the gravitational interaction resembles QED. In general, the

procedure from here is straightforward. We introduce the commutation relations:

$$[a(\mathbf{k},\sigma), a^\dagger(\mathbf{k}',\sigma')] = \delta_{\sigma\sigma'}\delta(\mathbf{k},\mathbf{k}') \tag{2.38}$$

And the field operator becomes:

$$\mathbf{f}_{\mu\nu} = \sum_\sigma \int \frac{d^3\omega}{\sqrt{2\omega}} [a(\omega,\sigma) e_{\mu\nu} e^{i\vec{k}\cdot\vec{x}} + a^\dagger(\omega,\sigma) e^*{}_{\mu\nu} e^{-i\vec{k}\cdot\vec{x}}] \tag{2.39}$$

However if we expand around a non flat metric the Pauli-Fierz Lagrangian is not the right Lagrangian. What we want to discuss now is the failure of such an approach[10]. It is well known that the first request, in the framework of Quantum Field Theory, is that the theory we are going to deal with is renormalizable. The nowadays accepted meaning of nonrenormalizability is the impossibility to fix, in a finite number of experiment, all the free constants of the theory. With the use of some tools of renormalization theory we can partly understand, looking only at the Lagrangian, if our theory is renormalizable or not. In fact, if the coupling constant of the theory has the dimension of a mass, the theory is non renormalizable. The Einstein-Hilbert Lagrangian has, in front of it, the coupling G that has the dimension of the inverse of a mass square. The same happens for the effective Fermi theory of weak interactions, where we know that such kind of interaction is the low energy theory of the Weinberg-Salam theory of elettroweak theory, that is renormalizable. Since we know that Einstein's theory of General relativity is right

[10]This approach is basically made of three steps: 1) Find a Hamiltonian for the equations of motion; 2) Apply the canonical quantization 3) Check if theory is renormalizable; 4) Calculate observable physical effects.

(too many phenomena can be explained with it, as the Mercury anomaly, the bend of light, the Hubble law and the red shift) we expect that the Einstein theory is the low energy theory of some other high energy one. At one loop[133] the theory turns out to be renormalizable. The counterterm, calculated explicitly from (2.16) is

$$\mathcal{L}_{1L}^{(div)} = \frac{1}{8\pi^2\epsilon}\big(\frac{1}{120}\bar{R}^2 + \frac{7}{20}\bar{R}_{\mu\nu}\bar{R}^{\mu\nu}\big), \tag{2.40}$$

where the $\epsilon = 4 - d$ is a hint that the calculation was performed with the use of dimensional regularization[11]. If we do not add matter, we have $R_{\mu\nu} = 0$, and so the terms vanish for all solutions of the Einstein equations. At 2-loops[134][135], instead, the renormalization involves R^3 terms, moreover with contractions of the Riemann tensor which were not present at the beginning. The result is that the theory is non renormalizable: it involves an infinite number of coupling constants and so it cannot be renormalized. Still, however, the effective quantum field theory approach [162] assumes that a quantum field theory quantization can be used as an effective low energy description of a hypothetical quantum theory of gravity. Moreover, a perturbative non-renormalizability does not imply that nonperturbative techniques cannot make sense of the quantum theory [61].

[11] Also, a Gauss-Bonnet relation has been used in order to reduce to this form.

Chapter 3

Motivations for an analogue description of General Relativity

As we will argue in this section, there are many reasons why a theorist should hope for a theory of gravity to replace current Einstein theory. We believe that the fact that gravity might be emergent is a serious possibility to consider. There are many deep questions related to this. For instance, what is time, and why in our approach it should be considered as a parameter. As a matter of fact, not having a real time in Quantum Gravity causes to have many interpretational problems. This is the well known problem called "The problem of time"[147]. In the canonical quantization of gravity, for instance, the Wheeler-DeWitt equation encodes this fact: the universe is still and timeless and there is no time evolution. The Hamiltonian of general relativity is, in fact, operatorially zero. Why, then, we observe the flow of time? Is it of thermodynamical origin (and its arrow given by the direction of increasing entropy)? Is it gravity of thermodynamical origin? During the last two decades, this matter has been investigated deeply, without, however,

achieving a real conclusion.

Black holes, for instance, display several features which relate gravity and thermodynamics. It is now well known that Black Holes possess an entropy proportional to the area of their horizons [34] and that this requires a modification of the laws of thermodynamics[35]. For instance, many academics argue that the entropy associated to the horizon must be associated with a microscopic description of general relativity. In this sense, gravity might be only an emergent theory, thus not fundamental. Moreover, as showed in [63], the emergence of gravity might also be related to the holographic principle. Further insights come from the investigations of the thermodynamical properties of gravity [48].

The collection of all this facts motivates the research in Analogue Models [163]. Analogue models are, in general, real systems unrelated to gravity in which many gravitational phenomena, as for instance the Hawking radiation, can appear. The study of these models could give many insights into the real nature of gravity.

3.1 Condensed Matter, Quantum Mechanics and Analogue models

So far we were concerned with pure general relativity or slight modifications of it. It is however hard to imagine how, once the diffeomorphism symmetry is broken and time becomes a mere parameter, the beautiful picture of Einstein's general relativity breaks down. There are plenty of ways this can happen and no experiments, at the moment, can probe those scales of energy. It is then important to understand that an effective theory

does not require the knowledge of the fundamental constituents. The effective theory of sound in air does not require the knowledge of the physics of its underlying constituents. In condensed matter and fluidodynamics, for instance, the Boltzmann equation allows to forget the microphysics and obtain an effective theory which propagates the modes. These modes are usually not coupled with the underlying constituents, not directly, but emerge as their normal modes.

It might seem unnatural, then, to imagine general relativity as an effective theory. How can it be that such a deep and beautiful theory, which predicts the curvature of spacetime as a result of its matter content and viceversa, can be just a fluidodynamical description? An easier exercise, however, is the one treating its tangent space as emergent. It is possible to imagine, in fact, how Lorentz geometry could be emergent [163]. We cite a Theorem of fluidodynamics to give a rough example:

Theorem. *If a fluid is barotropic and inviscid, and the flow is irrotational (though possibly time dependent) then the equation of motion for the velocity potential describing an acoustic disturbance is identical to the d'Alembertian equation of motion for a minimally-coupled massless scalar field propagation in a (3+1)-dimensional Lorentzian geometry,*

$$\triangle\phi \equiv \frac{1}{\sqrt{-g}}\partial_\mu(\sqrt{-g}g^{\mu\nu}\partial_\nu\phi) = 0. \tag{3.1}$$

Under these conditions, the propagation of sound is governed by an acoustic metric $-g_{\mu\nu}(t,x)$. This acoustic metric describes a (3+1)-dimensional Lorentzian (pseudo-Riemannian) geometry.

The metric depends algebraically on the density, velocity of flow, and local speed of sound in the fluid.

Of course, this is not the same as general relativity: this is merely how we describe the movement of particles in a medium. General relativity is much more and is encoded in the Einstein equations, i.e. which metrics have to be plugged into eqn. (3.1). In this thesis we will mostly be focused in the kinematical aspects of general relativity. In particular, how graph models can turn useful in studying the emergence of curvature, how surface trapping can be encoded into the graph, or the phenomenon described in the previous section, e.g. VSL theories, and how this can happen in a quantum mechanical model. The relevant questions for this type of approach are: how to derive the Einstein equations? Is the entropy of a black hole the effect of a quantum mechanical entropy of an underlying theory?

3.2 Variable Speed of Light theories and the major cosmological problems

Our current cosmological model, the Cosmological Standard Model (CSM), heavily relies on inflation. Inflation plays the same role in the CSM that the Higgs particle has in the Standard Model of Particles. An exponential growth of the scale factor, in fact, would explain not only the structure of the Universe, but solve the flatness problem and the horizon puzzle. However, this exponential growth has to be driven by some field, which

then vanish leaving a cosmological constant. Cosmologists are nowadays working on trying to constrain this type of theories. The theory of inflation had an incredible effect on cosmologists, and together with the scale factor, also the number of cosmological model is currently growing. We are here not different in this respect, and we will argue that one solution to this problem might come from a quantum gravity model. However, in our case we will not rely on an inflaton field, but indeed we will show that a different phenomenon could have taken place at 10^{-43} s, the Planck time, when we expect the quantum gravitational effects to have switched off.

In this section we will describe the so-called Variable Speed of Light (VSL) theories and how these might solve the problems which Inflation solves[164]. The simpler way to describe a VSL is that the speed of light might not be constant, by but instead varying with time, $c(t)$. This breaks the Lorentz group, from $SO(3,1)$ down to $O(3) \times \mathcal{R}$. Here we will consider a particular VSL [164], one in which the speed of light varies as

$$c(t) = \bar{c}\,\theta(t - t_0) + c\,\theta(t_0 - t), \tag{3.2}$$

with c and $\bar{c}$ constants. This could be achieved if the speed of light is, for instance, related to a phase transition in the early Universe. In the spontaneously broken phase of the evolution of the universe, the 3-dimensional space with $O(3)$ symmetry is assumed to be the homogeneous and isotropic Friedmann-Robertson-Walker metric,

$$dx^2 = R^2(t)[\frac{dr^2}{1 - kr^2} + r^2(d\theta^2 + \sin^2(\theta)d\phi^2)] \tag{3.3}$$

with $k = \pm 1, 0$ corresponding to de Sitter or anti-de Sitter, or flat universes. The time variable, t, is here an external parameter, or Newtonian time. The full metric is

$$ds^2 \equiv g_{\mu\nu} dx^\mu dx^\nu = dt^2 c^2(t) - R^2(t)[\frac{dr^2}{1-kr^2} + r^2(d\theta^2 + \sin^2(\theta) d\phi^2)] \tag{3.4}$$

with $c(t)$ given by (3.2). Thus, the metric can be split into two pieces, or bimetric form, $g_{\mu\nu} = g_{0\ \mu\nu} + \bar{g}_{\mu\nu}$. The phase transition produces two light cones, given by the two different speeds of light. The proper horizon is given by:

$$d_H(t) = R(t) \int_0^t \frac{dt' c(t')}{R(t')}. \tag{3.5}$$

Please note that in a radiation dominated universe, $R(t) \approx t^{\frac{1}{2}}$, and therefore

$$d_H \approx 2c(t)t. \tag{3.6}$$

This is the radius such that all the matter within it is in causal contact. We briefly state the horizon problem of the Cosmic Microwave Background (CMB). Observations have shown that the CMB is, apart from small fluctuations[1], isotropic, i.e. its temperature is pretty much uniform over the sky. Its distribution is, apart from resonances due to barions, a Planck spectrum. Cosmological models, prior to the advent of Inflation, suffered from the following question: how can be the CMB so isotropic? In other words, how could it thermalize? In fact, the proper horizon was too large for the CMB to interact and

[1]Which are, however, important in order to confirm a particular cosmological model.

then thermalize. A mechanism was needed in order to stretch this horizon, and stretch fast enough. Inflation implies a period of exponential expansion of the scale factor of the Universe, such that the horizon can be stretched fast enough in the early Universe and solve the thermalization problem of CMB. Another problem was associated to the flatness of the Universe: how can it be that the Universe is so flat, i.e., null spatial curvature? Inflation solves also this problem.

We now show how a Variable Speed of Light theory could solve these two problems. In the case of a VSL, e.g. using eqn. (3.2), the horizon of eqn. (3.6) is suddenly increased if $\bar{c} \gg c$. Due to the Heaviside step function being discontinuous, no diffeomorphism can produce such a sudden change in the metric. This is a departure from general relativity, as it could have been expected by having broken the Lorentz group. It is then clear that such a change depends on the dimensionless ratio $\gamma = \bar{c}/c$. The flatness problem is resolved in a similar way. The Friedmann equations in the broken phase are:

$$H^2 + \frac{c^2 k}{R^2} = \frac{8\pi G\rho}{3} \tag{3.7}$$

where $H = \dot{R}/R$ is the Hubble parameter and we have set the cosmological constant to zero, as it plays no role in what follows. We have that the parameter which measure the spatial curvature, is given by $\epsilon \equiv |\Omega - 1| = c^2|k|/\dot{R}^2$, where $\Omega = 8\pi G\rho/3H^2$. Taking a time derivative, we obtain:

$$\dot{\epsilon} = -\frac{2c^2|k|\ddot{R}}{\dot{R}^3} + 2\frac{\dot{c}}{c}\frac{c^2|k|}{\dot{R}^2} \tag{3.8}$$

If the Universe is radiation dominate, we have $\ddot{R} < 0$, and if the speed of light decreases in the phase transition, $\dot{c}/c < 0$ as well at the moment of the transition, and zero elsewhere. We thus see that $\dot{\epsilon} < 0$, which means that the universe curvature is automatically driven to zero. One might ask if γ has to be fine-tuned. A standard calculation shows that

$$|\Omega(10^{-43}) - 1| \approx \mathcal{O}(\gamma^2 10^{-60}). \tag{3.9}$$

Therefore, $\gamma \equiv \bar{c}/c \approx 10^{-30}$ is required in order to have the right amount of curvature in order to explain current observations. Such a big number requires, apart from a fast transition, also an underlying theory which, seen from the observer after the transition, is highly non-local.

Regarding the scale invariant fluctuations of the Cosmic Wave Background, it is obvious that it is impossible that the proper wavelengths can catch up with the Hubble horizons, if the transition happens fast enough. Thus, a rapid crossing of the horizon freezes the modes, which then are left scale invariant. How fast is probably the right question to ask to each individual physical model mimicking (3.2) and aiming to explain current cosmology observations.

It is fair to say that these models are not free of debates[158]. Within the context of general relativity *per se*, in fact, it has been argued that a variable speed of light might be only a coordinate effect. Moreover, it is not clear in these proposals, what is a clock measurement in proper time, as this is strictly related to the varying $c(t)$. Moreover, since the Lorentz group is broken, it should be made clear, model by model, how the limiting

dynamical speed $c(t)$ is determined, i.e. what physical mechanism drives it.

In the case of Quantum Graphity, where a similar effect is observed, many of these points are not valid. In fact, we will have a physical mechanism to drive the speed of propagation of signals, and we will have a newtonian clock.

PART II

GRAPH MODELS

Chapter 4

Quantum Graphs without matter

In this first part of the thesis we will pursue a very particular idea which we want to anticipate here. The first model we will introduce in the next sections is aimed at modeling the following physical picture.

In the early Universe, close to the Big Bang singularity, space was a crumbled object, in which there was no notion of distance. This can be modeled in terms of graphs, for instance, by considering a graph in which all the nodes are connected, i.e. a complete graph. This graph describes a high energy phase of the Universe. When the Universe cooled down, then the most of the edges of the graph turned off, leaving a lattice which at low temperature took a structure which is local, i.e. to each node there are only few neighbors.

For this reason, the first Quantum Graphity model is considered as a model of *emergent locality*. In the following, we will study the properties of this process and see how this model is related to Variable Speed of Light theories.

4.1 Graph Models

There are several reasons why graph models are attractive. First of all, a graph is a clear implementation of the relational content of general relativity. As we previously said in the introduction, general relativity is a background independent theory. The notion of vicinity and distance could be encoded, in simple models based on graph, in the connectivity structure of a graph. Graph models do not rely on any background metric and thus are the background independent objects *par excellence*. This might be the reason why graphs are the most common objects among many approaches to Quantum Gravity [1, 33, 2, 120, 82].

Moreover, it has been previously argued in the literature that at the discrete level, spatial diffemorphisms should appear as the permutation invariance of these fundamental constituents [83, 43], i.e. the nodes of the graph. This can be implemented by starting with a complete graph $\mathcal{K}_N$, which is a graph on N nodes such that, between any two nodes of the graph, there is an edge, or by using a dynamics which is permutation invariant. Moreover, the dynamics of the various models is chosen such that the energy depends on natural graph properties, as number of links, closed and open paths.

It should be stressed that graph models, asunder from being interesting on their own, are the simplest choice to study phenomena related to background independence. In particular, there is in principle no obstruction in studying these models in the continuum. In fact, very often the continuum limit will be considered.

In the following we will first review the String-Net condensation mechanism to generate a $U(1)$ gauge theory and motivate the Quantum Graphity approach. Some useful graph-theoretic properties and techniques and the necessary quantum mechanical nota-

tion are introduced.

4.2 A brief review of the String-Net condensation

The concept of topological order is one of the most productive recent ideas in condensed matter theory [100]. It provides explanations for phases of matter (for example, fractional quantum Hall liquids) that cannot be described by the paradigm of local order parameters and symmetry breaking. If local order parameters cannot describe such phenomena, then their order could be of topological nature [100], which will mean that long range correlations could be protected by quantum entanglement.

Topological order gives rise to a ground state degeneracy that depends on the topology of the system and is robust against any local perturbations [101]. Because of this property, topologically ordered systems appear to be good candidates for robust quantum memory and fault-tolerant quantum computation [102], and thus are useful for quantum information as well. Recently, experimental studies have been performed on particular materials [160].

From the point of view of a "Quantum Gravitist" interested in an emergent picture, topological order offers a whole new perspective to the problem of elementary particles. Particles regarded as fundamental, like photons and fermions, and other particles that can be interpreted as collective modes of a crystal. Recently, detailed studies on graphene show that also the spin itself could be emergent from an underlying discrete structure[119] [1]. In fact, if quantum gravity is emergent, the best possible picture is given

[1] As Wheeler himself pointed out[109], we will not understand the nature of space and time until we

by one in which not only gravity is emergent, but also particles.

The understanding of the phases of matter provides an explanation for the phonon and other gapless excitations. However, one can also ask whether photons, electrons, or gravitons are emergent phenomena too, not elementary particles.

Let us consider the case of light. Photons are $U(1)$ gauge bosons and they cannot correspond to the breaking of any local symmetry [31]. However, models with topological order can feature photons, fermions and even gravitons as emerging collective phenomena [100, 12]. The reason is that the mechanism to obtain emergent particles is not the same as ordinary symmetry breaking.

In the case of String-Net condensation, light emerges from topological order as the effective low-energy theory of a quantum spin system.

The quantum spin system is a local bosonic model, in the sense that the Hilbert space decomposes in a direct product of local Hilbert spaces. All the observables have to commute when far apart.

Moreover, the Hamiltonian must be a sum of local observables. In the low-energy sector, and in the continuum limit, the effective theory can be described by the Lagrangian of electromagnetism. A theory of light as an emergent phenomenon needs to explain why we do not see signals faster than light. A unified model of all interactions, should also explain why the speed of light is so universal. However, let us focus on a single interaction and neglect this problem for the time being.

A local bosonic model is a theory where the total Hilbert space is the tensor product

explain the nature of spin.

of local Hilbert spaces, local physical operators are finite products acting on nearby local Hilbert spaces, and the Hamiltonian is a sum of local physical operators. If we restrict ourselves to the case of a discrete number of degrees of freedom and finite-dimensional local Hilbert spaces, we have a *quantum spin model*.

A quantum spin model can be defined as follows. To every vertex x in a graph G we associate a finite dimensional Hilbert space $\mathcal{H}_x$. The total Hilbert space of the theory is

$$\mathcal{H} = \otimes_{x \in G} \mathcal{H}_x, \tag{4.1}$$

and to every subset of vertices $X \subset G$, we can associate local physical operators with support in X.

The Hamiltonian will take the form $H_{local} = \sum_{X \subset G} \Phi_X$, where to every $X \subset G$ we associate an hermitian operator Φ_X with support in X. An example of local bosonic model is given by a spin $1/2$ system on a lattice, where to every vertex x in the lattice we associate a local Hilbert space $\mathcal{H}_x \cong \mathbb{C}^2$.

String-net condensation emerges from a collection of quantum rotors on a lattice[100]. Consider a square lattice whose vertices are labeled by i, with angular variable $\hat{\theta}_{ij}$ and angular momentum S^z_{ij} on the links L_{ij} of the graph. The Hamiltonian for the quantum

rotor model is given by

$$H_{rotor} = U \sum_{i} \left(\sum_{\alpha} S^z_{\mathbf{i},\alpha} \right)^2 + J \sum_{\mathbf{i},\alpha} (S^z_{\mathbf{i},\alpha})^2 + \sum_{\substack{i,\alpha_1,\alpha_2 \\ s.t.\ \alpha_1 \cdot \alpha_2 = 0}} \left(t_{\alpha_1,\alpha_2} e^{i\left(\theta_{\mathbf{i}+\alpha_1} - \theta_{\mathbf{i}+\alpha_2}\right)} + h.c. \right), \tag{4.2}$$

where $\alpha = \{\pm 1/2(1,0), \pm 1/2(0,1)\}$ are the spinors of length $1/2$ pointing towards the lattice axes [31]. In the limit $t, J \ll U$, the first term of the Hamiltonian H_{rotor} behaves like a local constraint and makes the model a local gauge theory. Defining

$$g \equiv \frac{2}{U(t_{12}t_{-1-2} + t_{2-1}t_{-21})}, \tag{4.3}$$

the effective low-energy theory becomes

$$H_{eff} = J \sum_{i,j} (S^z_{ij})^2 - g \sum_{p} \frac{W_p + h.c.}{2} \equiv \sum_{i,j,p} (\Phi^1_{ij} + \Phi^2_p) \tag{4.4}$$

where $W_p = e^{i(\theta_{12} - \theta_{23} + \theta_{34} - \theta_{41})}$ is the operator which creates a string around a plaquette p, while the t's are couplings. Here H_{eff} is just an effective theory and thus its nonlocality is not troublesome. In the $g \gg J$ limit, the continuum theory for the Hamiltonian H_{eff} is the Lagrangian of electromagnetism[100]:

$$L = \int d^2\mathbf{x} \left(\frac{1}{4J} \mathbf{E^2} - \frac{g}{2} \mathbf{B}^2 \right), \tag{4.5}$$

with speed of light given by $c = \sqrt{2gJ}$.

4.3 Graph theory preliminaries

The complete undirected graph on N vertices is denoted by $\mathcal{K}_N$. It is a graph in which every two vertices are connected by an edge. If the vertices are labeled by $1, 2, \ldots, N$, then $\mathcal{K}_N$ has an edge e_{ab} connecting any two a and b.

It should be stressed that any graph G on N vertices can be regarded as a subgraph of the complete graph $\mathcal{K}_N$; in particular, it can be obtained by removing edges from $\mathcal{K}_N$. A convenient way to represent G is via its set of edges $E(G)$ or via its $N \times N$ adjacency matrix

$$A_{ab}(G) = \begin{cases} 1 & \text{if } e_{ab} \in E(G) \\ 0 & \text{otherwise.} \end{cases} \tag{4.6}$$

By construction, the adjacency matrix is symmetric and it has zero diagonal elements. This matrix enjoys many properties. Powers of the adjacency matrix,

$$A^N{}_{ij} = \sum_{r_1,\cdots,r_{N-1}} A_{ir_1} A_{r_2 r_3} \cdots A_{r_{N-1} j} \tag{4.7}$$

contain information about open and closed paths in the graph. In particular, paths which go several times on the same edges, or *retracing paths*.

For future use, it is also useful to define the notion of nonretracing paths. A *nonretracing path* is an alternating sequence of vertices and edges, in which any particular edge appears exactly once. It is useful to specify that nonretracing paths can be *open* or *closed* and that a nonretracing path is not necessarily a geodesic between two vertices. A closed

nonretracing path is also said to be a *cycle*. The number of cycles can be computed algorithmically but not with the straight forward use of powers of the adjacency matrix. Some questions regarding counting the number of cycles of a given length can be very difficult (see, *e.g.*, [84]).

4.4 Quantum mechanics preliminaries

All the subgraphs of the graph $\mathcal{K}_N$ can be encoded in a Hilbert space that we will now define. In general, it is possible to associate a Hilbert space $\mathcal{H}_{edge}$ to each edge e_{ab} and a Hilbert space $\mathcal{H}_{vertex}$ to each vertex. The total Hilbert space of the system is then given by the tensor product

$$\mathcal{H}_{total} = \bigotimes^{N(N-1)/2} \mathcal{H}_{edge} \bigotimes^{N} \mathcal{H}_{vertex}. \tag{4.8}$$

In the following, we will specialize to models in which all the degrees of freedom are on the edges of the graph as opposed to both the edges and vertices. In Chapter 5, instead, we will consider also the case with degrees of freedom on the vertices.

The basic Hilbert space associated with an edge is chosen to be that of a fermionic oscillator. That is, $\mathcal{H}_{edge}$ will be

$$\mathcal{H}_{edge} = \mathrm{span}\{|\,0\rangle,\, |\,1\rangle\}; \tag{4.9}$$

the state $|\,0\rangle$ is called the empty state and the state $|\,1\rangle$ is said to contain one particle. (One

can alternatively think of $|\,0\rangle$ and $|\,1\rangle$ as being states in the computational basis of a qubit.) A general state in the total space of edges $\mathcal{H}_{edge}^{\otimes N(N-1)/2}$ is

$$|\psi\rangle = \sum_{\{n\}} c_{\{n\}} \, |n_{12}\rangle \otimes |n_{13}\rangle \otimes |n_{23}\rangle \otimes \cdots \,, \tag{4.10}$$

i.e., a superposition of all possible states which are themselves tensor products of states $|n_{ab}\rangle$ associated with single edges; $n_{ab} = 0, 1$ are occupation numbers and $c_{\{n\}}$ are complex coefficients.

A given edge of the graph is interpreted as being on or off depending on whether the corresponding qubit state takes the value 1 or not. The collection of on states define a subgraph of the complete graph $\mathcal{K}_N$. Thus, the total Hilbert space of edges can be decomposed as (recall that we ignore degrees of freedom on the vertices)

$$\mathcal{H}_{total} = \bigoplus_{G} \mathcal{H}_G \tag{4.11}$$

with the tensor sum being over all subgraphs G of $\mathcal{K}_N$. Each term in (4.10) corresponds to a state in one of the blocks $\mathcal{H}_G$. Since we treat the vertices as distinguishable, there may be many blocks in the sum that correspond to isomorphic graphs [2].

Acting on the Hilbert space of each edge can be done through creation and annihilation operators $a^\dagger$ and a. They act in the usual way,

$$a|\,0\rangle = 0, \qquad a|\,1\rangle = |0\rangle, \tag{4.12}$$

[2]Two graphs are isomorphic if they are identical up to a relabeling of vertices.

and obey the anticommutation relation

$$\{a, a^\dagger\} = aa^\dagger + a^\dagger a = 1. \tag{4.13}$$

The other anticommutators are zero, $\{a, a\} = \{a^\dagger, a^\dagger\} = 0$. There is a Hermitian operator $a^\dagger a$, whose action on a state $|n\rangle$ with $n = 0, 1$ is

$$a^\dagger a|\, n\rangle = n\,|\, n\rangle. \tag{4.14}$$

This operator is commonly called the number operator because it reveals the number of particles present in a state.

It is now possible to define operators (4.14) that act on each of the copies of $\mathcal{H}_{edge}$. These will be denoted by subscripts and defined in the intuitive way, *e.g.*

$$\begin{aligned} &N_{13}\ (|n_{12}\rangle \otimes |n_{13}\rangle \otimes \cdots) \\ &\qquad = (1 \otimes a^\dagger a \otimes \cdots)\ (|n_{12}\rangle \otimes |n_{13}\rangle \otimes \cdots) \\ &\qquad = n_{13}\ (|n_{12}\rangle \otimes |n_{13}\rangle \otimes \cdots)\,. \end{aligned} \tag{4.15}$$

From the definition of the operators on the middle line, one can see that number operators acting on different edges commute. Since the graphs are undirected (that is, the edges are unordered pairs of vertices), the identity $N_{ab} = N_{ba}$ holds.

The set of operators N_{ab} can be understood as analogous to elements of an adjacency matrix A_{ab} and thus all the properties described in the previous section are understood.

There are some differences, however, due to the fact that the creation and annihilation operators a_{ab} and $a_{ab}^\dagger$ acting on the same edge do not commute. Terms which contain at least two creation operators and two annihilation operators can in principle be ordered in several inequivalent ways. In setups involving the harmonic oscillators, there is a standard convention for ordering operators called *normal ordering* and denoted by putting colons around an operator. In this convention, all annihilation operators a_{ab} are set to the right of the creation operators $a_{ab}^\dagger$. When $b = d$, the same two annihilation operators appear on the right. It is then easy to understand that

$$: N_{bc} N_{cb} : \; = 0. \tag{4.16}$$

Consequently, whenever a term of $: N_{ab}^{(L)} :$ with $L \geq 2$ acts on the same edge more than once, that term does not contribute. Therefore, the eigenvalues of operators $: N_{ab}^{(L)} :$ for each a, b return the number of *nonoverlapping paths* between vertices a and b. We will make use of the normal ordering convention and this property, in particular, when defining and analyzing the quantum Hamiltonian for the graph model and in the mean field theory approach.

4.5 The Hamiltonian

We would now like to describe the Quantum Graphity Hamiltonian introduced in [80].

For this purpose we consider Hamiltonian function (operator) H acting on states in the Hilbert space $\mathcal{H}_{total}$ defined in (4.8). A Hamiltonian operator associates an energy

$E(G)$ to a state $|\psi_G\rangle$. We can thus define, using a normal-ordering prescription,

$$E(G) = \langle\psi_G| : H : |\psi_G\rangle. \tag{4.17}$$

This notation for the energy should not be confused with the set of edges of a graph; the meaning of the symbol $E(G)$ should be clear from the context.

The Hamiltonian will preserve the permutation invariance symmetry of $\mathcal{K}_N$ by construction.

4.5.1 Valence term

The general form of this valence Hamiltonian should depend only on the number of on edges attached to a given vertex,

$$H_V = g_V \sum_a f_a \left(\sum_b N_{ab}, v_0 \right). \tag{4.18}$$

Here g_V is a positive coupling constant and v_0 is a free real parameter. The function f_a will be chosen such that its minimum occurs when vertex a has exactly v_0 on-links attached to it. The outer sum over vertices a indicates that all vertices in the graph should have the same valence v_0 to minimize the total energy.

A specific choice of H_V is

$$H_V = g_V \sum_a e^{p\left(v_0 - \sum_b N_{ab}\right)^2} \tag{4.19}$$

where p is another real constant. The exponential is defined by its series expansion in p,

$$\begin{aligned} e^{p\left(v_0-\sum_b N_{1b}\right)^2} = 1 + p\left(v_0 - N_{12} - N_{13} - \cdots\right)^2 \\ + \frac{p^2}{2}\left(v_0 - N_{12} - N_{13} - \cdots\right)^4 + O(p^3) \end{aligned} \tag{4.20}$$

The ellipses within the parentheses stand instead of the summation over the other N_{1b}.

The effect of the valence Hamiltonian H_V is to set the preferred valence for a graph to v_0 in the ground state.

4.5.2 Closed Paths

This term of the Hamiltonian counts the number of closed paths of the graph. This is given by,

$$H_B = \sum_a H_{B_a} \tag{4.21}$$

where H_{B_a} is rooted at a vertex a and is given by

$$H_{B_a} = -g_B \sum_b \delta_{ab}\, e^{r N_{ab}}. \tag{4.22}$$

Here g_B is a positive coupling and r is a real parameter. The exponential is defined in terms of a series expansion in the parameter r, and thus N_{ab}^L at the Lth order. When these powers of the number operator are normal-ordered, overlapping paths become unimportant and only nonoverlapping paths contribute. The sum over b and the delta function δ_{ab}

in (4.22) together ensure that only closed paths are counted.It is easy to understand that the Hamiltonian H_B starts contributing at $L = 3$.

4.5.3 Interaction Terms

The terms H_V and H_B do not change the graph state. A generic graph model Hamiltonian might also have some interaction terms which change the graph state. Interaction terms are necessary in a because they define how a graph state can evolve from one configuration to another.

Some examples of such possible interactions are the N-dimensional Pachner moves depending on which space dimensionality ones tries to emulate. However, in the following we will not consider these terms and we find not important to describe them here.

Thus, the final form of the Hamiltonian reads, not neglecting the interaction terms:

$$H = H_V + H_L + H_B \tag{4.23}$$

This is the Hamiltonian that we will study in the following.

4.6 Extensions with More Degrees of Freedom and String-Net condensation

In this section we see how generalization of the previous model can be related to quantum field theories, including quantum gravity.

The Hilbert space $\mathcal{H}_{edge}$ associated to each edge in the complete graph can be altered in order to add more degrees of freedom. There is still a requirement that the new $\mathcal{H}_{edge}$ contains a state $|0\rangle$, which can be interpreted as the physical link between two vertices being *off*.

In order to get string-net condensation, it is necessary to consider an infinity of labeling. Here instead we focus on the case $s = \{1, 2, 3\}$. The Hilbert space of the new edge is the span of all possible states, given by

$$\mathcal{H}_{edge} = \text{span}\{|\,0\rangle,\, |\,1_1\rangle,\, |\,1_2\rangle,\, |\,1_3\rangle\}. \tag{4.24}$$

The difference between the edge Hilbert space (4.24) and the old one (4.9) is that there are now multiple on states that can be distinguished by an internal label s. This will change the phase space of the model in the mean field theory approximation.

The total Hilbert space for this extended model is defined as in (4.8) and can still be decomposed according to (4.11). However, the spaces $\mathcal{H}_G$ in the tensor sum decomposition are here no longer zero-dimensional but reflect the internal degrees of freedom of the *on* links.

This Hilbert space can be considered as the one of spin operators, M which has the states $|j,\, m\rangle$ as eigenstates,

$$M\,|\,j,\, m\rangle = m\,|\,j,\, m\rangle, \tag{4.25}$$

and operators $M^{\pm}$ that change the internal m labels,

$$\begin{aligned} M^{+}\,|j,\,m\rangle &= \sqrt{(j-m)(j+m+1)}\,|\,j,\,m+1\rangle \\ M^{-}\,|j,\,m\rangle &= \sqrt{(j+m)(j-m+1)}\,|\,j,\,m-1\rangle. \end{aligned} \tag{4.26}$$

These are the familiar operators of angular momentum and all the known facts about them follow trivially.

A Hamiltonian for a model with this edge structure can be written, for instance, as

$$H = H_V + H_B + H_C + H_D + H_{\pm}, \tag{4.27}$$

where H_V and H_B are the same as in Sec. 4.1, while the other terms are

$$H_C = g_C \sum_a \left(\sum_b M_{ab} \right)^2, \tag{4.28}$$

$$H_D = g_D \sum_{ab} M_{ab}^2, \tag{4.29}$$

$$H_{\pm} = -\sum_{\text{cycles}} g_{\pm}\,(L) \prod_{i=1}^{L} M_i^{\pm}. \tag{4.30}$$

This Hamiltonian mimics the action of the one of Section. 4.1 [3]

Note the similarity of this coupling function to that of in the loop term H_B without the extended phase space . This is just a choice, and in principle many others could be made. For the time being, no detailed analysis of the $H_\pm$ has been made. Later on, when discussing the mean field theory analysis of the model, a simpler choice for counting the loops will be chosen.

Since the new terms of the Hamiltonian contain only M and $M^\pm$ operators and not a_s and $a_s^\dagger$ operators by themselves, they do not change the linking configuration. At low temperatures, we can consider the base graph to be frozen in a particular configuration which the Hamiltonian will choose, and discuss the action of H_{CD} and $H_\pm$ on this background. If the Hamiltonian is well chosen and the ground state graph is hexagonal, the terms of (4.28), (4.29) and (4.30) reduce to a model of string nets [44].

Since the loop Hamiltonian $H_\pm$ does not commute with H_C or H_D, the eigenstates of the full Hamiltonian will generally be superpositions of states involving different m configurations. Nonetheless, intuitively, the model can be developed by first describing the eigenstates of the $H_C + H_D$ terms alone, and then considering the effect of the loop

[3] Though, there are some clear differences. The couplings g_C, g_D, and $g_\pm$ are additional terms. In the $H_\pm$ term, referred to as the loop term below, the product is taken around a cycle of length L (i.e., consisting of L edges) and with alternating raising and lowering operators:

$$\prod_{i=1}^{L} M_i^\pm = M_{ab}^+ M_{bc}^- ... M_{yz}^+ M_{za}^-. \tag{4.31}$$

Thus, the loop operator is naturally restricted to act on cycles of even length. The coupling $g_\pm(L)$ is

$$g_\pm(L) = \frac{r^L}{L!} g_\pm, \tag{4.32}$$

and thus resemble a term of the Taylor expansion of an exponential.

term.

The ground state of $H_C + H_D$ consists of all links having $m = 0$. When $g_C \gg g_D$, low-energy excited states appear as closed chains of links on which the m variables have alternating values $m = +1$ and $m = -1$. These excitations are called strings and their energy above the ground state is proportional to the coupling g_D times their length (number of edges.) Thus g_D can be thought of as a string tension. The coupling g_C can instead be related to the mass of pointlike particles [44].

Given a graph with all on edges labeled by $m = 0$, a loop operator (4.31) acts as to create a closed string of alternating $m = +1$ and $m = -1$ edges (a loop operator cannot create open strings.). Of course, these closed strings acquire tension (energy) through the g_D term. However, since the sign of the $g_\pm$ term is negative, the overall energy of the state may either increase or decrease as a result of string creation and so there is the possibility of two distinct scenarios. Depending on the choice of the couplings, the tension in a string could be greater than the contribution from the loop term, so the overall effect of creating a string is to increase the energy of the system. If this is the case, then the string represents an excited state over the vacuum in which all m values are set to zero. If the tension is small compared to the contribution from $H_\pm$ so that creating a string decreases the energy, then the creation of the string actually lowers the energy and indicates that the original configuration cannot be the ground state. Instead, the true ground state consists of a superposition of a large number of strings - a string condensate. The Hamiltonian is bounded from below due to the finiteness of the graph, which acts as a regulator.

The characterization of the string-condensed ground state is difficult but its excita-

tions are conjectured to be that of a $U(1)$ gauge theory [44]. In fact, the Hamiltonian is close in form to the Kogut-Susskind formulation of lattice gauge theory [85]. The two main differences between this formulation of the model and the original string-net condensation model proposed by Levin and Wen [44] are that in the present case the background lattice is dynamical and has different types of plaquettes in the ground state, rather than only square plaquettes. This is in general more complicated than this, as the Konopka showed in [14]. In fact, in the model with a generalized phase space, in general the ground state has been found to be effectively one-dimensional, though with a degree fixed by the Hamiltonian. This latter fact will be confirmed later on through a mean field theory approach. Interestingly enough, a different formulation, but still close in spirit to Quantum Graphity but based on simplices [123], obtained a 2-dimensional ground state. More recently[65], a study of the domain structures in this type of models has shown that typical phenomena like gravitational lensing can occur in these models.

4.7 Lieb-Robinson Bounds and (non-)locality

4.7.1 Locality and non-locality

So far we have dealt with Quantum Mechanical models. As it is well known, Quantum Mechanics is non-local in a very strict sense. While information cannot be propagated faster than the speed of light, Quantum Mechanics propagates signals (i.e. probability) outside the local light-cone fixed by the speed of light. The solution to this non-locality problem is well known: Quantum Field Theory. In Quantum Field Theory the idea is to

replace a point-particle with a field and quantize it imposing that equal time commutators between fields are zero if not acting on the same point. This is the *principle of locality*.

The principle of *locality* is one of the most fundamental and powerful ideas of modern physics and is strictly connected to the concept of *causality*. Roughly, it states that given any local piece of a physical system can be influenced only by those pieces in its neighborhood. The principle of *causality*, instead, states that the cause precedes the effect. In special relativity, *information* cannot propagates faster than the speed of light.

Relativistic quantum mechanics, as we said, is built by taking the locality principle as a central feature. In non-relativistic quantum mechanics the situation is more subtle: signals can propagate at every speed and quantum correlations are non-local in their nature.

One can, in fact, send information over any finite distance in an arbitrary small time [95]. However, the amount of information that can be sent decreases exponentially with the distance if the Hamiltonian of the system is the sum of local Hamiltonians. This statement, as we will see, can be made very precise through the Lieb-Robinson bounds.

Specifically, there is an effective light cone resulting from a finite maximum speed of the interactions in quantum systems.

This interesting fact has attracted interest in the context of quantum information theory, condensed matter physics, and the creation of topological order [95, 98, 161, 97].

Later, we will see that a real light cone emerge for particles hopping on the graph, in a different model that we will introduce.

4.7.2 Lieb-Robinson Bounds and the emergent speed of sound

Here we recall the standard proof of the Lieb-Robinson bounds [96, 98, 97]. Let us consider a Hamiltonian of the form $H := \sum_{X \subset G} \Phi_X$. Also, let us consider an operator O_Y with support in a set $Y \subset G$. The time evolution for this operator, in Quantum Mechanics, is under the unitary 1-parameter transformation induced by H, and is $O_Y(t) = e^{itH} O_Y e^{-itH}$.

The Lieb-Robinson bound is an upper bound estimate of the commutator of these two operators $O_P(t), O_Q(t')$ with support in different regions P and Q and at different times t and t'.

In principle we could time evolve the two operators, but only the time difference will result relevant, as it will be clear during the proof.

If the interaction map Φ_X couples only nearest-neighbor degrees of freedom, the Hamiltonian can be written as $H = \sum_{<\mathbf{ij}>} h_{\mathbf{ij}}$ and the Lieb-Robinson bound reads

$$\begin{aligned} \|[O_P(t), O_Q(0)]\| &\leq 2\|O_P\|\|O_Q\| \sum_{n=0}^{\infty} \frac{(2|t|h_{max})^n}{n!} N_{PQ}(n) \\ &\leq 2\|O_P\|\|O_Q\| C \exp\left[-a(d(P,Q) - vt)\right] \end{aligned} \tag{4.33}$$

where $h_{max} = \max_{<\mathbf{ij}>\in G} h_{\mathbf{ij}}$ and $N_{PQ}(s)$ is the number of paths of length $s/2$ between the points P, Q at distance $d(P,Q)$ in G [95]; $||\cdot||$ is instead the operatorial norm, $||\hat{T}|| = \sup_v \frac{|\hat{T}v|}{|v|}$. The constants C, a, v have to be determined in order to get the tightest possible bound. This bound is loose for several reasons: the crude maximization over $h_{\mathbf{ij}}$, the overlook about the Hamiltonian's details, and the fact that all interactions are summed in modulus instead than amplitude, so that destructive interference is not taken in account.

4.7.3 Lieb-Robinson Bound for the emergent $U(1)$ model

What do the Lieb-Robinson bounds tell us about the model H_{eff} with emergent light? Here we recall the results of [54], where this question has been undertaken. We have argued that the effective model of Levin and Wen has an emergent $U(1)$ gauge-symmetry. Is the maximum speed of the interactions something like the speed of the emergent light or something completely different? As we have seen, this is of great importance if we want to take seriously the theory of light as an emergent phenomenon. More importantly, we will see that the degree of the graph, which in the model is a function of the temperature, plays a major role in the speed of propagation.

If we apply naively the Lieb-Robinson bounds to the Hamiltonian of the $U(1)$ lattice gauge theory, we see that the speed v is proportional to the strongest of the coupling constants, $v \propto g$. Since light only exists in the phase $g \gg J$, we would have $v \gg \sqrt{gJ}$.

However, the bound can be made much tighter by examining the details of the Hamiltonian and the specific way the interactions propagate [54]. Consider the function $f(t) := [O_P(t), O_Q(0)]$ and consider the set $Z_1 := \{Z \subset G : [\Phi_Z, O_P] \neq 0\}$, the support of the complement of the commutant of O_P in the set of interactions. The function $f(t)$ obeys a differential equation [97]

$$f'(t) = -i \sum_{Z \subset Z_1} \left([f(t), \Phi_Z(t)] + [O_P(t), [\Phi_Z(t), O_Q(0)]] \right), \tag{4.34}$$

where $\Phi_Z(t) = e^{iHt} \Phi_Z e^{-iHt}$. From the above equation, and using the norm-preserving

property of unitary evolutions, one can establish [97] the bound

$$\|[O_P(t), O_Q(0)]\| \leq \|[O_P, O_Q]\| \\ +2\|O_P\| \int_0^{|t|} \| \sum_{Z \subset Z_1} [\Phi_Z(t), O_Q(0)]\|. \tag{4.35}$$

Successive iterations of the above formula yield

$$\|[O_P(t), O_Q(0)]\| \leq 2\|O_P\|\|O_Q\| \sum_{n=0}^{\infty} \frac{(2|t|)^n}{n!} a_n, \tag{4.36}$$

where

$$a_n := \sum_{Y_i \subset Z_i} \prod_{i=1}^{n} \|\Phi_{Y_i}\|, \tag{4.37}$$

and where we define $Z_{i+1} := \{Z \subset G : [\Phi_Z, \Phi_{Z' \subset Z_i}] \neq 0\}$. The operators O_1 and O_2 are non-commuting and local operators of the Hamiltonian.

It is clear, at this point, that every element of the sum is a product of the type $\prod_i \|\Phi_i\|$ such that $[\Phi_i, \Phi_{i-1}] \neq 0$ for every i. If each Φ_i is a local bosonic operator, every one of those products is a path on the lattice.

These considerations can be applied to the case of the effective Hamiltonian H_{eff} [54]. Let us consider O_P, O_Q to be the spin operator S^z at the points P, Q. For this Hamiltonian, the only non commuting operators are W_p and S_i^z when they have a vertex in common. Therefore, a path in (4.37) consists of steps from a plaquette to any of the four links bordering it, alternated with steps from a link to any of the two incident plaque-

ttes. To every path of length n on G' will then correspond an operator whose norm is $\prod_{i=1}^{n} \|\Phi_i\| = (gJ)^{n/2}$. Thus, denoting with $N'_{PQ}(n,d)$ the number of paths of length n on G' from P to a given point Q at a distance $2d$, the following bound can be obtained

$$a_n \leq N'_{PQ}(n,d)(gJ)^{\frac{n}{2}}. \tag{4.38}$$

A bound has been given in [54] to $N'_{PQ}(n,d) \leq 2\sqrt{8}^{n} e^{\kappa(n-2d+4)}$, for every $\kappa > 0$. Moreover, the iteration of Eq.(4.36) can be built by replacing the $2|t|$ with $\|[\Phi^1,\Phi^2]\|(\|\Phi^1\|\|\Phi^2\|)^{-1}|t| = \sqrt{2}|t|$, and obtain

$$\begin{aligned} \|[O_P(t), O_Q(0)]\| &\leq \frac{4e^{4\kappa}}{e^{2\kappa d}}\|O_P\|\|O_Q\| \sum_{n=0}^{\infty} \frac{(\sqrt{16gJ}e^{\kappa}|t|)^n}{n!} \\ &= \leq 4e^{4\kappa}\|O_P\|\|O_Q\| e^{-2\kappa(d-\frac{\sqrt{2}\sqrt{2gJ}e^{\kappa}}{\kappa}|t|)}. \end{aligned} \tag{4.39}$$

Optimizing for κ, one could get $v_{LR} = \sqrt{2}e\sqrt{2gJ} \equiv \sqrt{2}e \times c$.

The speed v has been estimated numerically as $v \approx \sqrt{2}e\sqrt{2gJ} \equiv v_{LR} = \sqrt{2}e \times c$ and it is tighter than the ordinary Lieb-Robinson bound.

Eq. (4.39) establishes that all the observables that are outside of the effective light cone centered on P with speed of light v_{LR} will have an exponentially small commutator with the observables in P. It proves that any signal outside of a light cone generated with a speed that is of the same order of magnitude (and with the same dependence on coupling constants) of light will be exponentially suppressed. This result is a strong indication that the maximum speed of signals is light. Thus, the theory of emerging light explains why its speed is also the maximum speed for any signal at low energies. If we were able to

probe energies of order U one could still find faster signals. This is still, however, an open problem[74].

4.8 Mean field theory approximation at Low Temperature

We will now study the mean field theory approximation[4]. As we have seen in the previous sections, Quantum Graphity models are built such that at low temperatures the model mimics the Levin-Wen Hamiltonian. We have also seen as the degree of the graph is very relevant for the Lieb-Robinson bounds. We ask ourselves what is, then, the effective degree of the graph as a function of the temperature, in the Quantum Graphity model introduced in [80, 107]. We tackle this problem by means of a Mean Field theory approach. We will first relate the model to an Ising model, and then study the degree on this reformulation. For this, we will introduce line graphs, which are special graph duals.

4.8.1 Graphs and Line Graphs

We start by defining line graphs. Let $G = (V, E)$ denote a graph with vertex set $V = \{v_1, v_2, ...\}$ and edge set $E = \{e_1, e_2, ...\}$. The line graph $\mathcal{L}(G) = (\widetilde{V}, \widetilde{E})$ is the graph of the adjacencies of G, containing information on the connectivity of the original graph. Each vertex $\tilde{v} \in \widetilde{V}(\mathcal{L}(G))$ corresponds to an edge $e \in E(G)$. Two vertices $\tilde{v}_1$ and $\tilde{v}_2$ in $\widetilde{V}(\mathcal{L}(G))$ are adjacent if and only if the edges in G corresponding to $\tilde{v}_1$ and $\tilde{v}_2$ share a vertex. The correspondence between G and $\mathcal{L}(G)$ is not one to one. From a given graph

[4]This section is based on [64]. The role of the author of the present thesis was to find the relation between the speed of propagation of perturbations and the temperature.

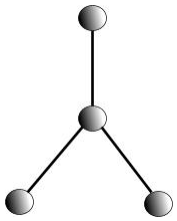

Figure 4.1: The simplest example of element of the Beineke classification of a minimal graph that is not a line graph of any other one. This means that in general there is not a one-one correspondence between a graphs and *line-duals*.

G we can construct only one $\mathcal{L}(G)$ but it is not true that any graph is a line graph. In fact, according to the Beineke classification, there are 9 non-minimal graphs that are not line graphs of another graph and each graph containing them is not a line graph[49]. The simplest example of a line graph is depicted in Fig. 4.1.

Given a graph G, we can construct its line graph using the following procedure:

1. Enumerate the vertices of G.
2. Enumerate the edges of G with a fixed prescription (see example below) and put a blob on them.
3. If two edges share a vertex, draw a bold line between them.
4. Remove G and its enumeration.

What is left is the line graph of G where the blobs represent its vertices.

Let us now introduce some useful quantities:

Definition. *(Kirchhoff matrix) Let G be a generic graph, $V = \{v_1, v_2, \cdots, v_n\}$ be the set of vertices of G and $E = \{e_1, e_2, \cdots, e_p\}$ be the set of edges of G. Let us define the matrix P of size $n \times p$ with entries $P_{i\beta}$, where i is an integer between 1 and n on the set of vertices and β is an*

integer between 1 *and* p *on the set of edges, such that:*

$$P_{i\beta} = \begin{cases} 1 & \textit{if the edge } \beta \textit{ has an vertex on the vertex } i, \\ 0 & \textit{otherwise .} \end{cases} \tag{4.40}$$

The Kirchhoff matrix K *is the* $p \times p$ *matrix built from* P*, such that:*

$$K = P^t \, P, \tag{4.41}$$

P^t *representing the transpose of* P*.*

A well-known theorem now gives the incidence matrix of the line graph $\mathcal{L}(G)$:

Theorem. *Let* G *be a graph with p edges and n vertices and let* $\mathcal{L}(G)$ *be its line graph. Then the matrix:*

$$J = K - 2\,\boldsymbol{I}, \tag{4.42}$$

where $\boldsymbol{I}$ *is the* $p \times p$ *identity matrix, is the incidence matrix of* $\mathcal{L}(G)$*.*

In the next section we will show how the graphity hamiltonian can be recast on the line graph using (4.40) and (4.42).

4.8.2 The line graph representation

Since in the hamiltonian (4.23) we neglect the terms in which vertices are interacting because we assume there are no degrees of freedom on them, one could expect that it can be

rewritten only in terms of the connectivity of the graph. To carry out such a reformulation, let us expand the first term in (4.23) for small values of the parameter p:

$$\begin{aligned}\widehat{H}_V &= g_V \sum_i \widehat{1} + p g_V \sum_i \left(v_0 - \sum_j \widehat{N}_{ij} \right)^2 + \mathcal{O}(p^2) \\ &= g_V \left(1 + v_0^2 p\right) \sum_i \widehat{1} + p g_V \sum_{ijk} \widehat{N}_{ij} \widehat{N}_{jk} - 2 g_V p v_0 \sum_{ij} \widehat{N}_{ij} + \mathcal{O}(p^2). \end{aligned} \tag{4.43}$$

As we will see later, such an expansion does not modify the properties of the model at low temperature. The first term in (4.43) is an energy shift and, for what is to come, can be neglected. We should now be able to recognize some particular terms in the expansion (4.43). The third term is proportional to the operator $\sum_{ij} \widehat{N}_{ij}$. It is the sum over all the edges of the graph, zero or not, of the number operator. We will change the notation to

$$\sum_{ij} \widehat{N}_{ij} \to 2 \sum_{\beta} \widehat{N}_{\beta}, \tag{4.44}$$

where β, as in the previous section, runs from 1 to $N(N-1)/2$ and labels the edges of $\mathcal{K}_N$ or, equivalently in what follows, the vertices of its line graph.

To rewrite the second term in (4.43), we need the matrix $P_{i\beta}$ of (4.40) in this context. This matrix maps the graph to its line graph, as we will see. We first fix a prescription to label edges. Let $\mathcal{K}_N$ be the complete graph of N vertices. Let $\mathcal{I}$ be any enumeration of $V(\mathcal{K}_N)$, $i \in \mathcal{I} = 1, ..., N$. We identify edges by their endpoint vertices (i, j), with $i, j \in \mathcal{I}$. A *labeling* S_β, $\beta \in \mathcal{B} = \{1, \cdots, N(N-1)/2\}$ is an enumeration of $\widetilde{E}(\mathcal{L}(\mathcal{K}_N))$, according to

the following prescription:

$$
\begin{aligned}
&S_1, \cdots, S_{N-1} \text{ label the edges connecting the vertices } \{(1,2), \cdots, (1,N)\};\\
&S_N, \cdots, S_{2(N-1)} \text{ label the edges connecting the vertices } \{(2,3), \cdots, (2,N)\};\\
&\vdots\\
&S_{N(N-1)/2} \text{ labels the edge connecting the vertices } (N-1,N).
\end{aligned}
\tag{4.45}
$$

Using this prescription it is easy to see that the matrix $P_{i\beta}$ introduced in (4.40), for the complete graph $\mathcal{K}_N$, has the simple (recursive) form:

$$
P^N = \begin{pmatrix} \vec{V}_{N-1} & \vec{0} \\ \mathbf{I}^{N-1}_{b'c'} & P^{N-1}_{a'\alpha'} \end{pmatrix}, \tag{4.46}
$$

where $\vec{V}_{N-1}$ is a row vector of length $N-1$, $\mathbf{I}^{N-1}$ is the identity matrix of size $(N-1)\times(N-1)$ and $\vec{0}$ represents a null row vector of length $N(N-1)/2-(N-1)$. The indices $\{a', b', c'\}$ and α' run from 1 to $N-1$ and 1 to $(N-1)(N-2)/2$ respectively. As an example, for the graphs of Fig. 4.2 the P matrices are:

$$
P^3 = \begin{pmatrix} 1 & 1 & 0 \\ 1 & 0 & 1 \\ 0 & 1 & 1 \end{pmatrix}, \tag{4.47}
$$

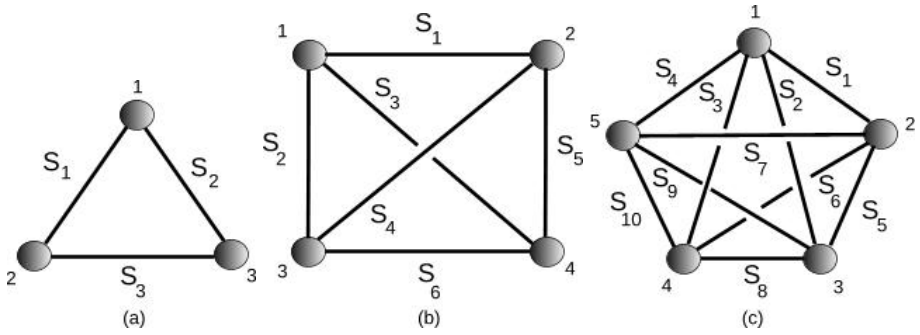

Figure 4.2: Three examples of complete graphs labeled according to the prescription (4.45).

$$P^4 = \begin{pmatrix} 1 & 1 & 1 & 0 & 0 & 0 \\ 1 & 0 & 0 & 1 & 1 & 0 \\ 0 & 1 & 0 & 1 & 0 & 1 \\ 0 & 0 & 1 & 0 & 1 & 1 \end{pmatrix}, \tag{4.48}$$

$$P^5 = \begin{pmatrix} 1 & 1 & 1 & 1 & 0 & 0 & 0 & 0 & 0 & 0 \\ 1 & 0 & 0 & 0 & 1 & 1 & 1 & 0 & 0 & 0 \\ 0 & 1 & 0 & 0 & 1 & 0 & 0 & 1 & 1 & 0 \\ 0 & 0 & 1 & 0 & 0 & 1 & 0 & 1 & 0 & 1 \\ 0 & 0 & 0 & 1 & 0 & 0 & 1 & 0 & 1 & 1 \end{pmatrix}, \tag{4.49}$$

for (a), (b) and (c) respectively.

It is easy to see that two edges α and β have a common vertex if and only if we have:

$$\sum_{i\in\mathcal{I}} {P^t}_{\beta i} P_{i\alpha} = c \neq 0, \tag{4.50}$$

where ^{t} is the transposition operation. By construction, c can take the following values only:

$$c = \begin{cases} 2 & \text{if } \alpha = \beta, \\ 1 & \text{if } \alpha \neq \beta \text{ and } \alpha \text{ and } \beta \text{ have a common vertex,} \\ 0 & \text{if } \alpha \neq \beta \text{ and } \alpha \text{ and } \beta \text{ do not have a common vertex.} \end{cases} \tag{4.51}$$

In particular, for $N = 4$, K is given by:

$$K^4 = \begin{pmatrix} 2 & 1 & 1 & 1 & 1 & 0 \\ 1 & 2 & 1 & 0 & 0 & 1 \\ 1 & 1 & 2 & 0 & 1 & 1 \\ 1 & 0 & 0 & 2 & 1 & 1 \\ 1 & 0 & 0 & 1 & 2 & 1 \\ 0 & 1 & 1 & 1 & 1 & 2 \end{pmatrix}, \tag{4.52}$$

Using now the matrix $P_{i\beta}$ just introduced, we want to construct generic *n-string matrices* as composition of n edges of the graph, thus a *path* on the graph. The n-string matrices will be needed both for the non-retracing loop term and the 2-edge interaction term in

equation (4.43). The quantity:

$$K^i_{\alpha\beta} = P^t_{\alpha i} P_{i\beta} \tag{4.53}$$

is the definition of the Kirchhoff matrix of equation (4.42) if we sum over the index i. From $K^i_{\alpha\beta}$ we can construct strings of P's of the form

$$Q^{i_1\cdots i_n}_{\alpha_1\cdots\alpha_{n+1}} = K^{i_1}_{\alpha_1\alpha_2} K^{i_2}_{\alpha_2\alpha_3} \cdots K^{i_n}_{\alpha_n\alpha_{n+1}}, \tag{4.54}$$

that we call *string matrices* of nth order. These string matrices represent paths through vertices $i_1 \cdots i_n$ and they are zero unless the edges corresponding to $\alpha_1 \cdots \alpha_{n+1}$ are in the correct order, that means, they represent an actual path on the graph. For instance, the number of paths of length 2 on the complete graph is given by

$$\#\text{2-strings} = \sum_{\alpha\neq\beta\in\mathcal{B}} \sum_{i\in\mathcal{I}} Q^i_{\alpha\beta} = \sum_{\alpha\neq\beta\in\mathcal{B}} K_{\alpha\beta}, \tag{4.55}$$

or, equivalently, we can use (4.40) and rewrite (4.55) as

$$\#\text{2-strings} = \sum_{\alpha\beta\in\mathcal{B}} \sum_{i\in\mathcal{I}} Q^i_{\alpha\beta} = \sum_{\alpha\beta\in\mathcal{B}} \left(K_{\alpha\beta} - 2\,\mathbf{I}_{\alpha\beta}\right). \tag{4.56}$$

The subtraction of twice the identity in (4.56) is the same as the subtraction of the self-energy of each edge. We now clearly see that this matrix is precisely the incidence matrix of the line graph of $\mathcal{K}_N$ introduced in (4.42), with $\alpha, \beta \in \widetilde{V}(\mathcal{L}(\mathcal{K}_N))$.

So far we have dealt with the complete graph only. We wish to extend this formalism to a dynamical graph. In order to do that we return to the Hilbert space formulation of the graph with *on/off* edges. Recall that any graph on N vertices is a subgraph of the complete graph $\mathcal{K}_N$, with some edges *off*. Thus, since we can always map a graph on a complete graph, we can count paths on any graph by modifying (4.56) so that it counts paths of only *on* edges on the corresponding complete graph. To do so, we introduce in the sum the number operators $\widehat{N}_\beta$ in the following way:

$$\begin{aligned} \#\text{2-strings} &= \sum_{\alpha\beta\in\mathcal{B}} (K_{\alpha\beta} - 2\, I_{\alpha\beta})\, \widehat{N}_\alpha \widehat{N}_\beta \\ &= \sum_{\alpha\beta\in\mathcal{B}} J_{\alpha\beta}\, \widehat{N}_\alpha \widehat{N}_\beta. \end{aligned} \tag{4.57}$$

This term does not contribute if any of the two edges α, β is off. It is easy to see that this term of the hamiltonian is an Ising interaction. The important difference between these two Hamiltonians is that in our case the spin system is on the line graph a complete graph $\mathcal{K}_N$.

By extension of the above, we are now able to construct a generic *path operator* out of $K^i_{\alpha\beta}$'s. We define

$$\begin{aligned} \widehat{P}(n) &:= \sum_{\Omega} \sum_{\alpha_1\cdots\alpha_n} K^{i_1}_{\alpha_1\alpha_2} K^{i_2}_{\alpha_2\alpha_3} \cdots K^{i_{n-1}}_{\alpha_{n-1}\alpha_n}\, \widehat{N}_{\alpha_1} \cdots \widehat{N}_{\alpha_n} \\ &= \sum_{\Omega} \sum_{\alpha_1\cdots\alpha_n} Q^{i_1\cdots i_{n-1}}_{\alpha_1\cdots\alpha_n}\, \widehat{N}_{\alpha_1} \cdots \widehat{N}_{\alpha_n}, \end{aligned} \tag{4.58}$$

where the set $\mathcal{Q}$ is

$$\mathcal{Q} = \begin{cases} i_1 \neq \cdots \neq i_{n-1} \in \mathcal{I} \text{ for non-retracing paths,} \\ i_1, \ldots, i_{n-1} \in \mathcal{I} \text{ for retracing paths.} \end{cases} \tag{4.59}$$

It is easy to see that it counts the number of paths of length n in the graph, that is why we call the Q's *string matrices*. Note that $Q^{i_1 \cdots i_{n-1}}_{\alpha_1 \cdots \alpha_n}$ can take values 0 and 1 only because it is a product of 0's and 1's. This string matrix is *not* the matrix multiplication of the Kirchhoff matrices: it only reduces to matrix multiplication for retracing paths where we sum over all possible vertices.

In the following, we will denote the two sets in (4.59) as $\mathcal{Q}^r$ and $\mathcal{Q}^{nr}$ for the retracing and non retracing cases respectively; moreover, we may explicitly show the indices on which we are doing the sum as $\mathcal{Q}^{r/nr}(i_{b(j)})$. In order to count loops, we just need to impose $\alpha_1 = \alpha_n$:

$$\underbrace{P_{\alpha_1 i_1} P_{i_1 \alpha_2}}_{K^{i_1}_{\alpha_1 \alpha_2}} \underbrace{P_{\alpha_2 i_2} P_{i_2 \alpha_3}}_{K^{i_2}_{\alpha_2 \alpha_3}} \underbrace{P_{\alpha_3 i_3} P_{i_3 \alpha_1}}_{K^{i_3}_{\alpha_3 \alpha_1}} . \tag{4.60}$$

Thus we have discovered that, when there are no degrees of freedom on the vertices of the graph and we neglect the interaction terms, we can recast the Quantum Graphity hamiltonian on the line graph $\mathcal{L}(\mathcal{K}_N)$ representation in the weak coupling regime at finite N.

We end this section with two properties of the nth-order string matrices. Let us define:

$$\widetilde{Q}^{r/nr}_{\alpha_1\cdots\alpha_n} = \sum_{Q^{r/nr}} Q^{i_1\cdots i_{n-1}}_{\alpha_1\cdots\alpha_n}. \tag{4.61}$$

The following properties of the sum of these string matrices on complete graphs will be required next:

Property 1: Let $\mathcal{G} = \mathcal{K}_N$. Then, for a loop of n edges:

$$\sum_{\alpha_1\neq\alpha_2\neq\cdots\neq\alpha_n} \widetilde{Q}^{nr}_{\alpha_1\cdots\cdots\alpha_L\alpha_1} = N(N-1)\cdots(N-L) \tag{4.62}$$

and

$$\sum_{\alpha_1\neq\alpha_2\neq\cdots\neq\alpha_n} \widetilde{Q}^{r}_{\alpha_1\cdots\cdots\alpha_L\alpha_1} = N^L. \tag{4.63}$$

Proof. These two facts follow trivially if we note that the equations (4.62) and (4.63) count the number of retracing and non-retracing paths of length L on the complete graph respectively.

Property 2: Let $\mathcal{G} = \mathcal{K}_N$. Then, for a loop of n edges, and for $L \geq 4$, we have:

$$\textstyle\sum_{\alpha_3\neq\alpha_4\neq\cdots\neq\alpha_n} \widetilde{Q}^{nr}_{\alpha_1\cdots\cdots\alpha_L\alpha_1} = (N-3)\cdots(N-3-(L-4))K_{\alpha_1\alpha_2}, \tag{4.64}$$

while, for $L = 3$:

$$\sum_{\alpha_3} \widetilde{Q}^{nr}_{\alpha_1\alpha_2\alpha_3\alpha_1} = K_{\alpha_1\alpha_2}, \tag{4.65}$$

if $\alpha_1 \neq \alpha_2 \neq \alpha_3 \cdots \neq \alpha_n$.

Proof. Note that $\sum_{\alpha_3\neq\alpha_4\neq\cdots\neq\alpha_n} \widetilde{Q}^{nr}_{\alpha_1\cdots\cdots\alpha_n\alpha_1}$ is the number of *non-retracing* loops of length L on the complete graph $\mathcal{K}_N$ which pass by the edges α_1 and α_2. Now, it is easy to see that if the edges α_1 and α_2 do not share a link this quantity is zero. Also note that, by the symmetry of the complete graph, the number of non-retracing loops based on two neighboring edges must be the same for each pair of edges α_{j_1},α_{j_2} sharing a node. Since the matrix $K_{\alpha_{j_1}\alpha_{j_2}}$ takes values 1 or 0 depending on whether the edges α_{j_1},α_{j_2} are neighbors or not, $\sum_{\alpha_3\neq\alpha_4\neq\cdots\neq\alpha_n} \widetilde{Q}^{nr}_{\alpha_1\cdots\cdots\alpha_L\alpha_1}$ must be proportional to the matrix $K_{\alpha_1\alpha_2}$. In order to evaluate the proportionality constant, let us note that each loop is weighed by a factor of 1 because n-string matrices take values 1 or 0 only. The combinatorial quantity $(N-3)\cdots(N-3-(L-4))$ is then the number of non-retracing loops of length L passing from two consecutive fixed edges on the complete graph of N vertices, as can be easily checked. The special case (4.66) follows from the fact that if we fix two edges there is only one edge which closes the 3-loop.

Note that, for $N \gg L$, we have:

$$\sum_{\alpha_3 \neq \alpha_4 \neq \cdots \neq \alpha_n} \widetilde{Q}^{nr}_{\alpha_1 \cdots\cdots \alpha_L \alpha_1} \approx \sum_{\alpha_3 \neq \alpha_4 \neq \cdots \neq \alpha_n} \widetilde{Q}^{r}_{\alpha_1 \cdots\cdots \alpha_L \alpha_1} = N^L. \tag{4.66}$$

We can now collect the results of this section to write the hamiltonian (4.43) as

$$\widehat{H} = A \sum_{\alpha,\beta \in \mathcal{B}} J_{\alpha\beta} \widehat{N}_\alpha \widehat{N}_\beta - B \sum_{\alpha \in \mathcal{B}} \widehat{N}_\alpha - C \sum_{\alpha \neq \beta \neq \gamma \in \mathcal{B}} \widetilde{Q}^{nr}_{\alpha,\beta,\gamma}\, \widehat{N}_\alpha \widehat{N}_\beta \widehat{N}_\gamma, \tag{4.67}$$

where

$$\begin{aligned} A &= p\, g_V, \\ B &= 2\, g_V\, p\, v_0, \\ C &= g_L\, \frac{r^3}{6}, \end{aligned} \tag{4.68}$$

and neglecting higher order loop terms.

4.8.3 Mean field theory approximation and low temperature expansion

Having rewritten the hamiltonian in an Ising fashion, we now can approach the problem of finding a graph observable and its equilibrium distribution using mean field theory. As we will see, the natural graph observable to consider is the average valence of the graph. We will assume that the system is at equilibrium and we neglect the interaction terms. In this case, it is straightforward to use mean field theory analysis [53]. In what follows, we assume units in which the Boltzmann constant $k_B = 1$.

We start by replacing the number operators $\widehat{N}_\alpha$ with semi-classical analogs, imposing that their expectation value must lie in the interval $I = [0, 1]$:

$$\widehat{N}_\beta \to \langle \widehat{N}_\beta \rangle_P = m_\beta, \tag{4.69}$$

where P is a probability measure of the following form:

$$P(m_\beta) = m_\beta \delta_{1,m_\beta} + (1 - m_\beta)\delta_{0,m_\beta}. \tag{4.70}$$

It is easy to see that this probability distribution forces the spin-average to lie in I. Recall that in order to obtain the mean field theory distribution we have to extremize the Gibbs functional given by

$$\Phi[m] = H[m] - \frac{1}{\beta} S[m], \tag{4.71}$$

where $\beta = T^{-1}$, $H[m]$ is the energy and $S[m]$ is the entropy functional. The latter can be written as:

$$S[m] = -\sum_{m_\beta = \{0,1\}} n_i P(m_\beta(i)) \log P(m_\beta(i)), \tag{4.72}$$

where n_i is the degeneracy of the state.

Case I: Non-degenerate edge states

In this subsection we focus on the case in which the states *on* and *off* are not degenerate, so that $n_i = 1$. In the next subsection we will deal with non-degenerate edge states and in particular with 3-degenerate *on* states.

In the process of extremizing the Gibbs functional we will see how the average valence of the graph naturally emerges. We impose:

$$\partial_{m_\beta} \Phi[m] = 0. \tag{4.73}$$

Using

$$\partial_{m_\beta} S[m] = -\log(\frac{m_\beta}{1 - m_\beta}) \tag{4.74}$$

and

$$\partial_{m_\beta} H[m] = A \sum_{\alpha \in \mathcal{B}} J_{\alpha\beta} m_\alpha - B - C \sum_{\alpha\gamma \in \mathcal{B}, \alpha \neq \gamma \neq \beta} \tilde{Q}_{\alpha\beta\gamma} m_\alpha m_\gamma, \tag{4.75}$$

we find that the distribution for the m_α is

$$m_\beta = \frac{e^{-\beta \partial_{m_\beta} H[m]}}{1 + e^{-\beta \partial_{m_\beta} H[m]}} = \frac{1}{1 + e^{\beta \partial_{m_\beta} H[m]}}. \tag{4.76}$$

The solution of this equation gives the equilibrium value of m_β once the value of the temperature is fixed.

We now want to write (4.76) as a function of an average quantity on the graph. Let us first note that, in the mean field theory approximation, we have

$$\sum_{\alpha} J_{\alpha\beta} m_\alpha = 2\, d(T), \tag{4.77}$$

where $d(T)$ is the mean valence of the graph. The valence $d(T)$ is a good graph observable that we can use also as a double check for our procedure since it appears explicitly in the original formulation of the hamiltonian and in the low temperature regime must take the value v_0. First, we note that:

$$m_\alpha = \frac{N_{\text{on edges}}}{N(N-1)/2} = \frac{\sum_{i\in\mathcal{J}} d(i)/2}{N(N-1)/2} = \frac{d(T)}{N-1}. \tag{4.78}$$

In the first equality, $N_{\text{on edges}}$ is the number of edges of the graph which are in an *on* state. In the second equality, the average valence (the sum over all the local valencies divided by the number of vertices) is explicitly written as a temperature dependent quantity. In the third equality we used the graph property:

$$\sum_{i\in\mathcal{J}} \frac{d(i)}{N-1} = \langle d \rangle \equiv d(T). \tag{4.79}$$

The most complicated term in the hamiltonian is the 3-loop one. The simplest way to deal with it is to use the Ansatz dictated by the mean field theory:

$$\sum_{\alpha\gamma\in\mathcal{B}} \tilde{Q}_{\alpha\beta\gamma} m_\alpha m_\beta \approx \xi(T) d^2(T). \tag{4.80}$$

Let us replace m_β with its average value: $d(T)/N - 1$. Using eq. (4.62) for non-retracing paths and assuming $N \gg 1$ we obtain the dependence on $d(T)$. $\xi(T)$ is a function of order ~ 1 at low temperature, which we assume is dependent on T. Using these approximations we can see that $d(T)$ is a natural order parameter for our mean field theory since it is easily recognized as implicitly defined in the stable distribution:

$$d(T) = \frac{N-1}{1 + e^{\beta[2d(T)A - \xi\frac{C}{2}d^2(T) - B]}}. \tag{4.81}$$

Again, in order to double check our procedure, we can ask if such an order parameter behaves as expected at low temperature. We must keep in mind that the starting hamiltonian (4.23) was constructed in such a way that the average valence at zero temperature was a fixed value of the parameter v_0 at finite N. We can now use (4.81) to check if this is the case. To do so, we Taylor expand both sides and match the zeroth and first order coefficients on the left and right hand side of the equation. That is, we start with the expansion

$$d(T) = \tilde{\alpha} + \tilde{\beta}T + O(T^2), \tag{4.82}$$

and, for the approximation to be consistent at $T = 0$, we require analicity of the order parameter (this has to be the case for a finite volume system in ordinary statistical mechanics, which is the case for finite N) . We then require that inside the exponential of equation (4.81) the temperature independent terms in the numerator cancel out so that at

$T = 0$ the exponent is well defined. This gives the second order equation in α:

$$2\alpha A - \xi(0) C \alpha^2 = B. \tag{4.83}$$

Now note that, while this equation has two solutions, we need to only look for the one which is analytical in the parameters of the model and tends smoothly to the solution $\tilde{\alpha} = \frac{B}{2A}$ in the $C \to 0$ limit. This fixes α to the value $\tilde{\alpha}$, given by

$$\tilde{\alpha} = \frac{A}{\xi(0) C} \left(1 - \sqrt{1 - \frac{C \xi(0) B}{A^2}} \right). \tag{4.84}$$

We can now plug $\tilde{\alpha}$ at $T = 0$ into (4.81):

$$\tilde{\alpha} = \frac{N - 1}{1 + e^{(2A - \xi(0) C \tilde{\alpha}) \tilde{\beta}}}, \tag{4.85}$$

to obtain the value of $\tilde{\beta}$ in (4.82):

$$\tilde{\beta} = \frac{1}{2A - \xi(0) C \tilde{\alpha}} \log \left(\frac{N - 1}{\tilde{\alpha}} - 1 \right). \tag{4.86}$$

It is easy to see that in the limit $N \to \infty$ we have $\tilde{\beta} \to \infty$, indicating a second-order phase transition (a discontinuity in the first derivative of the order parameter). In our case, this happens at $T = 0$, meaning that this transition is not possible because there is no way to cool down the system to zero temperature with an external bath. However, we have to remember that we are just approximating the real system with a semi-classical

analog. We then simply interpret the above result as the fact that the system reaches the ground state very quickly when the temperature approaches zero.

It is interesting now to plug in the couplings. Inserting equations (4.68) into (4.84), we find that at $T = 0$

$$d(T=0) = \tilde{\alpha} = \frac{A}{\xi C}\left(1 - \sqrt{1 - \frac{C\xi B}{A^2}}\right) = \frac{6pg_V}{\xi(0)g_L r^3}\left(1 - \sqrt{1 - \xi(0)\frac{g_L r^3 v_0}{3pg_V}}\right). \quad (4.87)$$

Note that, for small values of r, when $r^3 \ll \frac{3pg_V}{g_L v_0}$, we have $\tilde{\alpha} = v_0$, meaning that at low temperature the mean degree is the one imposed by the degree term of the hamiltonian, as expected. We can, however, see how the 3-loops term contributes to this quantity by a Taylor expansion in r:

$$d(T=0) = \tilde{\alpha} = v_0\left(1 + \frac{2}{3}\xi(0)\frac{g_L r^3 v_0}{pg_V}\right). \quad (4.88)$$

From this expression it is clear that the loop terms are suppressed if $g_V \gg g_L$. This is the main result derived in this section using the line graph representation. A plot of the function $d(T)$ is shown in Figure 3.

We now have the tools to calculate the susceptibility function for the theory in the mean field theory approximation. Recall that the susceptibility function tells us how the system reacts to a variation of the external magnetic field. In our case, the magnetic field is the combination $2g_V p v_0$ and we note that the parameter v_0 in the hamiltonian appears only here. We have the following analogy: v_0 represents the external magnetic field, while $2g_V p$ represents the spin-coupling combination.

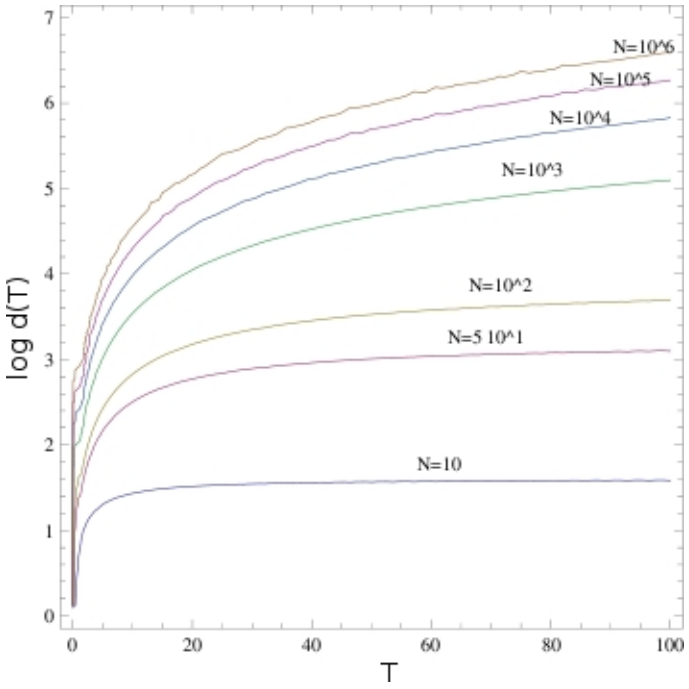

Figure 4.3: The behavior of $\log(\mathrm{d(T)})$ (y-axis) against T (x-axis), for increasing N.

In order to calculate the susceptibility, we assume that the constant B is site-dependent (i.e. a field). Thus, we have

$$\langle G_{\alpha\beta}\rangle_B = -\frac{1}{\beta}\frac{\partial}{\partial B_\beta}\frac{\partial}{\partial B_\alpha}F[h] = \frac{1}{\beta}\frac{\partial m_\beta}{\partial B_\alpha}. \tag{4.89}$$

In particular, we are interested in the susceptibility function when $T \approx 0$. From the study of it we can gain some information about the low energy behavior of the model. We expand the equilibrium distribution

$$m_\beta = \frac{1}{2}\left[1 - \beta\left(A\sum_{\alpha\in\mathcal{B}} J_{\alpha\beta}m_\alpha - B_\beta - C\sum_{\alpha\gamma\in\mathcal{B}}\tilde{Q}_{\alpha\beta\gamma}m_\alpha m_\gamma\right)\right]. \tag{4.90}$$

Using the notation $\rho_{\alpha\beta} := \sum_{\gamma\in\mathcal{B}} \tilde{Q}_{\alpha\beta\gamma} m_\gamma$, we obtain

$$\tilde{B}_\beta = B_\beta - \frac{1}{2} = \sum_{\alpha\in\mathcal{B}} \left(2\frac{\delta_{\alpha\beta}}{\beta} + AJ_{\alpha\beta} + C\tilde{\rho}_{\alpha\beta} \right) m_\alpha. \tag{4.91}$$

To invert this equation, we approximate $\rho_{\alpha\beta}$ by replacing $m_\gamma \to d(T)/(N-1)$:

$$\sum_{\gamma\in\mathcal{B}} \tilde{Q}_{\alpha\beta\gamma} m_\gamma \to \frac{d(T)}{N-1} \sum_{\gamma\in\mathcal{B}} \tilde{Q}_{\alpha\beta\gamma}. \tag{4.92}$$

We can now can use property (4.66) of the $\tilde{Q}$ matrices to find that the sum of the $\tilde{Q}$'s reduces to the incidence matrix of $\mathcal{L}(K_N)$. Hence, inverting equation (4.91), we obtain

$$m_\beta = \sum_\gamma Q_{\gamma\beta} \tilde{B}_\gamma, \tag{4.93}$$

where $Q_{\gamma\beta} = (2\frac{\delta}{\beta} + c_0\mathbf{J})^{-1}{}_{\gamma\beta}$ and c_0 is an effective constant in front of the Ising term of the hamiltonian:

$$c_0 \approx p g_V + g_L \frac{r^3}{3!} \frac{d(T)}{N-1}. \tag{4.94}$$

It is interesting to note that, thanks to property (4.65), we can sum all the loop terms up to a finite number $1 \ll \tilde{L} \ll N$ in the hamiltonian if we assume the mean field theory approximation. Inserting the couplings, we find

$$c_0 \approx p g_V + g_L \sum_{L=3}^{\tilde{L}} \frac{r^2}{L!} \left(r\frac{d(T)}{N} \right)^{L-2} N^{L-3} \approx p g_V + \frac{g_L r^2}{N d(T)^2} \left(e^{r\ d(T)} - 1 - r\ d(T) - \frac{r^2}{2} d(T)^2 \right).$$

(4.95)

It is interesting to note that in the limit $r \to 0$, or $T \to 0$ (where $d(T)$ tends to a finite number for $N \gg 1$), this effective constant tends to pg_V. We interpret this as the fact that at low temperature the loops become less and less important and the model is dominated by the Ising term. In particular, since the external "magnetic" field is given by v_0 and is assumed to be nonzero, it is not surprising that at $T = 0$ the average valence, the equivalent "magnetization", approaches this value. We note that the $N \to \infty$ limit does not behave well unless $L = 3$. Higher loops are highly non-local objects. For a given pair of edges, all the L-loops based on these edges span the whole graph already at $L = 4$, while of course this is not the case for 3-loops. As a result, in formula (4.95) there is a factor proportional to N^{L-3} which is not present at $L = 3$.

Case II: Degenerate edge states

The Quantum Graphity model [80] allows for degenerate *on* states on the edges or the vertices of the graph. Degeneracy of edge states is necessary, for instance, in order to have emergent matter via the string-net condensation mechanism of Levin and Wen. Degeneracy requires modifying our calculations above and we will address it in this subsection.

The first possible generalization of the Quantum Graphity model is to introduce a Hilbert space on the edges of the form:

$$\mathcal{H}^e_\beta = \text{span}\{|0\rangle_\beta, |1_1\rangle_\beta, |1_2\rangle_\beta, |1_3\rangle_\beta\}. \tag{4.96}$$

This changes the degeneracy number in equation (4.72). With $n_1 = 3$ and $n_0 = 1$, we obtain

$$\partial_{m_\beta} S[m] = -\log(\frac{m_\beta^3}{1-m_\beta}) - 2. \tag{4.97}$$

The equilibrium distribution solves this equation. If we put $Q = \exp[\beta(\partial_{m_\beta} H[m] - 2)]$, we have

$$m_\beta = \left(\frac{2}{3}\right)^{\frac{2}{3}} \frac{Q}{\left(9+\sqrt{3}\sqrt{27+4Q^3}\right)^{\frac{2}{3}}} + \frac{\left(9+\sqrt{3}\sqrt{27+4Q^3}\right)^{\frac{1}{3}}}{2^{\frac{1}{3}}3^{\frac{2}{3}}}, \tag{4.98}$$

obtained from the only real solution of the third order polynomial equation $m_\beta^3 + Qm_\beta - 1 = 0$.

Using the same procedure as before, it is easy to see that equation (4.84) remains unchanged: the low energy average valence is the same in both cases. However, the first derivative, that is, the coefficient of the T term in the Taylor expansion of the average valence in the temperature, changes, so that $\tilde{\beta}_{3,1} \geq \tilde{\beta}_{1,1}$ (with the obvious notation for the two coefficients). This phenomenon can be understood using the following argument. At high temperature, the two models behave in the same way, forcing the valence to be high. When the temperature drops, $d(T)$ also goes down. While in the (1,1) case the phase space of the *on* edges is the same as that of the *off* edges, in the (3,1) case the system prefers to stay in the *on* state. Thus, when the temperature decreases the system (3,1) is, at first, slowly converging to the ground state, but at $T = 0$ it is forced to go to the ground state.

For this reason the function $d(T)$ has a greater derivative near $T = 0$ in the (3,1) case.

4.9 The cosmological horizon problem and the speed of propagation of signals

The isotropy of the cosmic microwave background presents us with the *horizon problem*: how is it possible that regions that were never causally connected have the same temperature? We discussed this issue in section the section on the Variable Speed of Light theories. As we said, the horizon problem arises from the stipulation that interactions cannot travel faster than a finite speed, which defines a causal cone. Inflation solves the horizon problem by introducing an exponentially fast early expansion which allows for initial causal contact and thermalization of the observable universe [103]. Alternative proposed solutions require a mechanism for changing the speed of light as we trace the history of the universe backwards in time [104] or a bimetric theory [105]. Dynamically emerging light could also resolve the horizon problem. We now wish argue that the results on the maximum speed of interactions in speed systems can be used to justify this. In fact, the Lieb-Robinson bound which we described earlier shows that the maximum speed of interactions is directly proportional to the degree of the graph. As the plot in Fig. 4.3 shows, the degree as a function of the temperature is a monotonically increasing function. Thus, the physical picture which we would like to argue is the following. As the Universe cooled, the graph became more and more sparse, thus decreasing the average degree. With the degree, also the speed of interaction decreased, and the light cone

became more and more wide.

However, as we argued in the section on the variable speed of light, this phenomenon has to happen suddenly. In our picture instead, no phase transition occurs, if not at $T = 0$. Thus, this model cannot describe the Universe. Still, it remains an interesting attempt.

4.10 Problems with this model and the external bath

So far, we described a model of a time-varying graph. Since we took a thermodynamical description, time is encoded into the temperature, $T \equiv T(t)$. An adiabatic transformation cools down the Universe down to the present value, which is assumed to be constant[5]. However, what is the Temperature of the Universe? In standard thermodynamics, a gas is kept at a fixed temperature by an external bath, with a specific heat much larger than the sample we are doing experiments on. What keeps the graph (our model of Universe) at a particular temperature? Having an external bath is very troublesome if we are dealing with the Universe. This is the reason why a new model has been introduced, where the graph interacts with matter, i.e. degrees of freedom on the vertices of the graph, which allow the graph to thermalize.

[5]Here we are implicitly assuming that the temperature of the Universe is the same as the one of the CMB. This assumption is in principle not exact, as the Universe is not at thermal equilibrium.

Chapter 5

Quantum Graphs with matter

We now introduce a different model for quantum graphs, based on [111][1].

5.1 Bose-Hubbard model on Dynamical Graphs

An important issue in the research on quantum gravity is the dynamical nature of geometry in general relativity. Usually, lattice-type of methods in condensed matter theory use a fixed background, for example, a spin system on a fixed lattice. The lattice determines the locality of the interactions and hence is a discretization of geometry. This is studied in many approaches to quantum gravity. For example, CDT is based on path integral dynamics on an ensemble of all lattices (each lattice is a regularization of a Lorentzian geometry), thus providing a proper non-perturbative approach to the problem. Elsewhere, ideas from quantum information theory have been introduced in order to deal with this problem [82, 42, 80].

[1]The role of the author of the present thesis, in this section, was to solve numerically the model in the classical and the quantum case.

An alternative direction, and the one we are pursuing in the present thesis, is to make the lattice itself dynamical. The basic idea is to promote the lattice links to dynamical quantum degrees of freedom and construct a Hamiltonian such that, at low energy, the system "freezes" in a configuration with recognizable geometric symmetries, interpreted as the geometric phase of the model. In the present section we revisit the same idea but in a different model with two central properties:

- The model is a spin system on a *dynamical* lattice.
- There are lattice and matter degrees of freedom. The lattice interacts with the matter: matter tells geometry how to curve and geometry tells matter where to go.

The starting point for the implementation of the above is considerations of locality. In general relativity, locality is specified by the metric $g_{\mu\nu}$ on a manifold $\mathcal{M}$. Dynamics of matter on $(\mathcal{M}, g_{\mu\nu})$ is given by a Lagrangian which we call local if the interaction terms are between systems local according to $g_{\mu\nu}$. That is, the matter dynamics is made to match the given space-time geometry. We will do the reverse and define geometry via the dynamics of the matter. Our principle is that if particles i and j interact, they must be adjacent. This is a dynamical notion of adjacency in two ways: it is inferred from the dynamics and, being a quantum degree of freedom, it changes dynamically in time. This amounts to a spin system on a dynamical lattice and to interaction of matter with geometry.

To summarize, we present a toy model for the emergence of locality from the dynamics of a quantum many-body system. No notion of space is presupposed. Extension, separateness, distance, and all the spatial notions are emergent from the more fundamental

notion of interaction. The locality of interactions is now a consequence of this approach and not a principle. We will promote the interaction terms between two systems to quantum degrees of freedom, so that the structure of interactions itself becomes a dynamical variable. This makes possible the interaction and even entanglement between matter and geometry.

This toy model is also a condensed matter system in which the pattern of interaction itself is a quantum degree of freedom instead of being a fixed graph. It can be regarded as a Hubbard model where the strength of the hopping emerges as the mean field value for other quantum degrees of freedom. We show a numerical simulation of the quantum system and results on the asymptotic behavior of the classical system. The numerical simulation is mainly concerned with the entanglement dynamics of the system and the issue of its thermalization as a closed system. A closed system can thermalize in the sense that the partial system shows some typicality, or some relevant observables reach a steady or almost steady value for long times. The issue of thermalization for closed quantum system and the foundations of quantum statistical mechanics gained recently novel interest with the understanding that the role of entanglement plays in it [29]. The behavior of out of equilibrium quantum system under sudden quench, and the approach to equilibrium has been recently the object of study to gain insight in novel and exotic quantum phases like topologically ordered states.

From the point of view of Quantum Gravity, the interesting question is whether such a system can capture aspects of the dynamics encoded by the Einstein equations. We start investigating in this direction by studying an analogue of a trapped surface that may

describe, in more complete models, black hole physics. We discuss physical consequences of the entanglement between matter and geometry.

The model presented here is very basic and we do not expect it to yield a realistic description of gravitational phenomena. We now introduce the basic facts of the model. We first recall the Bose-Hubbard model

5.1.1 The Bose-Hubbard model

As we will see shortly, the Bose-Hubbard model is the discrete version of a scalar field in which the number of particles is conserved[2]. In order to see this, let us consider the Hamiltonian of a 1-dimensional scalar field,

$$H = \int \mathcal{D}x \left(\frac{1}{2}\pi^2(x) + \frac{1}{2}\left(\frac{\mathcal{D}\phi}{\mathcal{D}x}(x)\right)^2 + \frac{1}{2}M^2\phi^2(x) \right), \tag{5.1}$$

where M is the mass of the field $\phi(x)$, and $\pi(x)$ is the canonical momentum density. This model is used widely for the classification of the various phases of superfluids (Mott insulator/superfluid). In order to discretize eqn. (5.1), let us first define the following operators

$$\phi(x) \longrightarrow x_n = \phi(na)$$

$$\pi(x) \longrightarrow p_n = \pi(na) \tag{5.2}$$

$$\frac{\mathcal{D}\phi}{\mathcal{D}x} \longrightarrow \frac{x_n - x_{n-1}}{a} \tag{5.3}$$

[2]We thank Arnau Riera for the present derivation.

With this transformation, the Hamiltonian reads

$$H = \frac{1}{2}\sum_{n=0}^{N-1}\left(p_n^2 + \frac{1}{a^2}(x_n - x_{n-1})^2 + M^2 x_n^2\right) = \frac{1}{2}\sum_{n=0}^{N-1}\left(p_n^2 + \frac{2}{a^2}(x_n^2 - x_n x_{n-1}) + M^2 x_n^2\right) \tag{5.4}$$

where the operators x_n and p_n fulfill the canonical commutation relations $[x_n, p_m] = \mathrm{i}\,\delta_{nm}$. We will consider that the system has periodic boundary conditions, such that we can identify $x_0(p_0)$ as $x_N(p_N)$. In analogy with the quantization of the continuous version of the scalar field, let us introduce the transformation

$$\begin{aligned} x_n &= \frac{1}{\sqrt{N}}\sum_{k=0}^{N}\frac{1}{\sqrt{2\omega_k}}\left(\mathrm{e}^{\mathrm{i}\,\frac{2\pi}{N}kn}\,\hat{a}_k + \mathrm{e}^{-\mathrm{i}\,\frac{2\pi}{N}kn}\,\hat{a}_k^\dagger\right) \\ p_n &= \frac{1}{\sqrt{N}}\sum_{k=0}^{N}(-\mathrm{i})\sqrt{\frac{\omega_k}{2}}\left(\mathrm{e}^{\mathrm{i}\,\frac{2\pi}{N}kn}\,\hat{a}_k - \mathrm{e}^{-\mathrm{i}\,\frac{2\pi}{N}kn}\,\hat{a}_k^\dagger\right)\,. \end{aligned} \tag{5.5}$$

This transformation implies that the commutation relations for $\hat{a}_k$ an $\hat{a}_q^\dagger$ are

$$[\hat{a}_k, \hat{a}_q^\dagger] = \delta_{kq}\hat{1}\,. \tag{5.6}$$

By changing the limits of the sum in Eq. (5.5) and reshuffling its terms, x_n and p_n become

$$\begin{aligned} x_n &= \frac{1}{\sqrt{N}}\sum_{k=-\lfloor N/2\rfloor}^{\lfloor N/2\rfloor}\frac{1}{\sqrt{2\omega_k}}\,\mathrm{e}^{\mathrm{i}\,\frac{2\pi}{N}kn}\left(\hat{a}_k + \hat{a}_{-k}^\dagger\right) \\ p_n &= \frac{1}{\sqrt{N}}\sum_{k=-\lfloor N/2\rfloor}^{\lfloor N/2\rfloor}(-\mathrm{i})\sqrt{\frac{\omega_k}{2}}\,\mathrm{e}^{\mathrm{i}\,\frac{2\pi}{N}kn}\left(\hat{a}_k - \hat{a}_{-k}^\dagger\right)\,, \end{aligned} \tag{5.7}$$

where we have assumed that $\omega_k = \omega_{-k}$ and N is an odd number. The terms of the Hamiltonian can be written in terms of $\hat{a}_k$ and $\hat{a}_k^\dagger$ as

$$\begin{aligned}
\sum_n p_n^2 &= -\sum_{k=-\lfloor N/2 \rfloor}^{\lfloor N/2 \rfloor} \frac{\omega_k}{2} \left(\hat{a}_k - \hat{a}_{-k}^\dagger\right)\left(\hat{a}_{-k} - \hat{a}_k^\dagger\right) \\
\sum_n x_n^2 &= \sum_{k=-\lfloor N/2 \rfloor}^{\lfloor N/2 \rfloor} \frac{1}{2\omega_k} \left(\hat{a}_k + \hat{a}_{-k}^\dagger\right)\left(\hat{a}_{-k} + \hat{a}_k^\dagger\right) \\
\sum_n x_n x_{n-1} &= \sum_{k=-\lfloor N/2 \rfloor}^{\lfloor N/2 \rfloor} \frac{1}{2\omega_k} \mathrm{e}^{\mathrm{i}\frac{2\pi}{N}k} \left(\hat{a}_k + \hat{a}_{-k}^\dagger\right)\left(\hat{a}_{-k} + \hat{a}_k^\dagger\right) \\
&= \sum_{k=-\lfloor N/2 \rfloor}^{\lfloor N/2 \rfloor} \frac{1}{2\omega_k} \cos\left(\frac{2\pi}{N}k\right) \left(\hat{a}_k + \hat{a}_{-k}^\dagger\right)\left(\hat{a}_{-k} + \hat{a}_k^\dagger\right) ,
\end{aligned} \tag{5.8}$$

where in the last equation we have used the fact that $[a_{-k} + a_k^\dagger, a_k + a_{-k}^\dagger] = 0$. If we put together Eqs. (5.1.1) and (5.8), the Hamiltonian reads

$$H = \sum_{k=0}^{N-1} \left(-\frac{\omega_k}{4} \left(\hat{a}_k - \hat{a}_{-k}^\dagger\right)\left(\hat{a}_{-k} - \hat{a}_k^\dagger\right) + \frac{2\left(1 - \cos\left(\frac{2\pi}{N}k\right)\right)/a^2 + M^2}{4\omega_k} \left(\hat{a}_k + \hat{a}_{-k}^\dagger\right)\left(\hat{a}_{-k} + \hat{a}_k^\dagger\right) \right) .$$

Thus,

$$H = \sum_{k=0}^{N-1} \omega_k \left(\hat{a}_k^\dagger \hat{a}_k + \frac{1}{2}\right) \tag{5.9}$$

with

$$\omega_k^2 = \frac{2}{a^2}\left(1 - \cos\left(\frac{2\pi}{N}k\right)\right) + M^2 . \tag{5.10}$$

From this approach, the particles are simply collective excitations of a field.

Let us now rewrite the Hamiltonian as

$$\frac{1}{\mu}H = \sum_n \frac{p_n^2}{2M} + \frac{1}{2}M^2 x_n^2 + \sum_n \frac{1}{a^2 M}\left(x_n^2 - x_n x_{n-1}\right) \tag{5.11}$$

where the first sum is a set of uncoupled Harmonic oscillators with frequency one and the second term is the nearest neighbor interaction among them.

If we introduce the standard creation and annihilation operators,

$$\begin{aligned}\hat{b}_n &= \sqrt{\frac{M}{2}}\left(x_n + \frac{\mathrm{i}}{M}p_n\right) \\ \hat{b}_n^\dagger &= \sqrt{\frac{M}{2}}\left(x_n - \frac{\mathrm{i}}{M}p_n\right) ,\end{aligned} \tag{5.12}$$

the Hamiltonian becomes a Bose-Hubbard model with a non-conserved number of particles

$$H = \frac{1}{2Ma^2}\sum_n \left(\hat{b}_n^\dagger b_{n-1} + b_{n-1}^\dagger b_n\right) + \left(M + \frac{1}{Ma^2}\right)\sum_n b_n^\dagger b_n + \frac{1}{2Ma^2}\sum_n \left(b_{n-1}b_n + b_n b_n + \text{h.c.}\right) \tag{5.13}$$

where we have used that

$$\begin{aligned}x_n^2 &= \frac{1}{M}\hat{b}_n^\dagger \hat{b}_n + \frac{1}{2M}\left(\hat{b}_n^\dagger \hat{b}_n^\dagger + \hat{b}_n \hat{b}_n + 1\right) , \\ x_n x_{n-1} &= \frac{1}{2M}\left(\hat{b}_{n-1}^\dagger \hat{b}_n + \hat{b}_n^\dagger \hat{b}_{n-1} + \hat{b}_{n-1}^\dagger \hat{b}_n^\dagger + \hat{b}_{n-1}\hat{b}_n\right) .\end{aligned}$$

In th efollowing, we will rename the parameters:

$$E_{hop} = \frac{1}{2Ma^2} \tag{5.14}$$

$$\mu = M + \frac{1}{Ma^2} \tag{5.15}$$

where we can see the relation between the various constants of the model and lattice spacing and mass of the scalar field.

Later on, we will consider eqn. (5.13) for the case in which the term which increase and decrease the number of particle are absent. This will allow to diagonalize the Hamiltonian in blocks of constant number operator and study the effective geometry. Here we derived the equation for the Fermionic case, but for the bosonic case an analogous derivation is possible. Bosons, for instance, can have an additional potential of the form:

$$H_p = -U \sum_i \hat{N}_j(\hat{N}_j - 1) \tag{5.16}$$

with $\hat{N}_j = \hat{b}_j^\dagger \hat{b}_j$. This hamiltonian gives a penalty to piling up bosons. Hard-core bosons have bosonic commutation relations but are defined by the property $\{b^\dagger\}^2 \equiv 0$. This property can be achieved in the $U \to \infty$ limit of eqn. (5.16).

The Hubbard model is not only an interesting model, but has physical applications which we briefly describe here[75]. The Bose-Hubbard, the Fermi-Hubbard and the Bose-Fermi-mixtures describe many features of optical lattices. The simplest optical lattice is a 3D cubic lattice. It is formed by three pairs of laser beams creating three orthogonal standing waves with orthogonal polarizations. The potential traps atoms in its minima,

creating the "virtual" lattice with no defects. These lattices are very robust as they have no phononic modes. Scattering length, instead, drive the on-site interactions. Long and short lengths interactions are achieved in different phases of the model.

Regarding the different phases, the Bose-Hubbard model has a rather non trivial phase structure. In particular, the model exhibits a Superfluid-Mott insulator quantum phase transitions[3]. This transition happens when the lattice filling factor, the number of atoms per site, is integer and is driven by the ratio E_{hop}/U. We will discuss these phases extensively later in the thesis.

5.1.2 Promoting the edges of the lattice to a quantum degree of freedom

In this Section we describe how the graph can be made dynamical by introducing an appropriate Hilbert space associated to the edges of a graph. We start with the primitive notion of a set of N distinguishable physical systems. We assume a quantum mechanical description of such physical systems, given by the set $\{\mathcal{H}_i, H_i\}$ of the Hilbert spaces $\mathcal{H}_i$ and Hamiltonians H_i of the systems $i = 1, ..., N$. This presumes it makes sense to talk of the time evolution of some observable with support in $\mathcal{H}_i$ without making any reference to space.

We choose $\mathcal{H}_i$ to be the Hilbert space of a harmonic oscillator. We denote its creation and destruction operators by $b_i^\dagger, b_i$, respectively, satisfying the usual bosonic relations. Our N physical systems then are N bosonic particles and the total Hilbert space for the

[3]The transition is quantum, as it happens ideally at zero temperature, and thus is driven only by the ratios of coupling constants.

bosons is given by

$$\mathcal{H}_{bosons} = \bigotimes_{i=1}^{N} \mathcal{H}_i. \tag{5.17}$$

If the harmonic oscillators are not interacting, the total Hamiltonian is trivial:

$$H_v = \sum_{i=1}^{N} H_i = -\sum_i \mu_i b_i^\dagger b_i. \tag{5.18}$$

If, instead, the harmonic oscillators are interacting, we need to specify which is interacting with which. Let us call $\mathcal{I}$ the set of the pairs of oscillators $\mathbf{e} \equiv (i, j)$ that are interacting. Then the Hamiltonian would read as

$$H = \sum_i H_i + \sum_{\mathbf{e}\in\mathcal{I}} h_{\mathbf{e}} \tag{5.19}$$

where $h_{\mathbf{e}}$ is a Hermitian operator on $\mathcal{H}_i \otimes \mathcal{H}_j$ representing the interaction between the system i and the system j.

We wish to describe space as the system of relations among the physical systems labeled by i. In a discrete setup like ours, a commonly used primitive notion of the spatial configuration of N systems can be provided by an adjacency matrix A, the $N \times N$ symmetric matrix defined as follows:

$$A_{ij} = \begin{cases} 1 & \text{if } i \text{ and } j \text{ are adjacent} \\ 0 & \text{otherwise.} \end{cases} \tag{5.20}$$

The matrix A is associated to a graph on N vertices whose edges are specified by its the nonzero entries. Now, it is clear that the set $\mathcal{I}$ of interacting nodes in the Hamiltonian (5.19) also defines a graph G whose vertices are the N harmonic oscillators and whose edges are the pairs $\mathbf{e} \equiv (i,j)$ of interacting oscillators. Here $\mathcal{I}$ is the edge set of G. We want to promote the interactions - and thus the graph itself - to a quantum degree of freedom.

To this goal, let us define $\mathcal{G}$ as the set of graphs G with N vertices. They are all subgraphs of $\mathcal{K}_N$, the complete graph on N vertices, whose $\frac{N(N-1)}{2}$ edges correspond to the (unordered) pairs $\mathbf{e} \equiv (i,j)$ of harmonic oscillators. To every such pair $\mathbf{e}$ (an edge of $\mathcal{K}_N$) we associate a Hilbert space $\mathcal{H}_{\mathbf{e}} \simeq C^2$ of a spin $1/2$. The total Hilbert space for the graph edges is thus

$$\mathcal{H}_{graph} = \bigotimes_{\mathbf{e}=\mathbf{1}}^{N(N-1)/2} \mathcal{H}_{\mathbf{e}}. \tag{5.21}$$

We choose the basis in $\mathcal{H}_{graph}$ so that to every graph $g \in \mathcal{G}$ corresponds a basis element in $\mathcal{H}_{graph}$: the basis element $\mid e_1 \dots e_{N(N-1)/2}\rangle \equiv \mid G\rangle$ corresponds to the graph G that has all the edges $\mathbf{e}_s$ such that $e_s = 1$. For every edge (i,j), the corresponding $SU(2)$ generators will be denoted as $S^i = 1/2\sigma^i$ where σ^i are the Pauli matrices.

The total Hilbert space of the theory is

$$\mathcal{H} = \mathcal{H}_{bosons} \otimes \mathcal{H}_{graph}, \tag{5.22}$$

and therefore a basis state in $\mathcal{H}$ has the form

$$\mid \Psi\rangle \equiv\mid \Psi^{(bosons)}\rangle\otimes \mid \Psi^{(graph)}\rangle \equiv\mid n_1,...,n_N\rangle\otimes \mid e_1,...,e_{\frac{N(N-1)}{2}}\rangle \tag{5.23}$$

The first factor tells us how many bosons there are at every site i (in the Fock space representation) and the second factor tells us which pairs e interact. That is, the structure of interactions is now promoted to a quantum degree of freedom. A generic state in our theory will have the form

$$\mid \Phi\rangle = \sum_{a,b} \alpha_{a,b} \mid \Psi_a^{(bosons)}\rangle\otimes \mid \Psi_b^{(graph)}\rangle, \tag{5.24}$$

with $\sum_{a,b} |\alpha_{a,b}|^2 = 1$. In general, our quantum state describes a system in a generic superposition of energies of the harmonic oscillators, and of interaction terms among them. A state can thus be a quantum superposition of "interactions". For example, consider the systems i and j in the state

$$\mid \phi_{ij}\rangle = \frac{\mid 10\rangle\otimes \mid 1\rangle_{ij} + \mid 01\rangle\otimes \mid 0\rangle_{ij}}{\sqrt{2}}. \tag{5.25}$$

This state describes the system in which there is a particle in i and no particle in j, but also there is a quantum superposition between i and j interacting or not. The following state,

$$\mid \phi_{ij}\rangle = \frac{\mid 00\rangle\otimes \mid 1\rangle_{ij} + \mid 11\rangle\otimes \mid 0\rangle_{ij}}{\sqrt{2}}. \tag{5.26}$$

represents a different superposition, in which the particle degrees of freedom and the graph degrees of freedom are entangled. It is a significant feature of our model that matter can be entangled with geometry.

An interesting interaction term is the one that describes the physical process in which a quantum in the oscillator i is destroyed and one in the oscillator j is created. The possibility of this dynamical process means there is an edge between i and j. Such dynamics is described by a Hamiltonian of the form

$$H_{hop} = -E_{hop} \sum_{(i,j)} P_{ij} \otimes (b_i^\dagger b_j + b_i b_j^\dagger) \tag{5.27}$$

where

$$P_{ij} \equiv S^+_{(i,j)} S^-_{(i,j)} = \mid 1\rangle\langle 1 \mid_{(i,j)} = \left(\frac{1}{2} - S^z\right)_{(i,j)} \tag{5.28}$$

is the projector on the state such that the edge (i,j) is present and the spin operators are defined as $S^+_{(i,j)} = \mid 1\rangle\langle 0 \mid_{(i,j)}$ and $S^-_{(i,j)} = \mid 0\rangle\langle 1 \mid_{(i,j)}$. With this Hamiltonian, the state Eq.(5.25) can be interpreted as the quantum superposition of a particle that may hop or not from one site to another. It is possible to design such systems in the laboratory. For instance, one can use arrays of Josephson junctions whose interaction is mediated by a quantum dot with two levels.

We note that it is the dynamics of the particles described by H_{hop} that gives to the degree of freedom $\mid e\rangle$ the meaning of geometry[4]. The geometry at a given instance is

[4] We use *geometry* and *space* as shorthand for the adjacency relations encoded in $|\Psi^{graph}\rangle$, even though the generic $|\Psi^{graph}\rangle$ will be a graph (or a superposition of graphs) without any symmetries and hence

given by the set of relations describing the dynamical potentiality for a hopping. Two points j, k can be "empty", that is, the oscillators j, k are in the ground state, but they can have a spatial relationship consisting in the fact that they can interact. For example, they can serve to have a particle to hop from i to j, then to k, then to l. We read out the structure of the graph from the interactions, not from the mutual positions of particles.

In addition, H_{hop} tells us that it takes a finite amount of time to go from i to j. If the graph is represented by a chain, it tells us that it takes a finite amount of time (modulo exponential decaying terms) for a particle to go from one end of the chain to another. This results to a "spacetime" picture (the evolution of the adjacency graph in time) with a finite lightcone structure. The hopping amplitude is given by t, and therefore all the bosons have the same speed. We can make the model more sophisticated by enlarging the Hilbert space of the links, and obtain different speeds for the bosons. Instead of considering spins $1/2$, consider an $S-$level system. The local Hilbert space is therefore

$$\mathcal{H}_e = \text{span}\{|\ 0\rangle, |\ 1\rangle, \ldots, |\ S-1\rangle\} \tag{5.29}$$

Now consider the projector onto the $s-$th state on the link (i,j): $P_{ij}^{(s)} = |\ s\rangle\langle s\ |_{ij}$. We can define a new hopping term whose amplitude depends on the level of the local system in the following way:

$$H_{hop} = -\sum_{s,(i,j)} E_{hop}^{s} P_{ij}^{(s)} \otimes (b_i^\dagger b_j + b_i b_j^\dagger) \tag{5.30}$$

not a candidate for a discretization of a smooth geometry. In this simple model, we make no attempt to dynamically flow to a $|\Psi^{graph}\rangle$ with recognizable geometric symmetries, as was done, for example, in [14, 15, 80]. One can address this in a future model by extending the Hamiltonian of the model.

where the hopping amplitudes E^s_{hop} depend on the state s of the system, and $E^0_{hop} = 0$. For instance, the E^s_{hop} can be chosen larger for larger s. In this way, moves through higher level links are more probable, and therefore the speed of the particles is not constant. In the following, we will study the model with just the two level system.

Of course, we need a Hamiltonian also for the spatial degrees of freedom alone. The simplest choice is simply to assign some energy to every edge:

$$H_{link} = -U \sum_{(i,j)} \sigma^z_{(i,j)} \tag{5.31}$$

Finally, we want space and matter to interact in a way that they can be converted one into another. The term

$$H_{ex} = k \sum_{(i,j)} \left(S^-_{(i,j)} \otimes (b^\dagger_i b^\dagger_j)^R + S^+_{(i,j)} \otimes (b_i b_j)^R \right) \tag{5.32}$$

can destroy an edge (i, j) and create R quanta at i and R quanta at j, or, vice-versa, destroy R quanta at i and R quanta at j to convert them into an edge.

The terms H_{link} and H_{ex} are so simple that we will not expect them to give us any really interesting property of how regular geometry can emerge in such a system. This is the subject for a more refined and future work. Nevertheless, this term has an important meaning because the nature of the spatial degrees of freedom is completely reduced to that of the quanta of the oscillators: an edge is the bound state of $2R$ quanta. When in the edge form, the quanta cannot hop around. When unbounded, they can hop around under the condition that there are edges from one vertex to another. One can replace the

separation of the fundamental degrees of freedom into bosons and graph edges with a unified set of underlying particle ones, single bosons and collections of $2R$ bound bosons. Therefore a bound state of $2R$ quanta in the pair $(\mathcal{H}_i, \mathcal{H}_j)$ tells us what physical systems are at graph distance one. The set of such bound states as we vary j is the neighborhood of the system i. This is the set of vertices j a free particle in i can hop to. The projector P_{ij} has thus the meaning that the hopping interaction must be *local* in the sense just defined.

Now we see that the term H_{ex} is not satisfactory because exchange interactions are possible between any pair of vertices, no matter their distance. So quanta that are far apart can be converted in an edge between two points that were very far just before the conversion. Moreover, also the conjugate process is problematic, because it can easily lead to a graph made of disconnected parts. We implement locality by allowing exchange processes only between points that are connected by some *other* short path of length L. Note that this refers to the locality of the state $|\Psi^{graph}\rangle$ at time t relative to the locality of the state at time $t-1$. Consider again the projector P_{ij} on the edge (i,j) being present. Its $L-$th power is given by

$$P_{ij}^L = \sum_{k_1,\ldots,k_{l-1}} P_{ik_1} P_{k_2k_3} \ldots P_{k_{L-1}j}. \tag{5.33}$$

For every state $|\ \Psi\rangle \in \mathcal{H}_{graph}$, we have that $P_{ij}\ |\ \Psi\rangle \neq \mathbf{0}$ if and only if there is at least another path of length L between i and j. We can now modify the term H_{ex} as follows:

$$H_{ex} = k \sum_{(i,j)} \left(S^-_{(i,j)} P^L_{ij} \otimes (b_i^\dagger b_j^\dagger)^R + P^L_{ij} S^+_{(i,j)} \otimes (b_i b_j)^R \right). \tag{5.34}$$

In the extended $S-$level system, the exchange term is modified as $|\ (s+1)(\mathrm{mod}S)\rangle\langle s(\mathrm{mod}S)\ |_{(i,j)}$ $\otimes(b_i b_j)^R$ and similarly for the hermitian conjugate.

This was the final step that brings us to the total Hamiltonian for the model which is

$$H = H_{link} + H_v + H_{ex} + H_{hop}. \tag{5.35}$$

In the following, we consider the theory for $L = 2$, which is the strictest notion of locality for the exchange interaction one can implement.

5.1.3 Discussion of the model

We can summarize the model in the following way. All we have is matter, namely the value of a function f_i, where the indexes i label different physical systems. We have chosen f_i to be the number of quanta of the i-th harmonic oscillator. The bound state of a particle in i and a particle in j has the physical effect that other particles in i and j can interact. When there is such a bound state, we say there is an edge between i and j. Then other particles at i and j can interact, for instance, they can hop from i to j. The collection of these edges, or bound states, defines a graph which we interpret as the coding of the spatial adjacency of the particles (in a discrete and relational fashion). The physical state of the many body system is the quantum superposition of configurations of the particles and of the edges. The system evolves unitarily, and particles can hop around along the edges. But the distribution of the particles also influences the edges because some particles at vertices i, j can be destroyed (if i and j are nearby in the graph) to form

another edge, and therefore making i and j nearer. The new edge configurations then influence the motion of the particles and so on. We have a theory of matter interacting with space. The intention of the model is to study to what extend such dynamics captures aspects of the Einstein equation and whether it (or a later extension of such a spin system) can be considered as a precursor of the gravitational force. From the condensed matter point of view, this is a Hubbard model for hopping bosons, where the underlying graph of the Hubbard model is itself a quantum dynamical variable that depends on the motion of the bosons. In the spirit of General Relativity, the edges (space) tell the bosons (matter) where to go, and the bosons, by creating edges, tell the space how to curve.

We note that, in this theory, all that interacts has a local interaction by definition. We defined locality using the notion of neighborhood given by the set of systems interacting with a given system [5]. We also note that, due to quantum superpositions, matter and space can be entangled. For this reason, the dynamics of the matter alone is the ruled by a quantum open system, the evolution for the matter degrees of freedom is described no more by a unitary evolution operator but by a completely positive map. We can show that the entanglement increases with the curvature. To fix the ideas, let us start with a flat geometry represented by the square lattice as the natural discretization of a two dimensional real flat manifold. In this model, a flat geometry with low density of matter can be described by a square (or cubic) lattice with a low density of bosons. This means

[5] There is, however, a way to define non-local interactions. For instance, consider the configuration of the graph of the square lattice. Pick two vertices i, j at large distance l_{ij} on this lattice (in the graph distance sense), and place a new edge connecting them. Now by definition the two vertices i and j are adjacent. Nevertheless, the ratio between the number of paths of distance one from i to j with the number of paths of distance l_{ij} goes to zero in the limit of large l_{ij}. This is what one can call a *non-local* interaction. It corresponds to the situation in lattice field theory where one has a fixed graph, and then some interactions between points that are far apart.

that a particle is most of the time alone in a region that is a square lattice. The model will not then allow interaction between the particle and the edges, and all that happens is a free walk on the graph. On the other hand, when we increase the degree of the vertices by adding more edges, we make interaction, and hence entanglement, between edges and particles possible. This corresponds to increasing the curvature. In a regime of very weak coupling, $k \ll E_{hop} \ll U, \mu$, entanglement will be possible only in presence of extremely strong curvature. From the point of view of the dynamics of the quantum system, this means that the evolution for the matter is very close to be unitary when curvature is low, while very strong curvature makes the evolution for the particles non-unitary and there will be decoherence and dissipation with respect to the spatial degrees of freedom.

How does the graph evolve in time in such a model? The quantum evolution is complex, and since the model is not exactly solvable, numerical study is constrained to very small systems. In the next section we simulate the system with 4 vertices and hard core bosons.

We can gain some insight from the analysis of the classical model, regarding H as the classical energy for classical variables. Since we delete edges randomly and build new edges as the result of a random walk of the particles, and there is nothing in this model that favors some geometry instead of others, we do not expect to obtain more than random graphs in the limit of extremely long times. Indeed, we can argue as follows. With the exception of a very small number or graphs, all the other graphs belong to the set of graphs in which one can - under the evolution of our model - reach a ring. In practice, this means that there is a configuration in which one deletes all the edges without disconnect-

ing the graph, and obtains many particles. This means that, starting from a state with zero particles, N vertices and L_0 edges the number of eligible edges for deletion is $L_0 - \alpha N$ with some constant α of order 1. So, as long as $L_0 > \alpha N$, the dynamical equilibrium between the number of edges and particles is realized when the rate of conversion of edges into particles equals the one of conversion of particles into edges. Let r be the number of edges destroyed (and pairs of particles created). If we assume that the particles move much faster than the edges, they will always be eligible for creating a new edge. The rates will be then the same when $L_0 - r = r$ which implies that at the dynamical equilibrium half of the initial edges are destroyed. Consider the case of the complete graph $\mathcal{K}_N$, with zero initial particles. The initial number of edges is $L_0 = N(N-1)/2$, and at long times, the dynamical equilibrium is reached when $r = L_0/2$. A similar reasoning can be applied to r instance, consider a square lattice of N vertices with periodic boundary conditions. In the state without particles, this is an eigenstate of the Hamiltonian, and therefore its evolution is completely frozen. Nevertheless, if we add a pair of particles, then all the other configurations of the graph can be reached, including the ring immersed in a gas of many particles. It turns out that the dynamical equilibrium is reached when $L_0/2 = N$ of the initial edges are destroyed. The equilibrium state is obtained by deleting the edges randomly, and thus we expect to obtain a random graph. In order to obtain more interesting stable geometries, one has to put other terms in the Hamiltonian, that involve more edges together, meaning that curvature has a dynamical importance. The rigorous treatment of the asymptotic evolution of such graphs requires an analysis in terms of Markov chains, and it is developed in the next section.

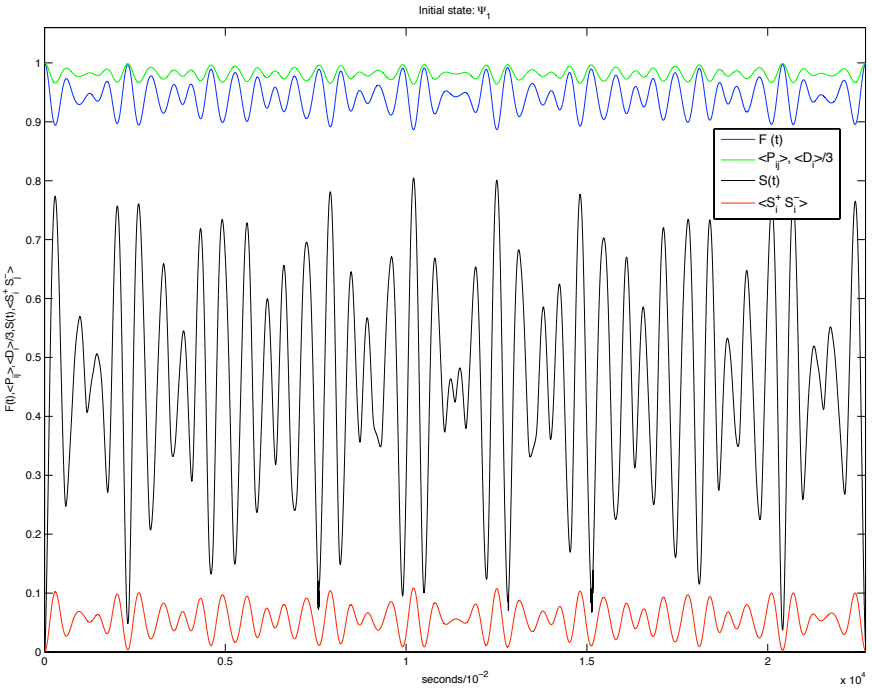

Figure 5.1: Simulation of the system $H_{1/2}$ for $N = 4$. The initial state is $\rho_1 =\mid \psi_1\rangle\langle\psi_1 \mid$ where $\mid \psi_1\rangle =\mid 0000111111\rangle$, that is, there are no particles and all edges are present. The parameters for this simulation are $U = \mu = 1, E_{hop} = k = .1$. In the figure are plotted the quantities $\langle S_i^+ S_i^-\rangle$ (red line), $\mathcal{F}(t)$ (blue line), $S(t)$ (black line), $P_{ij}(t), D_i(t)/3$ (green line) as a function of time. Revivals of the expectation value of the link operator coincide with revivals in the fidelity with the initial state. The initial value of the entanglement is $S(0) = 0$ because the initial state is separable. Notice that even though the fidelity is $\mathcal{F}(t) \gtrsim 0.85$, the state has a non negligible entanglement.

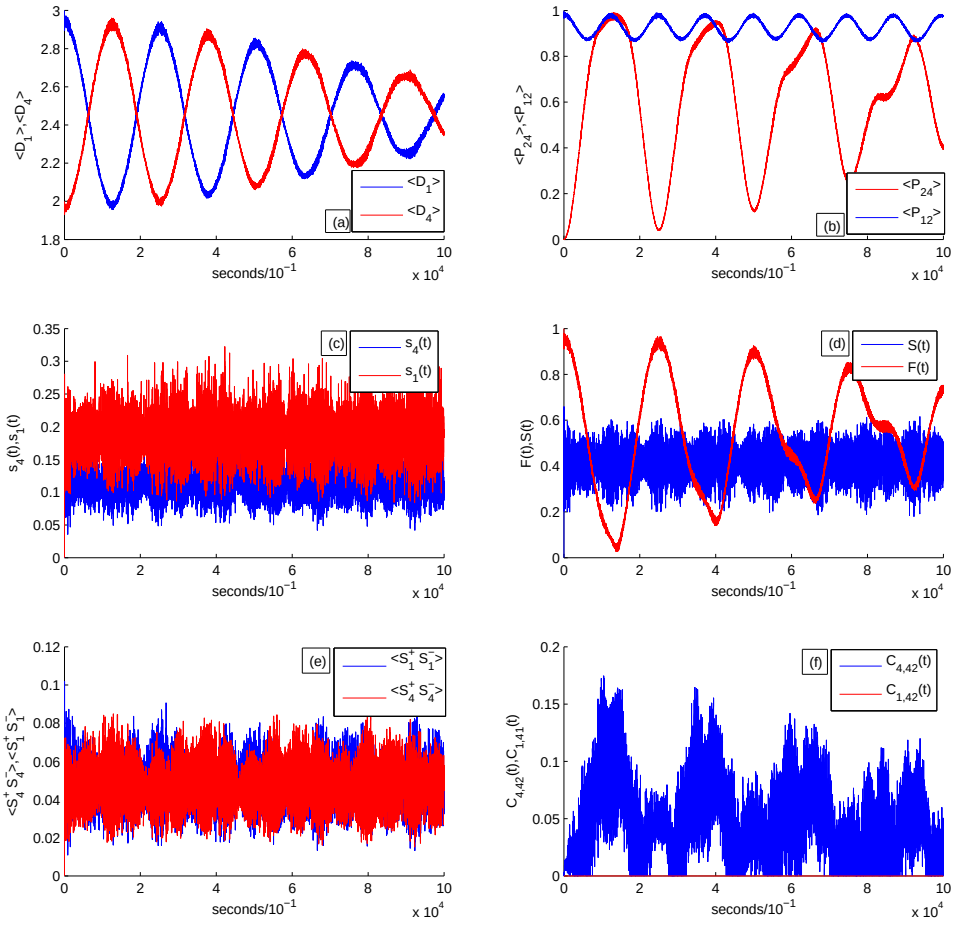

Figure 5.2: The initial state of this numerical integration is $\mid \psi_2\rangle = \mid 0000111101\rangle$, the parameters are in the "insulator" phase, $U = \mu = 1$, $E_{hop} = k = 0.1$. The temporal scale is in units of $\hbar$, on a range of 10^4 seconds. The diagonalization of the full system has been performed by means of Householder reduction. **a)** Time evolution of $\langle D_1(t)\rangle, \langle D_4(t)\rangle$. The damping of the oscillations is a sign of thermalization. **b)** Expectation values $\langle P_{12}(t)\rangle, \langle P_{24}(t)\rangle$. The latter observable is thermalizing. **c)** Von Neumann Entropy $s_i(t)$ for the sites $i = 1, 2$. We see that the entanglement dynamics is split in two different bands. The two vertices are only distinguished by the initial degree. **d)** Entanglement evolution $S(t)$ and overlap with the initial state $\mathcal{F}(t)$. The damping of $\mathcal{F}(t)$ is a clear sign of thermalization. The entanglement $S(t)$ between particles and edges shows the entangling power of the system. **e)** Expectation value of the particle operators at two different sites $i = 1, 4$. **f)** Concurrence $C(t)$ as a function of time of the particles on the site $i = 2$ with the edge $(2, 4)(blue)$. Again we notice a damping of oscillations. Instead, the concurrence between the site 1 and the link 5 (red) is identically zero.

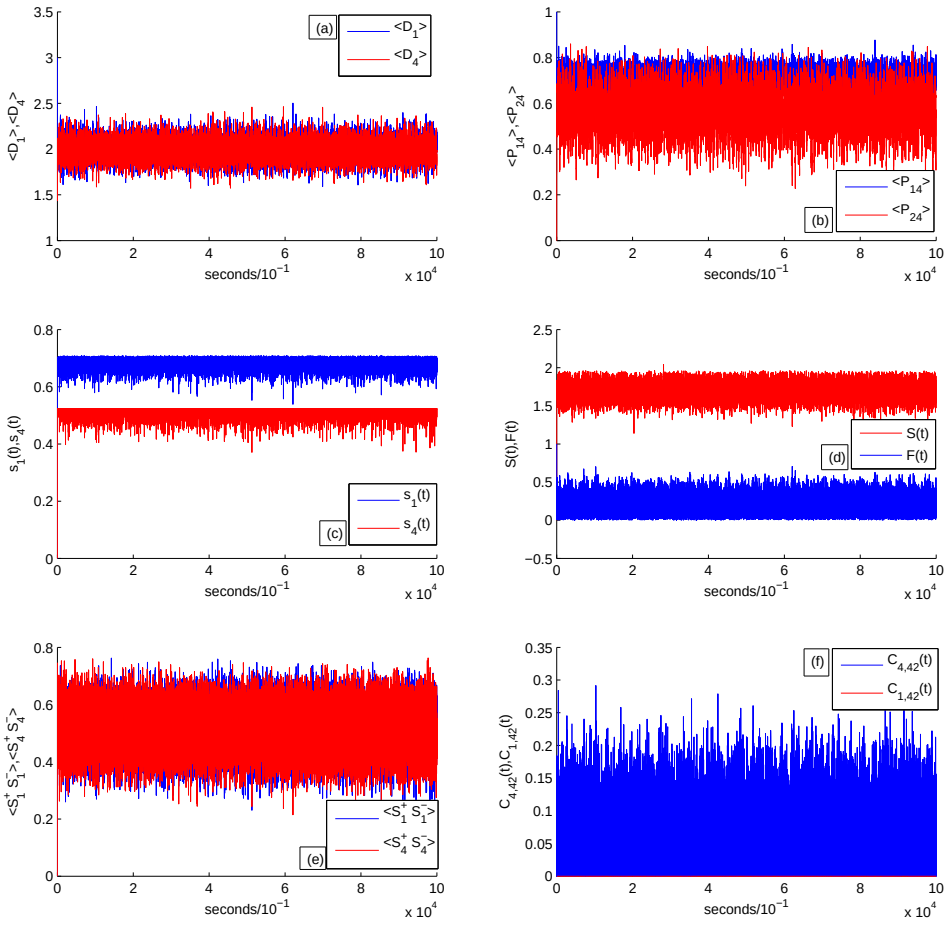

Figure 5.3: The initial state of this numerical integration is $\mid \psi_2\rangle = \mid 0000111101\rangle$, the parameters are in the "superfluid" phase, $U = \mu = 0.1$, $E_{hop} = k = 1$. The temporal scale is in units of $\hbar$, on a range of 10^4 seconds. The diagonalization of the full system has been performed by means of Householder reduction. **a)** Time evolution of $\langle D_1(t)\rangle, \langle D_4(t)\rangle$.. The oscillations have constant amplitude and the system does not present signs of thermalization. **b)** Expectation values of the link operators P_{14}, P_{24}. There is no sign of thermalization. The two values belong to two different bands depending on the initial value of the operator. **c)** Von Neumann Entropy $s_i(t)$ for the sites $i = 1, 2$. We see that the entanglement dynamics is split in two different bands. The two vertices are only distinguished by the initial degree and the splitting is more marked than in the "insulator" case. Compare the result with the higher overlap of the operators $D_{ij}(t)$. **d)** Entanglement evolution $S(t)$ and overlap with the initial state $\mathcal{F}(t)$. Again the plots show no signs of thermalization. The behavior of $\mathcal{F}(t)$ implies very long recurrence times. **e)** Expectation value of the particle operators at two different sites $i = 1, 4$. **f)** Time evolution of Concurrence $C(t)$. In blue is plotted the Concurrence between the vertex $i = 2$ and the edge $(2, 4)$ for the "superfluid" case. Unlike the insulator case, the behavior of $C(t)$ does not show any sign of thermalization. The concurrence between the site 1 and the link 5 is identically zero, as in the "insulator" case.

5.1.4 Setting of the model

In this section, we study the model Eq. (5.35) when the particles are hard core bosons. In this model, only at most one particle is allowed per site and the model can be mapped onto a spin system. We are particularly interested in the entanglement dynamics of the system. We have performed a numerical simulation of the time evolution of the model described by Eq. (5.35). Since we are interested also in describing the quantum correlations in the reduced density matrix, we have resorted to exact diagonalization. In this way, we are able to compute the entanglement of the matter degrees of freedom with respect to the spatial ones. Of course, the simulation of a full quantum system is heavily constrained by the exponential growth of the Hilbert space. In this work, we have resorted to the simulation of hard-core bosons: at most one particle is allowed at any site. Hardcore bosons creation and annihilation operators must thus satisfy the constraints

$$(\hat{b}_i^\dagger)^2 = (\hat{b}_i)^2 = 0,\ \{\hat{b}_i, \hat{b}_i^\dagger\} = 1 \tag{5.36}$$

With these constraints, the bosonic operators map into the $SU(2)$ generators

$$\hat{b}_i^\dagger \leftrightarrow S_i^+ \tag{5.37}$$

$$\hat{b}_i \leftrightarrow S_i^- \tag{5.38}$$

$$\hat{b}_i^\dagger \hat{b}_i \leftrightarrow \left(\frac{1}{2} - S^z\right)_i \tag{5.39}$$

The local Hilbert space of a site i for a hard core boson is therefore that of a spin one half: $\mathcal{H}_i^{hcb} \simeq \mathbb{C}^2$. After the projection onto the hard-core bosons subspace, the model becomes a purely spin $1/2$ model. For a system with n sites, the Hilbert space for the particles is thus the 2^N-dimensional Hilbert space $\mathcal{H}_{bosons} = \otimes_{i=1}^{N} \mathcal{H}_i^{hcb} \simeq \mathbb{C}^{2 \otimes N}$. The Hilbert space for the spatial degrees of freedom is still the $2^{N(N-1)/2}$-dimensional Hilbert space $\mathcal{H}_{graph} = \bigotimes_{\mathbf{e}=\mathbf{1}}^{N(N-1)/2} \mathcal{H}_{\mathbf{e}}$. The total Hilbert space is thus the $2^{N(N+1)/2}$-dimensional Hilbert space

$$\mathcal{H}_{spins} = \mathcal{H}_{bosons} \otimes \mathcal{H}_{graph} \simeq \bigotimes_{i=1}^{N} \mathcal{H}_i^{hcb} \bigotimes_{\mathbf{e}=\mathbf{1}}^{N(N-1)/2} \mathcal{H}_{\mathbf{e}} \tag{5.40}$$

As a basis for $\mathcal{H}_{spins}$ we use the computational basis. The basis is thus $\{\mid i_1, ..., i_{N(N-1)/2}; j_1, ..., j_N \rangle\}$, where the first $N(N-1)/2$ indices i_k label the edges of the graph, and the remaining N indices j_k label the vertices. Of course $i_k, j_k = 0, 1$ for every k.

After the projection onto the hard core bosons space $\mathcal{H}_{spins}$, the model Hamiltonian becomes thus the spin one-half Hamiltonian (for μ_i uniform):

$$\begin{aligned} H_{1/2} = & - U \sum_{(i,j)} S^z_{(i,j)} - \mu \sum_{i=1}^{N} \left(\frac{1}{2} - S^z \right)_i - t \sum_{(i,j)} P_{ij} \otimes (S_i^+ S_j^- + S_i^- S_j^+) \\ & - k \sum_{(i,j)} \left(S^-_{(i,j)} P^2_{ij} \otimes (S_i^+ S_j^+) + P^2_{ij} S^+_{(i,j)} \otimes (S_i^- S_j^-) \right) \end{aligned} \tag{5.41}$$

Let us examine the model in some limits. When the exchange term is vanishing, $k = 0$,

the model has particle number conservation

$$[H_{1/2}, \hat{N}] = 0, \qquad \hat{N} = \sum_i b_i^\dagger b_i \tag{5.42}$$

and therefore it has a $U(1)$ symmetry, corresponding to the local transformation at every site given by

$$\mid \psi\rangle \rightarrow \prod_l e^{i\phi b_l^\dagger b_l} \mid \psi\rangle, \qquad \phi \in [0, 2\pi) \tag{5.43}$$

while the total system with $k \neq 0$ does not have particle conservation because particles can be created or destroyed by means of the exchange term with the edges. Moreover, the $k = 0$ system is self dual at $\mu = 0$ under the transformation $b_i \rightarrow b_i^\dagger$. For every separable state of the form $\mid \psi\rangle = \mid i_1, ..., i_{N(N-1)/2}\rangle \otimes \mid \psi\rangle_{bosons}$, the system is just the usual Hubbard model on the graph specified by the basis state $\mid i_1, ..., i_{N(N-1)/2}\rangle$. In the limit of $-U$ positive and very large, all the edges degrees of freedom are frozen in the $\mid 1\rangle$ state. The model becomes a Bose-Hubbard model for hard-core bosons on a complete graph.

It is a typical feature of the richness of the Hubbard model that summing the potential and kinetic term gives a model with an incredibly rich physics. Depending on the interplay between potential and kinetic terms, it can accommodate metal-insulator transitions, ferromagnetism and antiferromagnetism, superconductivity and other important phenomena. The richness of the model comes from the interplay between wave and particle properties. The hopping term describes degrees of freedom that behave as 'waves', whereas the potential term describes particles [13]. As it is well known, the model is not

solvable in two dimensions. The present model is even more complicated by the fact that the graph itself is a quantum variable. It is therefore extremely difficult to extract results from such a model. The hopping term in t favors delocalization of the bosons in the ground state, while the chemical potential μ is responsible for a finite value of the bosonic density ρ in the ground state given by

$$\rho = \frac{1}{N}\sum_i \langle b_i^\dagger b_i \rangle. \tag{5.44}$$

The strength of $|\mu|$ determines how many bosons are present in the ground state. For $\mu > 0$, a large value of μ determines $\rho = 1$, meaning that the ground state has a boson at every site, whereas for $\mu < 0$, a large value of μ means there are no bosons in the ground state $\rho = 0$. In any case, there is no possibility for hopping and this situation describe what is called a Mott insulator. On the other hand, for $k = 0$ and $E_{hop} > \mu$ the hopping dominates and the system is in a superfluid phase. The non vanishing expectation value in the ground state is that of the average hopping amplitude per link

$$\sigma = \frac{2}{N(N-1)}\sum_{i,j} \langle b_i^\dagger b_j \rangle. \tag{5.45}$$

We expect this situation to hold even for the weakly interacting system $E_{hop} \gg k \neq 0$. As in the Hubbard model, there should be a quantum phase transition between the Mott insulator and the superfluid phase for a critical value of μ/E_{hop}. An extensive numerical simulation of the ground state properties of the model is necessary to understand if, for $k \neq 0$, such transition belongs to the same universality class or a different one. It would

also be interesting to understand whether there is a Lieb-Mattis theorem for such a system, namely that there are gapless excitations in the thermodynamic limit for the system of spins one-half.

It should also be evident that depending on the interplay between potential and kinetic energy, the ground state of the system is entangled in the bipartition edges-particles. Starting instead from some separable initial state, the unitary evolution induced by $H_{1/2}$ will entangle states initially separable.

5.1.5 Numerical analysis

We have analyzed several aspect of the dynamics of the system in two different situations. The "insulator" case is the one in which the potential energies are dominant over the kinetic terms: $U = \mu = 1; E_{hop} = k = 0.1$. The second situation is when the kinetic terms are much stronger, the so called "superfluid" case: $U = \mu = 0.1; E_{hop} = k = 1$. We have studied numerically the entanglement dynamics of the model, using as figures of merit the *(i)* Entanglement between particles and edges expressed by the von Neumann entropy $S(t)$ of the density matrix reduced to the system of the particles, *(ii)* the Entanglement per site j expressed by the von Neumann entropy $s_j(t)$ of the density matrix reduced to the system of just one site, and *(iii)* the Concurrence $C(t)$ between a pair of edges, or particles or the particle-edge pair. This expresses the entanglement between these two degrees of freedom alone.

We have simulated the system described by $H_{1/2}$ with $N = 4$ sites, which is 2^{10} dimensional. We have labeled the sites $i = 1, .., 4$ starting from the lower left corner of a square

and going clockwise. The basis states for the system are $\mid J_1 J_2 J_3 J_4; e_{14} e_{12} e_{23} e_{34} e_{24} e_{13} \rangle$ with $J_i, e_{kl} = 0, 1$. By direct diagonalization of the Hamiltonian, we compute the time evolution operator $U(t) = e^{-iHt}$. Starting from an initial state $\rho(0)$, the evolved state is $\rho(t) = U(t)\rho U^\dagger(t)$. The entanglement $S(t)$ as a function of time between particles and edges is obtained by tracing out the spatial degrees of freedom, we obtain the reduced density matrix for the hard core bosons: $\rho_{hcb}(t) = \text{Tr}_{graph}\rho(t)$. The evolution for the subsystem is not unitary but described by a completely positive map. The entanglement is computed by means of the von Neumann entropy for the bipartition $\mathcal{H} = \mathcal{H}_{bosons} \otimes \mathcal{H}_{graph}$, so we have

$$S(t) = -\text{Tr}\left(\rho_{hcb}(t) \log \rho_{hcb}(t)\right) \tag{5.46}$$

The single-site entanglement $s_j(t)$ is instead obtained by tracing out all the degrees of freedom but the site j and then computing the von Neumann entropy of such reduced density matrix. Finally, the last figure of merit to describe the entanglement dynamics of the model is the two-spins concurrence $C(t)$ defined in [20]. We define the $\tau(t)$ reduced system of any two spins in the model, i.e., an edge-edge pair, or an edge-particle pair or a particle-particle pair. The entanglement as function of time between the two members of the pair is given by

$$\mathcal{C}(\tau(t)) \equiv \max(0, \sqrt{\lambda_1} - \sqrt{\lambda_2} - \sqrt{\lambda_3} - \sqrt{\lambda_4}), \tag{5.47}$$

where λ_i's are the eigenvalues (in decreasing order $\lambda_1 > \lambda_2 > \lambda_3 > \lambda_4$) of the operator

$\tau(t)(\sigma_y \otimes \sigma_y)\tau^*(t)(\sigma_y \otimes \sigma_y)$.

There are other important quantity to understand the time evolution of the model. We have computed the expectation value of the particle number operator $S_i^+ S_i^- =\mid 1\rangle\langle 1 \mid_i$ at the site i, the link operator P_{ij}, and the vertex degree operator $D_i = \sum_{k \neq i} P_{ik}$, whose expectation value gives the expected value for the number of edges connected to the vertex i. The last important quantity is the fidelity $\mathcal{F}(t) := |\langle\psi(0)|\psi(t)\rangle|$ of the state $\mid \psi(t)\rangle$ with the initial state $\mid \psi(0)\rangle$. This quantity gives a measure of how much the state at the time t is similar to the initial state.

The simulations have been carried out using two initial states $\mid \psi_1\rangle, \mid \psi_2\rangle$. The state $\mid \psi_1\rangle$ is the basis state describing the complete graph K_4 without particles: $\mid \psi_1\rangle =\mid 0000111111\rangle$. In Fig. 5.1 is shown the result of the simulation using $\mid \psi_1\rangle$ as initial state, and for the model where the on-site potential energy is bigger than the kinetic energies, that is, in the "insulator" phase: $U, \mu > E_{hop}, k$. Due to the very high symmetry of the Hamiltonian in the initial subspace, the system is basically integrable and we can indeed see a short recurrence time. Due to the initial symmetry of the state and the fact that no more than one particle is allowed at every site, the system is very constrained and it is integrable. The entangling power of the Hamiltonian is elevated and despite the fact that the overlap with the initial state is very high, the entanglement is non negligible. The expectation value of every link is the same because of symmetry. For such an initial state, there is no qualitative difference other than different time scales between the "insulator" and "superfluid" case.

The time evolution starting from a just less symmetric state is far richer. The state

$\mid \psi_2\rangle = \mid 0000111101\rangle$ is the basis state describing the square with just one diagonal, and again no initial particles. As anticipated, we have studied the model for two sets of parameters. The case (a) is the "insulator" case with parameters $\mu = U = 1; E_{hop} = k = 0.1$. The case (b), or "superfluid" case has parameters $\mu = U = 0.1; E_{hop} = k = 1$.

"Insulator" case (a).— In the graph, Fig. 5.2(a) are plotted the time evolutions of $\langle D_1(t)\rangle, \langle D_2(t)\rangle$ which have initial values of $\langle D_1(0)\rangle = 3, \langle D_2(0)\rangle = 2$. The oscillations of these operators are damped as well and the system is thermalizing towards a state which represents an homogeneous graph. It is very remarkable to see the phenomenon of eigenstate thermalization in such a small system. Recently, there has been a revival in the study of how quantum systems react to a sudden quench in the context of equilibration phenomena in isolated quantum systems, and our results are showing indeed that for such an isolated quantum system, the reduced system can thermalize due to the entanglement dynamics [29, 30]. In Fig. 5.2 (b) are plotted the expectation value of the link operators P_{12}, P_{24} as a function of time In the initial state $\mid \psi_2\rangle$ we have $\langle \psi_2 \mid P_{12} \mid \psi_2\rangle = 1, \langle \psi_2 \mid P_{24} \mid \psi_2\rangle = 0$. The evolution of $\langle P_{12}(t)\rangle$ is almost periodic but we see that on the other hand the oscillations of $\langle P_{24}(t)\rangle$ are damping and the system is thermalizing. The behavior of the P_{13} operator is complementary to P_{24} and at long times $\lim_{t\to\infty}\langle P_{24}(t) - P_{13}(t)\rangle = 0$. In Fig. 5.2 (c) we plotted the entanglement per site measured by the von Neumann entropy $s_j(t)$ as a function of time. The sites considered are again $j = 1$ and $j = 4$. The two quantities split in two separated bands. Naively, one would expect that the vertices with higher degree are more entangled, but it is not so. Comparing with Fig.5.2 (a) we see that the degrees $\langle D_1(t)\rangle, \langle D_4(t)\rangle$ cross several time and have same time average. Surprisingly, the vertex

with consistent higher entanglement is the one that started with higher degree at time zero, *when the system was in a separable state*. The system has a memory of the initial state that is revealed in the entanglement dynamics. This means that there are some global conserved quantities that are not detected by any local observable, but are instead encoded in the entanglement entropy, which is a function of the global wavefunction. The thermalization process is also shown in the behavior of the fidelity $\mathcal{F}(t)$ that presents damped oscillations, see Fig. 5.2 (d). The behavior of the von Neumann entropy $S(t)$ in Fig. 5.2 (d) shows that the reduced system of the particles is indeed evolving as an open quantum system. Though some of the observables are thermalizing, the entanglement dynamics does not show any damping. In Fig. 5.2 (e) is shown the time evolution of the expectation values of the number operators $N_i(t) = S_i^+ S_i^-(t)$at the vertices $i = 1, 4$. The vertices are distinguished by the initial state of the graph, namely by their degree. The average number of particles per site is $\overline{N_i(t)} \sim 0.05$. This means that particles are basically involved in virtual creation/annihilation processes through which the graph acquires a dynamics. The next graphs show that the entanglement dynamics is all but trivial. The following Fig. 5.2 (f) shows the time evolution of the Concurrence $C(t)$ between the vertex $i = 2$ and the edge $(2, 4)$ which is in the state $\mid 0\rangle$ at the initial time. We see deaths and revivals of entanglement, and the damping of the oscillation signals again some thermalization.

"Superfluid" case (b).— In this case, the kinetic terms k, E_{hop} are dominant over the potential terms U, μ. The dynamics of this model for these parameters is completely different. We do not have any sign of thermalization. The degree expectation values $\langle D_1(t)\rangle, \langle D_2(t)\rangle$ have a similar oscillating behavior with an even higher overlap, see Fig. 5.3

(a). The link operators P_{14}, P_{24}, shown in Fig. 5.3 (b) oscillate with no damping and are almost completely overlapped. To such distinct behavior with respect to the insulator case, we find a very strong similarity in the behavior of the entanglement per site $s_i(t)$ (see Fig. 5.3 (c) where, again, and in a more pronounced way, there is a splitting in two bands depending on the initial state of the system, and not on the degree (or other interesting observables) of the system during the time evolution. As in the insulator case, the vertex that started off with a higher degree is constantly more entangled than the one that started off with a lower degree, even if in the initial state they are both separable states and during the evolution all the relevant observables overlap strongly and have same time averages. This phenomenon again reveals how the entanglement contains global information on the state of the system that is not revealed in the usual local observables one looks at. The entanglement between edges and particles has a similar behavior than in the "insulator" case, but it is an order of magnitude greater, which is consistent with the fact that now the terms that couple edges and particles (and thus create entanglement) are larger. The superfluidity is revealed also in the behavior of the fidelity $\mathcal{F}(t)$ that shows no sign of thermalization with constant amplitude of oscillations, see Fig. 5.3 (d). The average number of particles per site is now $\overline{N_i(t)} \sim 0.52$ and is homogeneous (Fig. 5.3 (e)). Particles are delocalized over the quantum graph with a non vanishing expectation value. The Concurrence $C(t)$ in Fig. 5.3 (f) confirms that there is no thermalization in the system.

To conclude this section, we have studied the model Eq.(5.35) in the case of hard-core bosons. The usual Hubbard model with hard-core bosons on a fixed graph presents two

quantum phases at zero temperature. An insulator phase, when the potential energy of the electrons is dominant, and a superfluid phase, when the kinetic energy is dominant. In our model, the graph interacts with the electrons and the graph degrees of freedom are themselves quantum spins that can be in a superposition. We have studied numerically the entanglement dynamics of the system with four vertices starting from a separable state. The evolution with insulator parameters shows typical signs of thermalization in some of the relevant observables. Moreover, the entanglement dynamics reveals a memory of the initial state that is not captured in the observables. The behavior of the dynamics of the "superfluid" system is completely different, in the fact that there is no apparent thermalization. The memory effect revealed by the entanglement dynamics is present in an even more pronounced way. There are many open questions to be answered: how the entanglement spectrum behaves and what it reveals of the system, what is the phase diagram of the model at zero temperature in the thermodynamic limit, and a systematic study of the correlation functions in the model. We barely started studying the features of this model that presents formidable difficulties, but that promises to be very rich.

5.2 Markov chains analysis of the model

In this section, we develop a general method to describe the evolution of graphs. We regard Eq.(5.35) as the Hamiltonian for a classical model and consider a configuration of the system with a fixed number of edges and particles. The sum of these two quantities is a constant of the evolution. Moreover, it is safe to assume that almost all edges can be po-

tentially converted in particles. The reason is simple: fixing the number of vertices, every connected graph (up to isomorphism) can be obtained by deleting and adding edges that are part of triangles. With this approximation, we expect that at long times a dynamical equilibrium is established between particles and edges. When considering the classical model, we can disregard superpositions and look at the dynamics as a discrete-time process with characteristics described as follows. For simplicity, we focus on the complete graph $\mathcal{K}_N = (V(\mathcal{K}_N), E(\mathcal{K}_N))$, with set of vertices $V(\mathcal{K}_N)$ and set of edges $E(\mathcal{K}_N)$. Note that this constraint is not necessary, since we can start from any graph containing a triangle. The process simply needs at least one triangle in order to run. The process, starting from time $t = 0$, can be interpreted as a probabilistic dynamics gradually transforming the complete graph into its connected spanning subgraphs. These are subgraphs on the same set of vertices. Methods from the theory of Markov chains appear to be good candidates to study such a dynamics. We identify with a "graph of graphs" the phase space representing all possible states of the system considered. In this way a random walk on the graph, driven by appropriate probabilities, will allow us to study the behavior of the Hamiltonian, at least restricting ourselves to the classical case. Thus, the Hamiltonian transforms graphs into graphs. The Markov chain method suggests different levels of analysis: a level concerning the *support* of the dynamics; a level concerning the *distribution of particles*. At the first level, we are interested in studying graph theoretic properties of the graphs/objects obtained during the evolution, if we disregard the movement of the particles. This consists of studying expected properties of the graphs obtained by running the dynamics long enough. It is important to remark that the presence of particles does

not modify the phase space, which, if we start from $\mathcal{K}_N$, is the set of all connected graphs. The graphs obtained cannot have more edges than the initial one. Notably, particles only alter the probability of hopping between elements of the phase space. At the second level, we are interested in studying how the particles are going to be distributed on the vertices of the single graphs, and therefore in what measure the particles determine changes on the graph structure and consequently modify the support of the dynamics. When considering only the support, the Hamiltonian for the classical model determines the next process:

- At time step $t = 0$, we delete a random edge of $G_0 \equiv \mathcal{K}_N$ and obtain G_1.
- At each time step $t \geq 1$, we perform one of the following two operations on G_t:
  - *Destroy a triangle:* We delete an edge randomly distributed over all edges in triangles of G_t. A *triangle* is a triple of vertices $\{i, j, k\}$ together with the edges $\{i, j\}, \{i, j\}, \{j, k\}$.
  - *Create a triangle:* We add an edge randomly distributed over all pairs $\{i, j\} \notin E(G_t)$ such that $\{i, k\}, \{j, k\} \in E(G_t)$ for some vertex k.

This process is equivalent to a random walk on a graph $\mathcal{G}_N$ whose vertices are all connected graphs. Each step is determined by the above conditions. The Hamiltonian gives a set of rules determining the hopping probability of the walk. The theory of random walks on graphs is a well established area of research with fundamental applications now ranging in virtually every area of science [19]. The main questions to ask when studying a random walk consist of determining the stationary distribution of the walk and estimating

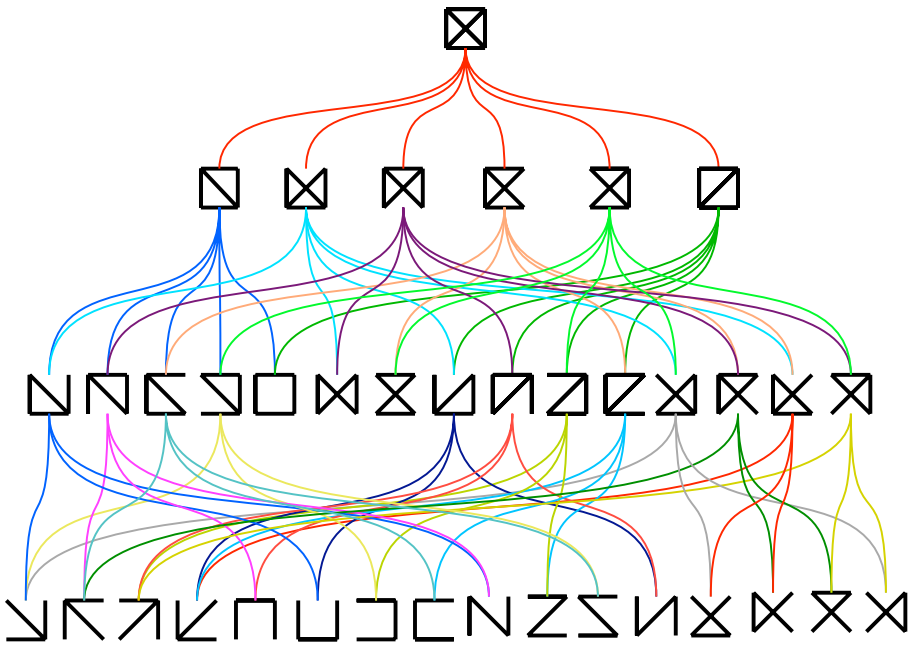

Figure 5.4: The graph $\mathcal{G}_4$. The number of vertices is 38 and 72 edges. The number of vertices of $\mathcal{G}_n$ is exactly the number d_n of connected labeled graphs on n vertices. The number d_n satisfies the recurrence $n2^{\binom{n}{2}} = \sum_k k d_k 2^{\binom{n-k}{2}}$ [17]. The walker starts from the vertex corresponding to the graph $\mathcal{K}_4$. Even when we add particles, the graph $\mathcal{G}_n$ remains the support of the dynamics. The vertices of $\mathcal{G}_n$ are the possible states of classical evolution. In the quantum evolution, we have a weighted superposition of vertices.

temporal parameters like the number of steps required for the walk to reach stationarity. The stationary distribution at a given vertex is intuitively related to the amount of time a random walker spends visiting that vertex. In our setting, the walker is a classical object in a phase space consisting of all connected graphs with the same number of vertices. Fig. 5.4 is a drawing of $\mathcal{G}_4$, the configuration space of all connected graphs on four vertices. This is a graph whose vertices are also graphs. The initial position of the walker is the vertex corresponding to $\mathcal{K}_4$.

The graph $\mathcal{G}_N$ ($N \geq 2$) is connected and bipartite. The number of vertices of $\mathcal{G}_N$ equals the number of connected *labeled* graphs on N vertices. We need labels on the vertices to distinguish between isomorphic graphs. From the adjacency matrix of a graph G, we can

construct the transition matrix $T(G)$ inducing a *simple random walk* on G: $[T(G)]_{i,j} = 1/d(i)$ if $\{i,j\} \in E(G)$ and $[T(G)]_{i,j} = 0$, otherwise. Here, $d(i) := |\{j : \{i,j\} \in E(G)\}|$ is the *degree* of a vertex i. Notice that the degrees of the vertices in $\mathcal{G}_N$ are not uniform, or, in other words, $\mathcal{G}_N$ is not a *regular* graph. In fact, the degree of the vertex corresponding to $\mathcal{K}_N$, which is the number of edges in this graph, is much higher than the degree of the graphs without triangles. In Fig. 5.4, it is easy to see that K_4 has degree 6 and that the path on 4 vertices, drawn in the bottom-right corner of the figure, has only degree 2.

The evolution of a random walk is determined by applying the transition matrix to vectors labeled by the vertices encoding a probability distribution on the graph. The law $\left(T(G)^T\right)^t \mathbf{v}_0^{(i)} = \mathbf{v}_t$ gives a distribution on $V(G)$ at time t, with the walk starting from a vertex i. The vector $\mathbf{v}_0^{(i)}$ is an element of the standard basis of $\mathbb{R}^N$. The vector $\mathbf{v}_t = (\mathbf{v}_t^{(1)}, \mathbf{v}_t^{(2)}, ..., \mathbf{v}_t^{(N)})^T$ is a probability distribution, being $\mathbf{v}_t^{(i)}$ the probability that the walker hits vertex i at time t. The distribution $\pi = (d(i)/2\,|E(G)| : i \in V(G))$ is the *stationary distribution*, that is $T(G)\pi{=}\pi$. If G is connected and non-bipartite then $\lim_{t\to\infty} \left(T(G)^T\right)^t \mathbf{v}_0^{(i)} = \pi$ [19]. The stationary distribution is independent of the initial vertex. Therefore, a walk on $\mathcal{G}_N$ can start from any vertex and the asymptotic dynamics remains the same. It is simple to see that $\mathcal{G}_N$ is bipartite. Then a random walk does not converge to a stationary distribution, but it *oscillates* between two distributions with support on the graphs with an odd and an even number of edges, respectively. In fact, for a bipartite graph G with $V(G) = A \cup B$, we have the following: $\lim_{t\to\infty,\text{even}} \left(T(G)^T\right)^t \mathbf{v}_0^{(i)} = \pi_{even}$ with $[\pi_{even}]_i = d(i)/\,|E(G)|$ if $i \in A$ and $[\pi_{even}]_i = 0$, otherwise; analogously for $\lim_{t\to\infty,\text{odd}} \left(T(G)^T\right)^t \mathbf{v}_0^{(i)} = \pi_{odd}$. For instance, it follows that

the stationary distribution of a random walk starting from any vertex of $\mathcal{G}_4$ oscillates between the two distributions

$$\pi_{odd} = (\underbrace{0}_{1}, \underbrace{1/12, ..., 1/12}_{6}, \underbrace{0, ..., 0}_{15}, \underbrace{1/24, ..., 1/24}_{4}, \underbrace{1/36, ..., 1/36}_{12})$$

and

$$\pi_{even} = (\underbrace{1/12}_{1}, \underbrace{0, ..., 0}_{6}, \underbrace{5/72, ..., 5/72}_{4}, \underbrace{1/31, ..., 1/31}_{3}, \underbrace{5/72, ..., 5/72}_{8}, \underbrace{0, ..., 0}_{4}, \underbrace{0, ..., 0}_{12}).$$

In particular, for π_{odd}, $\sum_{i:d(i)=6}[\pi_{odd}]_i = \frac{1}{2}$, $\sum_{i:d(i)=4}[\pi_{odd}]_i = \frac{1}{6}$, $\sum_{i:d(i)=2}[\pi_{odd}]_i = \frac{1}{3}$; for π_{even}, $\sum_{i:d(i)=6}[\pi_{odd}]_i = \frac{1}{12}$, $\sum_{i:d(i)=5}[\pi_{odd}]_i = \frac{5}{6}$, $\sum_{i:d(i)=2}[\pi_{odd}]_i = \frac{1}{12}$. Now, what is the most likely structure of a graph/vertex of $\mathcal{G}_N$ in which the random walker will spend a relatively large amount of time? In other words, where are we going to find the walker if we wait long enough and what are the typical characteristics of that graph or set of graphs? From the above description, one may answer this question by determining the stationary distribution of the walk in $\mathcal{G}_N$. We do not have immediate access to this information, because we do not know the eigenstructure of $T(\mathcal{G}_N)$. For this reason, we need some way to go around the problem. We can still obtain properties of the asymptotics by making use of standard tools of random walks analysis. In particular, as a first step, we are able to estimate the number of edges in the most likely graph in $\mathcal{G}_N$. Even if this information is not particularly accurate and it is far from being sufficient to determine the graphs, it still can give an idea of their structure. The probability $\pi(G)$ that the walk will be at a given graph G after a large number of time steps is given, up to a small error term, by the

stationary distribution π of the walk. As we have mentioned above, $\pi(G)$ is given by the number of possible transitions from G in the walk, divided by a normalizing constant E which is independent of G. Based on this, it is possible to find the expected number of edges in a graph visited by the walk. We will provide here a sketch of the proof. A more extensive discussion is the Appendix. In total there are $\binom{\binom{N}{2}}{k}$ graphs with N vertices and k edges. By some of the classical results in the theory of random graphs [18] we know that for $k \geq \frac{(1+\epsilon)\log N}{N}$, the probability that a random graph is connected converges to 1 as N grows. Let us recall briefly that a random graph is a graph whose edges are chosen with a fixed probability, equal and independent for each pair of vertices. The probability that a graph is visited by our walk will have k edges is given by $\sum_{V(\mathcal{G}_N):|E(\mathcal{G}_N)|=k} \pi(\mathcal{G}_N)$, where the sum is in fact taken over all connected graphs with k edges. In order to estimate this sum we must know how much $\pi(\mathcal{G}_N)$ can vary. However by the results mentioned earlier $\pi(\mathcal{G}_N)$ cannot be larger than $\binom{N}{2}/E$ and not smaller than $(N-1)/E$, since that is the largest and smallest number of edges in a connected graph, and every transition in the walk can be associated with an edge in the current graph. Hence, the probability that the graph will have k edges will lie between $\binom{\binom{N}{2}}{k}\binom{N}{2}/E$ and $\binom{\binom{N}{2}}{k}(N-1)/E$. However for large N and k this value is completely dominated by the first term, which is of order $2^{N^2}/N$ for $k = \binom{N}{2}/2$. A more careful use of these estimates shows that the expected number of edges will be close to $\binom{N}{2}/2 \sim N^2/4$. Furthermore this results will hold true for any walk where the ratio between probabilities for the most and least likely graphs is not exponentially large in N. This observation tells us that the most likely graphs obtained during the process tend to have less edges than regular objects as lattice-like graphs. The

number of edges in a square lattice with n^2 vertices is $2n\,(n+1)$. For a cubic lattice on n^3 vertices this number is $3n\,(n+1)^2$, from the general formula $dn\,(n+1)^{d-1}$, where d is the dimension of the lattice. It seems natural to try to establish a relation between our walk and random graphs. After a first analysis, such a relation does not appear obvious. In fact, the walk on $\mathcal{G}_N$ is based upon a *locality principle* which is not usually defined when considering random graphs. An attempt to implement this principle for random graphs would consist in constructing Erdös-Renyi graphs starting from a random tree instead of the empty graph, that is, the graph with zero edges. A random tree, insures connectivity. Each pair of vertices at distance two is then joined with a probability p. If we keep adding and deleting edges, we obtain a dynamics similar to the one induced by our Hamiltonian. It is important to observe that the differences with the standard notion of random graph are essentially two: vertices at distance larger than two cannot be joined with a single step of the process; there is an additional probability of deleting edges.

Let us keep in mind that so far we have not consider particles. Indeed, we have studied only a random walk on $\mathcal{G}_N$, where this is the space of objects obtained by deleting and adding edges that form triangles. However, our Hamiltonian describes an evolution including particles. Each edge deletion creates two particles sitting at the end vertices of the deleted edge. These particles are free to move in the graph. Creation of another edge will depends on the number of particles. Only when two particles are located on two different vertices at distance two from each other, then we have a nonzero probability of creating an edge between such vertices and therefore creating a new triangle. Including particles, we can define the following process:

- At time step $t = 0$, we delete a random edge of $G_0 := \mathcal{K}_N$ and obtain G_1.
- At each time step $t \geq 1$, we perform one of the following two operations on G_t:
  - *Destroy a triangle:* We delete an edge randomly distributed over all edges in triangles of G_t. When deleting an edge we *create* two (indistinguishable) particles. Each particle is located on a vertex of the graph according to the stationary distribution over G_{t+1}. This reflects the assumption that the particles thermalize.
  - *Create a triangle:* With a certain probability, we add an edge $\{i, j\} \notin E(G_t)$ such that $\{i, k\}, \{j, k\} \in E(G_t)$ for some vertex k. The probability of adding this edge is proportional to the probability of finding a particle at vertex i and a particle at vertex j at the same time t. When adding an edge, we *destroy* two particles. Specifically, the particles located in the two end vertices.

Notice that the probability of deleting an edge is independent of the number of particles in the graph and their locations. On the other side, the probability of adding an edge is fundamentally connected to the number of particles. Higher is the number of particles in the graph $G_t \in V(\mathcal{G}_N)$ and higher is the probability of adding edges. The process exhibits a conservative behavior since the number of particles is always

$$2\binom{N}{2} - |E(G_t)|\,. \tag{5.48}$$

So, the dynamics is again equivalent to a random walk on the graph $\mathcal{G}_N$. This time the random walk is not a simple random walk, since the probability of each step is deter-

mined by the above conditions. In the transition matrix $T(\mathcal{G}_N)$ we can have $[T(\mathcal{G}_N)]_{i,j} \neq [T(\mathcal{G}_N)]_{i,k} \neq 0$, whenever $j \neq k$. This fact gives different nontrivial weights on the edges of $\mathcal{G}_N$. The transition matrix of the walk is then not necessarily symmetric and we need a normalization factor to keep it stochastic (*i.e.*, the sums of the elements in each row is 1). Whenever an edge is deleted two particles are created. In the simplest version of our model all particles are distinguishable and at each time step of the walk all particles are redistributed according to a random walk on each graph/vertex of $\mathcal{G}_N$. By Eq. (5.48), there are N^{2p} possible particle configurations. By the standard behavior of a random walk, particles will tend to cluster at vertices with high degree. For this model the state of the walk will consist both of the current graph G and the vector x of positions of all particles. Here the number of possible transitions will depend both on the structure of G, as before, and the number of particles. Since the number of particle configurations grows rapidly while the number of edges decreases, the walk will concentrate on connected graphs with few edges, rather than the denser graphs favored by the model without particles. If we make a rough estimate of the number of states corresponding to graphs with $\binom{N}{2}/2$ edges, we see that they are fewer than $N^{\binom{N}{2}}2^{\binom{N}{2}}$ and that the number of states corresponding to graphs with $\mathcal{O}(N)$ edges are more than $N^{(2-\epsilon)\binom{N}{2}}$, for any $\epsilon > 0$. A comparison argument like the one used for the case without particles then shows that the expected number of edges for a graph/vertex will be $o(N^2)$. It has to be remarked that an *ad hoc* tuning of the deletion probability for each edges should plausibly allow to obtain sparser or denser graphs. We have give a rough bound on the number of edges in a typical graph obtained via the Hamiltonian in Eq.(5.35). The bound does not contradict the possibility that such

a graph has an homogeneous structure like a lattice. Additionally to the number of edges, it may be worth to have some information about cliques. A *clique* is a complete subgraph. Cliques are then the *densest* regions in a graph. Knowing the size of the largest cliques gives a bound on the maximum degree and clearly tells about the possibility of having dense regions. In the Appendix we will prove that the growth of the largest cliques is logarithmic with respect to the number of vertices. This behavior also occurs for random graphs.

Numerical simulations were performed to obtain information on the behavior of the classical system under different initial conditions. We are going to discuss the case of the complete graph $\mathcal{K}_N$ as initial state. Complete graphs are interesting for several reasons. First of all, every edge of $\mathcal{K}_N$ is eligible for interaction. This implies that edges rapidly transform in particles. As we can see in Fig. 5.5 (a), the number of particles increases rapidly until it reaches an equilibrium value $\tilde{N}_0(N)$. The number of steps to reach the equilibrium distribution is the same for all the graph sizes, and is of the order of the inverse of the only *time scale* introduced, given by $\sim P_i^{-1}$. It is interesting to understand the equilibrium distribution of the degree for the various graphs $\mathcal{K}_N$. To obtain a better shape for this distribution, we increased the number of simulations from 30 to 60. The result can be seen in Fig. 5.5 (b). We find that the distribution is Poisson (D_e is the degree), as it is for random graphs:

$$P_N(D_e) = \frac{1}{R} e^{-\frac{(D_e - f(N))^2}{Q(N)}} \tag{5.49}$$

where R is a normalization constant. In Fig. 5.5 (a) we find that the function $f(N)$ is, for the graph $\mathcal{K}_N$, given by

$$f(N) = \frac{N}{2}, \tag{5.50}$$

while the function $Q(N)$ of Fig. 5.5 (b) is

$$Q(N) = \frac{\sqrt{N}}{2}. \tag{5.51}$$

It has to be remarked that this result agrees for large N with the combinatorial proof in the last section.

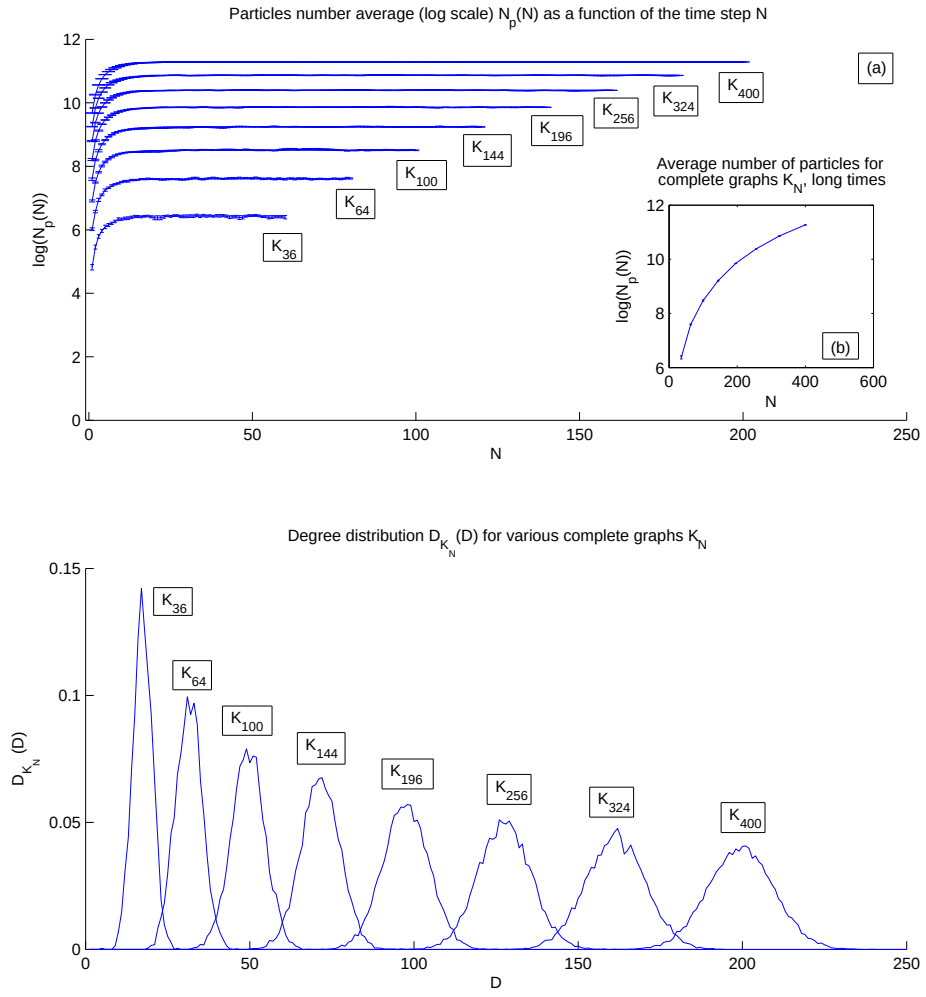

Figure 5.5: **a)** Plot of the logarithm of the average number of particles N_p as a function of the number of steps. The initial conditions were complete graphs with N vertices, $\mathcal{K}_N$, with hopping probability $P_h = 1$ and interacting probability $P_i = 0.1$. **b)** In this plot we have the same quantity of (a), $\log(N_p(N))$, plotted as a function of the graph size N at long times (when at equilibrium). **c)** Plot of the equilibrium degree distributions for each graph $\mathcal{K}_N$. The hopping and interaction probabilities for each simulation are $P_h = 1$ and $P_i = 0.1$ respectively. The distributions are obtained averaging over 60 simulations. At equilibrium, we obtain Poisson distributions centered on $\frac{N}{2}$, as shown in Fig. (5.6) (b), and variance $Q(N) = \frac{\sqrt{N}}{2}$, as shown in Fig. (5.6) (a). This agrees with standard results of the theory of random graphs.

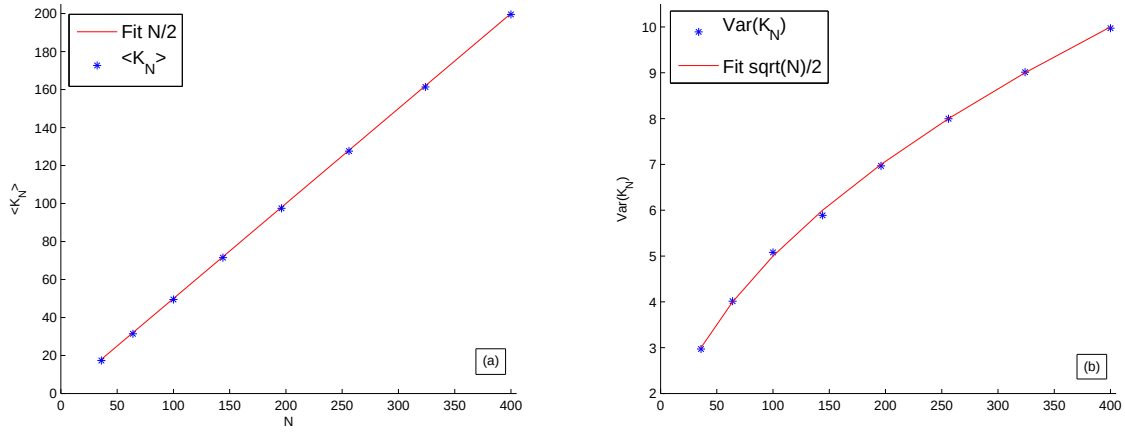

Figure 5.6: **a)** Plot of the average values of the equilibrium degree distributions of Fig. (5.5) (c). The red line is the fit, given $f(N) = \frac{N}{2}$. This agrees perfectly with the various $\mathcal{K}_N$. **b)** Plot of the variance of the equilibrium degree distributions of Fig. (5.5) (c). The red line is the fit, giving $Q(N) = \frac{\sqrt{N}}{2}$.

Part III

Emergence

Chapter 6

Geometry and Emergence

Since the discovery of the Hawking and Unruh effects, it was clear that gravity is fundamentally different from the other forces we know. A new thermodynamics had to be associated to black hole physics: they require a modification of the second law of thermodynamics. This is one of the biggest puzzles in theoretical physics.

In this chapter we will introduce a mapping between connectivity of the graph and the evolution equation for a scalar field in curved space [1]. We will find that the Bose-Hubbard Hamiltonian with homogeneous couplings on a lattice with varying vertex degree is equivalent to a Bose-Hubbard Hamiltonian on a regular-degree graph but with site-dependent effective couplings (similar to the behavior seen in [66]). This makes it possible to connect the coefficients in the Hamiltonian to geometric properties of the graph. The picture which emerges from this analysis is the one of Fig. 6.1: the graph modifies the strength of the interaction in the Bose-Hubbard Hamiltonian, and this ap-

[1] This section is based on [112]. The role of the author of the present thesis in the paper was mostly on the analytical results. He proved analytically that the trapped surface configuration has a Hamiltonian which is gapped, and derived the effective Hamiltonian and the effective equation for the probability. Also, the emergence of the mass from multi-particle interaction.

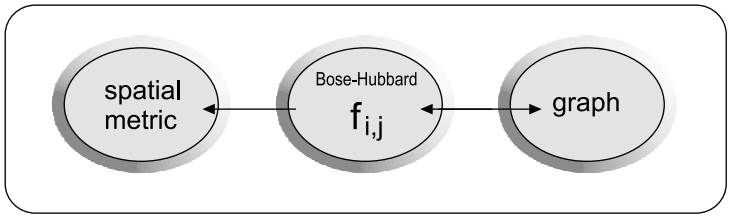

Figure 6.1: The scheme representing the relations between the graph, the hopping energies $f_{i,j}$ of the Bose-Hubbard model and the emergent metric: the graph modifies the strength of the interaction in the Bose-Hubbard Hamiltonian, which in turn translates into a curved geometry (for the appropriate states).

pears as a curved geometry to the propagating matter.

It is important to note that the emergent curved space is a *dynamical* property of the system. The geometry that the particles propagating on the graph see depends on the dynamics of the particles and it is not just a property of the graph and, in addition, the resulting motion of the particles will change the graph and so affect the geometry.

In the present Chapter, moreover, we study the model for a particular class of graphs that have been conjectured to be analogues of trapped surfaces. We are interested in the approximation $k \ll t$, which can be seen as the equivalent of ignoring the backreaction of the matter on the geometry. For simplicity, we will set $U = k = 0$ in eqn. (5.35), meaning that

$$\widehat{H} = \widehat{H}_v + \widehat{H}_{\text{hop}}. \tag{6.1}$$

In this case, the total number of particles on the graph is a conserved charge. $\widehat{H}_v$ and $\widehat{H}_{links}$ are constants on fixed graphs with fixed number of particles. The Hamiltonian is the ordinary Bose-Hubbard model on a fixed graph, but that graph can be unusual, with

sites of varying connectivity and with more than one edge connecting two sites. Our aim will then be to study the effective geometry that matter in this model sees.

Even on a fixed lattice, the Hubbard model is difficult to analyze, with few results in higher dimensions. It would seem that our problem, propagation on a lattice with connectivity which varies from site to site is also very difficult. Fortunately, it turns out that for our purposes it is sufficient to restrict attention to lattices with certain symmetries. To avoid confusion with the the time variable, in the following the coupling constant previously called t associated to the hopping of the particles will be renamed E_{hop}.

6.1 Foliated and rotationally invariant graphs

In this Section we define graphs with two particular properties which we call *foliation* and *rotational invariance*. These properties will allow us to greatly simplify the calculations that follow without loss of generality. We will see that the problem of finding the ground state of hopping Hamiltonians, on graphs with these properties can be simplified to the solution of the one-dimensional Bose-Hubbard model.

6.1.1 Foliated graphs

A *foliated graph* is a graph that can be decomposed into a set of subgraphs connected by edges in a successive way. More precisely, let g_i be a labeling of subgraphs of a graph G and E_i a labeling of the set of edges connecting the sets g_i, such that $\cup_i (g_i \cup E_i) = G$. Then,

Definition 1. *A graph G is* foliated *if it can be decomposed in several disjoint subgraphs g_i with*

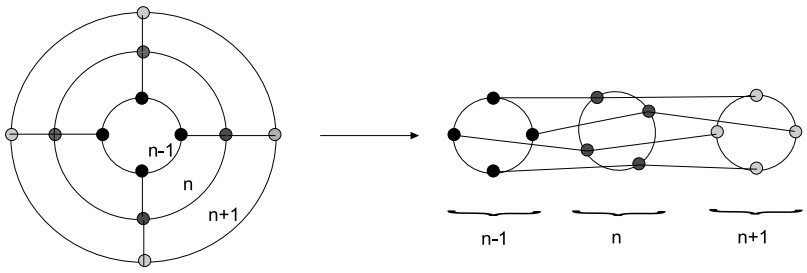

Figure 6.2: A 2-d lattice that can be foliated.

the following properties:

1. *All the subgraphs g_i are degree regular.*

2. *All the edges of a subgraph g_i connect a vertex in g_i to a vertex in g_{i-1} or g_{i+1}.*

3. *The number of edges connecting a vertex in g_i (g_{i+1}) to vertices in g_{i+1} (g_i) is the same for every vertex of g_i (g_{i+1}). This number is called* relative degree *and is represented by $d_{i,i+1}$ ($d_{i+1,i}$).*

Notice that the name, *foliated*, comes from the fact that these graphs can be decomposed into subgraphs such as any foliated structure can be separated into thin layers. Examples of foliated graphs are presented in Figs. 6.2 and 6.3.

The number of edges that connect two consecutive subgraphs g_i and g_{i+1} is given by

$$d_{i,i+1}N_i = d_{i+1,i}N_{i+1}\,, \tag{6.2}$$

where N_i is the number of vertices of g_i.

In order to discuss the properties of the hopping Hamiltonians defined by foliated graphs, let us introduce a natural coordinates (i, m) to specify a vertex of a foliated graph.

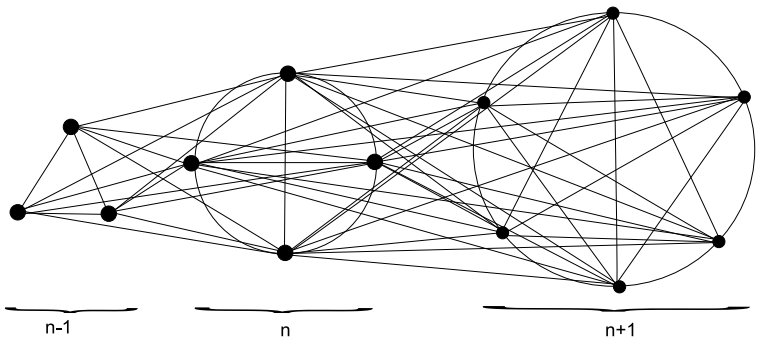

Figure 6.3: A non-planar lattice that can be 1-foliated.

The coordinate i specifies the subgraph g_i and m refers to the particular vertex in g_i. The hopping Hamiltonian of a foliated graph in terms of these coordinates can be written as

$$\begin{aligned}\widehat{H}_{\text{fol}} = &-\sum_{i=0}^{R-1}\sum_{m,m'=0}^{N_i-1} A^{(i)}_{mm'} b^\dagger_{i,m} b_{i,m'} + h.c. \\ &-\sum_{i=0}^{R-1}\sum_{m=0}^{N_i-1}\sum_{m'=0}^{N_{i+1}-1} B^{(i)}_{mm'} b^\dagger_{i,m} b_{i+1,m'} + h.c.\,,\end{aligned} \tag{6.3}$$

where $b^\dagger_{i,m}(b_{i,m})$ is the creation (annihilation) operator of a particle at the vertex (i,m), R is the number of layers g_i, $A^{(i)}_{mm'}$ is the adjacency matrix of the subgraph g_i, and $B^{(i)}_{mm'}$ stands for the edges between the vertices of g_i and g_{i+1}.

In this model, the *delocalized* states on the subgraphs g_i are particularly interesting. These are states of a particle which is completely and uniformly spread over the graph g_i, defined as follows:

Definition 2. *The* delocalized *state,* $\mid i\rangle$*, in* g_i *is defined by*

$$\mid i\rangle = \frac{1}{\sqrt{N_i}} \sum_{m=0}^{N_i-1} \mid i,m\rangle. \tag{6.4}$$

The delocalized state $\mid i\rangle$ is an eigenstate of the hopping Hamiltonian defined from the degree-regular subgraph g_i,

$$\widehat{H}_{\text{fol}}^{(i)} = -\sum_{m,m'=0}^{N_i-1} A_{mm'}^{(i)} b_{i,m}^{\dagger} b_{i,m'} + h.c.\,. \tag{6.5}$$

More explicitly,

$$\widehat{H}_{\text{fol}}^{(i)} \mid i\rangle = \frac{1}{\sqrt{N_i}} \sum_{m=0}^{N_i-1} \left(\sum_{m'=0}^{N_i-1} A_{m'm}^{(i)} \right) \mid i,m\rangle = -d_{i,i} E_{hop} \mid i\rangle \ , \tag{6.6}$$

where we have used the degree-regularity of the graph, $d_{i,i} = \sum_m A_{nm}^{(i)}$, for all n. For example, when the graph g_i is a chain, the completely delocalized state is the ground state of the system and has energy -2, with 2 is the degree of the vertices of a 1-dimensional chain.

The subspace spanned by the delocalized states $\mid i\rangle$ is an eigenspace of the system, since the projector onto this subspace,

$$\widehat{P}_d = \sum_{i=0}^{R-1} |i\rangle\langle i|, \tag{6.7}$$

commutes with the Hamiltonian (6.3), $[H_{fol}, P_d] = 0$. Therefore, the time evolution of any superposition of delocalized states lies always in this subspace (it is a superposition of delocalized states). This allows us to define an effective Hamiltonian for the delocalized

states,

$$\begin{aligned}\widehat{H}_{\text{eff}} &:= \widehat{P}_{\text{d}}\widehat{H}_{\text{fol}}\widehat{P}_{\text{d}} \\ &= \sum_{i=0}^{R-1} \left(f_{i,i+1} \left(|\, i+1\rangle\langle i \,| + |\, i\rangle\langle i+1 \,| \right) + \mu_i |i\rangle\langle i| \right),\end{aligned} \tag{6.8}$$

where $\mu_i = \langle i \mid \widehat{H}_{\text{fol}} \mid i\rangle = -E_{\text{hop}} d_{i,i}$ and

$$f_{i,i+1} := \langle i \mid \widehat{H}_{\text{fol}} \mid i+1\rangle = -E_{\text{hop}}\, d_{i,i+1} \sqrt{\frac{N_i}{N_{i+1}}}\,. \tag{6.9}$$

Note that the Hamiltonian (6.8) is a one-dimensional Bose-Hubbard Hamiltonian with chemical potential μ_i and tunneling coefficient $f_{i,i+1}$.

The mass term (or chemical potential) μ, is *fattened by the edges connecting the nodes within the subgraph g_i of the foliated graph*. This is one the main results of the thesis. This behavior resembles a scalar field not-minimally coupled to (classical) gravity, where the mass of the particle is multiplied by a curvature factor. In our case, the role of the curvature is played by $-E_{hop} d_{i,i}$ (see Sec. 6.3).

The extension to higher dimensions is straightforward. It requires the extension of one-dimensional foliated graphs to graphs which can be foliated in multiple directions, thus resembling an ordinary lattice, but with multiple links between pairs of sites. The coefficients $f_{k,k-1}$ will depend on the direction of the foliation that the particle is hopping to.

We have found an eigenspace of the foliated Hamiltonians for which the effective Hamiltonian is particularly simple. However, this eigenspace will not, in general, contain

relevant eigenstates of the Hamiltonian such as the ground state. In order to ensure this, we require another symmetry.

6.1.2 Rotationally invariant graphs

Let us present next our definition of the rotationally invariant graphs.

Definition 3. *A graph G is called* N-rotationally invariant *if there exists an embedding of G to the plane that is invariant by rotations of an angle $2\pi/N$.*

With the exception of those graphs that have a vertex in the center, *N-rotationally invariant* graphs allow for a labeling of their vertices $(n,\theta) \in \mathbb{N} \times \mathbb{Z}_N$ such that their adjacency matrix $A_{(n\theta),(n'\theta')}$ only depends on n, n' and $\theta - \theta'$. We can make use of these coordinates (n,θ) in order to write the Hamiltonian defined by a rotationally invariant graph

$$\begin{aligned} H_{\text{rot}} = &- \sum_{\theta=0}^{N-1} \sum_{n,n'} A_{nn'} b^\dagger_{n\theta} b_{n'\theta} + h.c. \\ &- \sum_{\theta=0}^{N-1} \sum_{\varphi=1}^{N-1} \sum_{n,n'} B^{(\varphi)}_{n,n'} b^\dagger_{n\theta} b_{n'\theta+\varphi} + h.c., \end{aligned} \tag{6.10}$$

where $b^\dagger_{n,\theta}$ ($b_{n,\theta}$) is the creation (annihilation) operator at the vertex (n,θ), $A_{nn'}$ is the adjacency matrix of the graph of any angular sector and $B^{(\varphi)}_{n,n'}$ is the adjacency matrix of two angular sectors at an angular distance φ in units of $2\pi/N$.

Let us introduce the rotation operator $\widehat{L}$ defined by

$$\begin{aligned}\widehat{L}b_{n,\theta} &= b_{r,\theta+1}\widehat{L} \\ \widehat{L}b^\dagger_{n,\theta} &= b^\dagger_{r,\theta+1}\widehat{L}\,.\end{aligned} \tag{6.11}$$

The effect of the operator L is particularly easy to understand in the single particle case:

$$\widehat{L} \mid n,\theta\rangle = \widehat{L}b^\dagger_{n,\theta} \mid 0\rangle = b^\dagger_{n,\theta+1}\widehat{L} \mid 0\rangle = \mid n,\theta+1\rangle\,, \tag{6.12}$$

where we have assumed that the vacuum is invariant under a rotation $\widehat{L} \mid 0\rangle = \mid 0\rangle$.

Note that $\widehat{L}$ is unitary and its application N times gives the identity, $\widehat{L}^N = \mathbb{1}$. This implies that its eigenvalues are integer multiples of $2\pi/N$.

Another interesting property of L is that commutes both with the rotationally invariant Hamiltonians and with the number operator $\widehat{N}_p$,

$$[\widehat{H}_{\text{rot}}, \widehat{L}] = [\widehat{N}_p, \widehat{L}] = [\widehat{H}_{\text{rot}}, \widehat{N}_p] = 0\,. \tag{6.13}$$

Therefore $\widehat{H}_{\text{rot}}$, $\widehat{N}_p$, and $\widehat{L}$ form a complete set of commuting observables and the Hamiltonian is diagonal in blocks of constant $\widehat{L}$ and $\widehat{N}_p$. This allows us to simplify the problem of finding the ground state and the first excited states of the system, a very useful fact we will use in the next section.

Note that rotational invariance and foliability are not equivalent. There are graphs which can be foliated and are not rotationally invariant and vice-versa. An example is

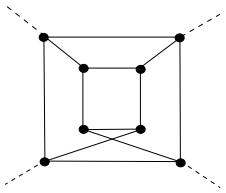

Figure 6.4: A foliated graph which is not rotationally invariant.

given in Fig. 6.4.

We have seen that both for the cases of foliated graphs and the rotationally invariant graphs, *the subspace spanned by the completely delocalized states is an eigenspace of the system.* In the foliated model, effective dynamics in this eigenspace are given by a one-dimensional Bose-Hubbard Hamiltonian. In the rotational invariant case, this eigenspace contains the ground state of the system. Thus, the ground state of graphs with both symmetries lies in the subspace of completely delocalized states and the computational effort to find it is equivalent to the solution of a one-dimensional Bose-Hubbard model. This allows us to analyze a complicated model using the approximation of a one-dimensional spin chain, with obvious advantages, especially for numerical work.

6.2 Regions of high connectivity as trapped surfaces

In [111], it has been observed that the Hamiltonian (6.63) caused trapping of matter in regions of higher connectivity. The basic mechanism is the following: consider a graph consisting of two set of nodes, A and B, separated by a set of points C on the boundary. Let the vertices in A be of much higher degree than the vertices in B, $d_A \gg d_B$ (see Fig. 6.5). If the number of edges departing from the set C and going to the set A is much higher than the number of edges going from C to B, then the hopping particles have a

high probability of being "trapped" into the region A.

Our task in this Section is to make this heuristic argument precise and determine whether these high connectivity configurations are spin-system analogues of trapped surfaces. We will do this by studying specific states that are graphs with symmetries that contain a core (trap) of N nodes. Fig. 6.6 is an example of such a graph. Such states are 1-foliated graphs and we will be able to use the properties we discovered above.

6.2.1 Classical trapping

In order to gain some intuition on the trapping, let us consider the classical analogue of the problem. In the classical setup, a particle has a well-defined position in some site of A. At each time step of length $\hbar/E_{\text{hop}}$, the particle randomly jumps to another site of the graph connected to its current site by an edge. This process is successively repeated until the particle escapes from A. How much time is required (on average) for the particle to escape from the highly connected region?

In this simple model, the probability that the particle jumps to a site outside A is

$$p_{\text{esc}} = \frac{N_{\text{ext}}}{N - 1 + N_{\text{ext}}}\,, \tag{6.14}$$

where N_{ext} is the number of links that connect a site in A with the environment, and N is the total number of sites in A. The evaporation time is then given by

$$t_{\text{ev}} = \frac{\hbar}{E_{\text{hop}}}\frac{1}{p_{\text{esc}}} \approx \frac{\hbar}{E_{\text{hop}}}\frac{N}{N_{\text{ext}}}\,, \tag{6.15}$$

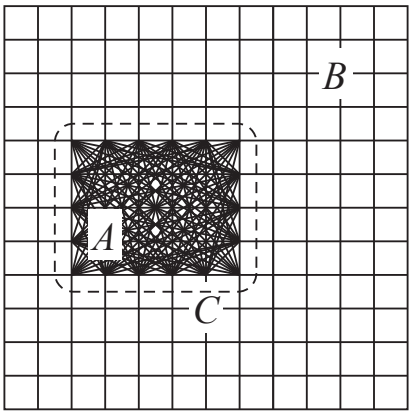

Figure 6.5: A region of higher connectivity in a regular graph.

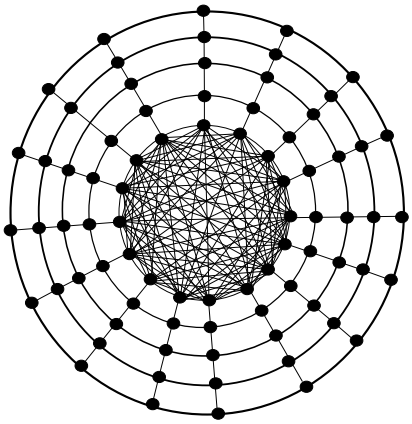

Figure 6.6: The $\mathcal{K}_N$ graph.

where we have assumed that $N \gg N_{\text{ext}}$. In the large N limit, the particle is trapped in A.

6.2.2 Quantum case: the $\mathcal{K}_N$ configuration

In this section we study the spectrum and the configuration of the ground state and the finite temperature states of the hopping Hamiltonian on the graph of Figure 6.6 which we will call the $\mathcal{K}_N$ graph. This is a 1-foliated graph with a completely connected core. We will show that the model on $\mathcal{K}_N$ can be solved analytically in the thermodynamic limit.

The position of a vertex of the $\mathcal{K}_N$ graph can be specified by means of the integer spherical coordinates r and θ, with ranges $0 \leq r \leq R-1$ and $0 \leq \theta \leq N-1$. Then, the

quantum state of a particle with a well-defined position in the graph can be written as

$$\mid r, \theta\rangle = b^{\dagger}_{r,\theta} \mid 0\rangle \,, \tag{6.16}$$

where $\mid 0\rangle$ is the vacuum state and $b^{\dagger}_{r,\theta}$ the corresponding creation operator. Using these coordinates, the hopping Hamiltonian defined by the $\mathcal{K}_N$ graph becomes

$$\begin{aligned} \widehat{H}_0 = \sum_{\theta=0}^{N-1} \sum_{r=0}^{R-1} \left(b^{\dagger}_{r+1,\theta} b_{r,\theta} + b^{\dagger}_{r,\theta+1} b_{r,\theta} + \text{h.c.} \right) \\ + \sum_{|\theta-\theta'|\geq 2} b^{\dagger}_{0,\theta'} b_{0,\theta} \,, \end{aligned} \tag{6.17}$$

where h.c. is the Hermitian conjugate. Note that the second term in Eq. (6.17) corresponds to hopping in the completely connected region, while the first sum is hopping outside that core. Our question is how the introduction of this completely connected region (the second sum) changes the spectrum and the eigenstates of the system.

Single particle case. Let us first work out the single particle sector of the Hamiltonian.

In order to determine the eigenstates and eigenvalues of $\widehat{H}_0$, we will write the Hamiltonian in the eigenbasis of the rotation operator $\widehat{L}$ defined in equation (6.11). The eigenstates of $\widehat{L}$ read

$$\mid r, \ell\rangle = \frac{1}{\sqrt{N}} \sum_{\theta=0}^{N-1} \mathrm{e}^{\mathrm{i}\, \frac{2\pi}{N} \ell\theta} \mid r, \theta\rangle \,, \tag{6.18}$$

with eigenvalues

$$\widehat{L} \mid r, \ell\rangle = \mathrm{e}^{\mathrm{i}\,\frac{2\pi}{N}\ell} \mid r, \ell\rangle \,, \tag{6.19}$$

where $\ell = 0, 1, \ldots, N-1$. The Hamiltonian is diagonal in blocks of constant ℓ and can be written as

$$\widehat{H} = \sum_{\ell=0}^{N-1} \widehat{H}_\ell \,, \tag{6.20}$$

where $\widehat{H}_\ell = \widehat{P}_\ell \widehat{H} \widehat{P}_\ell$ are the projections onto the eigenspaces of $\widehat{L}$ with the projectors $\widehat{P}_\ell$ defined as

$$\widehat{P}_\ell = \sum_{r=0}^{R-1} |r, \ell\rangle\langle r, \ell| \,. \tag{6.21}$$

Inserting Eq. (6.21) into the definition of $\widehat{H}_\ell$, we get

$$\begin{aligned} \widehat{H}_\ell = & -N\delta_{\ell 0}|0\rangle\langle 0| - 2\cos\left(\frac{2\pi}{N}\ell\right)\theta\left(r-\frac{1}{2}\right)|r\rangle\langle r| \\ & - (\mid r+1\rangle\langle r \mid + \mid r\rangle\langle r+1 \mid) \,, \end{aligned} \tag{6.22}$$

where $\theta(\cdot)$ is the Heaviside step function, introduced to make the second term of the right hand side vanish when $r = 0$.

Note that $\widehat{H}_\ell$ is translationally invariant in the limit $R \to \infty$ for $\ell > 0$. Therefore, it can

be analytically diagonalized by the discrete Fourier transform

$$\mid k_r, \ell\rangle = \frac{1}{\sqrt{R}} \sum_{r=0}^{R-1} \mathrm{e}^{\mathrm{i}\,\frac{2\pi}{R} k_r r} \mid r, \ell\rangle \,, \tag{6.23}$$

with $k_r = 0, \ldots, R-1$ and $1 \leq \ell \leq N-1$. We find

$$\widehat{H}_\ell \mid k_r, \ell\rangle = 2\left(1 - \cos\left(\frac{2\pi}{R} k_r\right) - \cos\left(\frac{2\pi}{N}\ell\right)\right) \mid k_r, \ell\rangle \tag{6.24}$$

up to $1/R$ corrections that vanish in the infinite limit.

Let us now consider the subspace $\ell = 0$ of the rotationally invariant states. Because the Hamiltonian commutes with $\widehat{L}$, the ground state $\mid GS\rangle$ of the system must be invariant under its action: $\widehat{L} \mid GS\rangle = \mid GS\rangle$. Therefore, $\mid GS\rangle$ belongs to this subspace. On it, we can explicitly construct the matrix for the Hamiltonian $\widehat{H}_{\ell=0}$:

$$\widehat{H}_{\ell=0} = -E_{\text{hop}} \begin{pmatrix} N & 1 & 0 & \cdots & 0 \\ 1 & 2 & 1 & \ddots & \vdots \\ 0 & 1 & 2 & \ddots & 0 \\ \vdots & \ddots & \ddots & \ddots & 1 \\ 0 & \cdots & 0 & 1 & 2 \end{pmatrix} . \tag{6.25}$$

It is a tridiagonal matrix with characteristic polynomial $p_R(\lambda) = \det(\widehat{H} - \lambda I)$ which can

be written in a recursive way as

$$
\begin{aligned}
&p_0(\lambda) = 1, \\
&p_1(\lambda) = -N\,, \\
&p_n(\lambda) = -(2-\lambda)p_{n-1}(\lambda) - p_{n-2}(\lambda)\,.
\end{aligned}
\tag{6.26}
$$

Note that because of the recursive relation, it is not clear whether the other eigenvalues apart from the first one depend on N or not.

It is easy to see that, if we rescale $E_{\text{hop}} = \tilde{E}_{\text{hop}}/N$ and take $N \to \infty$, the only element left in the matrix is the element associated to the $|0\rangle$ state. Thus, at $N \to \infty$, the ground state becomes $\mid r = 0, \ell = 0\rangle$ and the gap between it and the first excited state scales as N. In the thermodynamic limit, the ground state of the single particle sector corresponds to a particle completely delocalized in the complete graph,

$$
\lim_{N\to\infty} \mid GS\rangle = \mid r = 0, \ell = 0\rangle = \frac{1}{\sqrt{N}} \sum_{\theta=0}^{N-1} \mid 0, \theta\rangle\,. \tag{6.27}
$$

The rest of eigenvectors of the subspace $\ell = 0$ are orthogonal to $\mid GS\rangle = \mid r = 0, \ell = 0\rangle$, and therefore lie in the subspace spanned by $\mid r, \ell = 0\rangle$ with $r \geq 1$. The Hamiltonian can be analytically diagonalized in this subspace by the same transformation used in Eq. (6.23):

$$
\mid k, 0\rangle = \frac{1}{\sqrt{R}} \sum_{r=1}^{R-1} \mathrm{e}^{\mathrm{i}\,\frac{2\pi}{R}kr} \mid r, 0\rangle\,, \tag{6.28}
$$

with $k = 0, \ldots, R-2$.

In conclusion, we have seen that *the $\mathcal{K}_N$ model has a unique ground state which is protected by a gap which increases linearly with the size N of the completely connected region*. The rest of the eigenvalues form an energy band which is the same as if we had the $\mathcal{K}_N$ graph without the completely connected region,

$$E_{k\ell} = 2\left(1 - \cos\left(\frac{2\pi}{R}k_r\right) - \cos\left(\frac{2\pi}{N}\ell\right)\right) . \tag{6.29}$$

These results are numerically confirmed by Figs. 6.7 and 6.8. In Fig. 6.7, the energies of the ground state, the first excited state and the state with maximum energy are plotted against the size of the completely connected region. In Fig. 6.8, we have plotted the fidelity between the ground state of the system and the completely delocalized state in the completely connected region vs N.

Multi-particle case. Let us next analyze what happens when there are several particles in the $\mathcal{K}_N$ configuration, interacting with an on-site potential.

The Hamiltonian of the multi-particle $\mathcal{K}_N$ model can be decomposed in its one-body and two-body parts,

$$\widehat{H} = \widehat{H}_0 + \widehat{V} \tag{6.30}$$

where $\widehat{H}_0$ is defined in Eq. (6.17) and $\widehat{V}$ is an on-site interaction among the particles:

$$\widehat{V} = u\sum_{r=0}^{R-1}\sum_{\theta=0}^{N-1} b_{r\theta}^\dagger b_{r\theta}^\dagger b_{r\theta} b_{r\theta} , \tag{6.31}$$

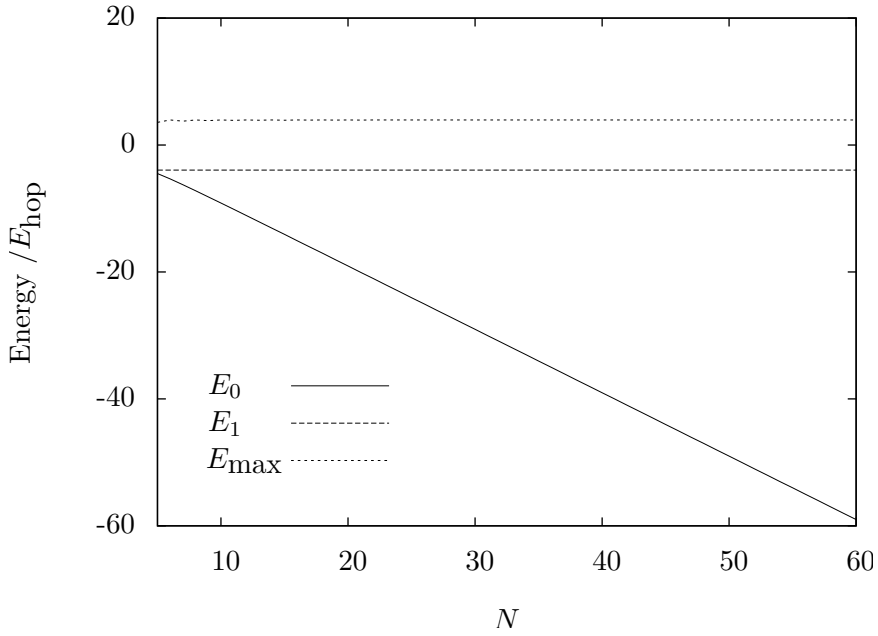

Figure 6.7: Plots of the energy E_0 of the ground state, the energy E_1 of the first excited state, and $E_{\rm max}$, the energy of the maximum energy state, against the size N of the completely connected region of the $\mathcal{K}_N$ graph, in the single particle sector. This plot has been realized for the full model with $R = 30$. Note that the gap $E_1 - E_0$ increases linearly with N.

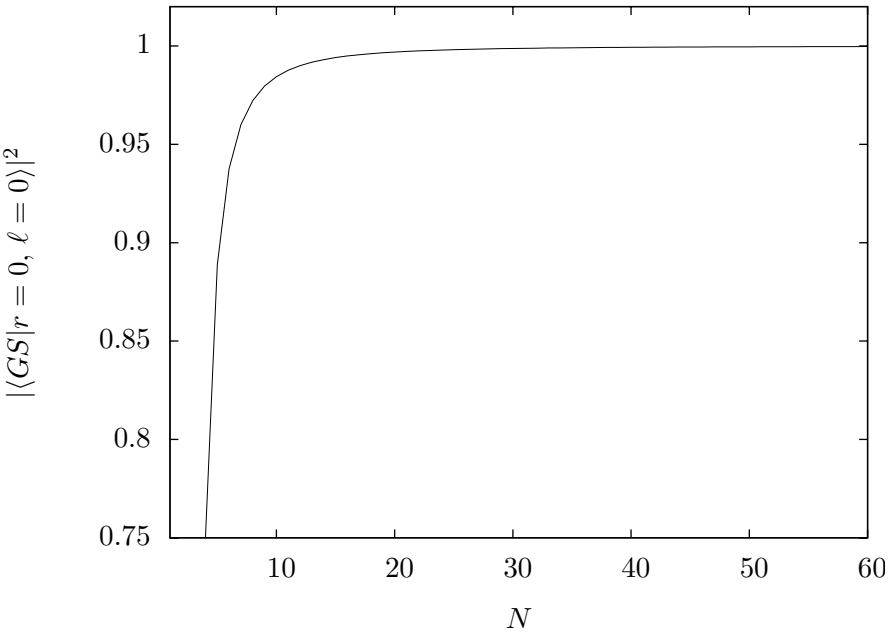

Figure 6.8: Fidelity between the completely delocalized state in the completely connected region $|r = 0, \ell = 0\rangle$ and the ground state against the size N of that region. The completely delocalized state $|r = 0, \ell = 0\rangle$ becomes the ground state of the system for large N.

with u the energy penalty for two particles in the same site.

Because the interaction $\widehat{V}$ commutes with the number operator $\widehat{N}$ and the rotation transformation $\widehat{L}$, $\widehat{H}$, $\widehat{L}$ and $\widehat{N}$ form a complete set of commuting observables. It is convenient to write $\widehat{H}_0$ and $\widehat{V}$ in terms of the creation and annihilation operators

$$\eta_{k\ell} = \frac{1}{\sqrt{RN}} \sum_{\theta=0}^{N-1} \sum_{r=0}^{R-1} \mathrm{e}^{\mathrm{i}\,\frac{2\pi}{R}kr}\, e^{\mathrm{i}\,\frac{2\pi}{N}\ell\theta} b_{r,\theta}, \quad \forall \ell \geq 1, \tag{6.32}$$

$$\eta_{k0} = \frac{1}{\sqrt{RN}} \sum_{\theta=0}^{N-1} \sum_{r=1}^{R-1} \mathrm{e}^{\mathrm{i}\,\frac{2\pi}{R-1}r}\, b_{r,0}, \tag{6.33}$$

$$\eta_{\mathrm{gs}} = \frac{1}{\sqrt{N}} \sum_{\theta=0}^{N-1} b_{0,\theta}\,. \tag{6.34}$$

As it has been previously shown, the one-body term in the Hamiltonian is

$$\widehat{H}_0 = -N\eta_{\mathrm{gs}}^\dagger \eta_{\mathrm{gs}} + \sum_{k\ell} E_{k\ell} \eta_{k\ell}^\dagger \eta_{k\ell}\,, \tag{6.35}$$

and the interaction reads

$$\begin{aligned}\widehat{V} = u \sum_{k\ell} \delta_{\ell_1+\ell_2,\ell_3+\ell_4} \delta_{k_1+k_2,k_3+k_4} \widehat{\eta}_{k_1\ell_1}^\dagger \eta_{k_2\ell_2}^\dagger \eta_{k_3\ell_3} \eta_{k_4\ell_4} \\ + u\, \eta_{\mathrm{gs}}^\dagger \eta_{\mathrm{gs}}^\dagger \eta_{\mathrm{gs}} \eta_{\mathrm{gs}}\,,\end{aligned} \tag{6.36}$$

where the sum runs over all possible k_i and ℓ_i for $i = 1, \ldots, 4$ and the Krönecker delta shows that the interaction conserves the quantum numbers ℓ and k. Note that the single-particle ground state is completely decoupled from the states of the energy band. There-

fore, the state of n particles,

$$\mid GS\rangle = \left(\eta_{\text{gs}}^{\dagger}\right)^{n} \mid 0\rangle \,, \tag{6.37}$$

is an eigenstate of the system with energy $-nN + un(n-1)/2$. Furthermore, as the interaction is a positive operator, we can ensure that $\mid GS\rangle$ is the ground state of the system as long as $n < N$.

Thus, *the ground state of the many-body problem is a Bose-Einstein condensate of delocalized particles at the completely connected region.* The large gap and the features of the on-site interaction make this condensate robust at finite temperatures and against adding interacting particles. Thus, the completely connected region of the $\mathcal{K}_N$ model can be considered a trapped surface.

However, it is not clear whether every completely connected region is a trapped surface. In particular, we would like to see what happens when the connectivity does not change as abruptly as in the $\mathcal{K}_N$ system. For this reason, in Section 6.4 we will parametrize the fall-off of the parameters and study the localization of particles. Moreover, we would like to relate this fall-off to an effective curved space-time geometry, as in an analogue gravity system. In order to do this, then, a correspondence between the connectivity of the graph and the curvature of the space-time is required. Establishing this relation is our task for the next section.

6.3 Correspondence between graph connectivity and curved geometry

In this section we establish a relation between the connectivity of a graph and the curvature of its continuous analogue geometry. In order to do this, we restrict the time-dependent Schrödinger equation to the manifold formed by the classical states, that is, single-particle states with a well-defined but unknown position. The equation of motion obtained corresponds to the equation of propagation of light in inhomogeneous media, similarly to black hole analogue systems. Once we have such a wave equation, we can extract the corresponding metric. In the second part of the section, the dispersion relation and the continuous limit are discussed for the transitionally invariant case.

6.3.1 Restriction of the time-dependent Schrödinger equation to the set of classical states

Since we want to study the dynamics of a single particle on a fixed graph, it is only necessary to consider the single particle sector. The one dimensional Bose-Hubbard model for a single particle reads,

$$\widehat{H}_0 = \sum_{n=0}^{M-1} f_{n,n+1} \left(\mid n\rangle\langle n+1 \mid + \mid n+1\rangle\langle n \mid \right) + \sum_n \mu_n |n\rangle\langle n| \,, \tag{6.38}$$

where $f_{n,n+1}$ are the tunneling coefficients between sites n and $n+1$, μ_n is the chemical potential at the site n, and M is the size of the lattice.

In this setup, let us introduce the convex set of classical states $\mathcal{M}_C$, parameterized as

$$\rho(\Psi) = \sum_{n=0}^{M-1} \Psi_n |n\rangle\langle n| \,, \tag{6.39}$$

where Ψ_n is the probability of finding the particle at the site n. The states in $\mathcal{M}_C$ are classical because the uncertainty in the position is classical, that is, they represent a particle with an unknown but well-defined position.

The aim of this section is to restrict the Schrödinger equation of the whole convex set of density matrices to the convex set $\mathcal{M}_C$ and obtain the effective equations of motion for the classical states. In order to do this we will follow the same procedure as in Ref. [67]. We will approximate the time evolution generated by $\widehat{H}_0$ without ever leaving the convex set $\mathcal{M}_C$. This procedure consists basically of two steps:

1. *Time evolution*. Insert the initial state $\rho(t) \in \mathcal{M}_C$ into the time-dependent Schrödinger equation to get its evolution $\rho(t + \Delta t)$ after a short time Δt.

2. *Restriction to $\mathcal{M}_C$*. Find the state in $\mathcal{M}_C$ that best approximates the evolved state $\rho(t + \Delta t)$.

If we take the infinitesimal limit $\Delta t \to 0$ of the previous steps we are going to get a differential equation for the field $\Psi_n(t)$.

Let us mention that the time-dependent Gross-Pitaevskii equation can also be derived by this method, that is, by restricting the Schrödinger equation to the manifold defined by states parametrized by $\mid \varphi\rangle = \exp\left(\int \mathcal{D}x\varphi(x)b_x^\dagger\right) \mid 0\rangle$, where $b_x^\dagger$ is the field operator that creates a particle at position x. In Ref. [67], the second step is something that must be done

in order to restrict the equations of motion to the desired manifold. Nevertheless, in our case, *decoherence* can give a physical interpretation to this step. Since our particle is under the effect of a noisy environment, its density matrix is going to be constantly dephased by the interaction between the particle and its reservoir.

If we insert $\rho(t)$ in the time-dependent Schrödinger equation we obtain:

$$\partial_t \rho(t) = \sum_n \partial_t \Psi_n(t) |n\rangle\langle n| = \mathrm{i}[\widehat{H}_0, \rho(t)]\,, \tag{6.40}$$

where, in general, the right hand side cannot be written in terms of the left hand side, and therefore the previous equation cannot be fulfilled. Note that the Hamiltonian pushes $\rho(t+\Delta t)$ out of the $\mathcal{M}_C$.

Thus, the best approximation to $\rho(t+\Delta t)$ in the convex set $\mathcal{M}_C$ is obtained by minimizing the distance

$$\| \sum_n \partial_t \Psi_n(t) |n\rangle\langle n| - \mathrm{i} \left[\widehat{H}_0, \rho(t)\right] \|\,, \tag{6.41}$$

For the Hamiltonian (6.38), the commutator $[\widehat{H}_0, \rho(t)]$ reads

$$[\widehat{H}_0, \rho(t)] = \sum_n f_{n,n+1} \left(\Psi_{n+1} - \Psi_n\right) \left(|\, n\rangle\langle n+1\,| + |\, n+1\rangle\langle n\,|\right)\,, \tag{6.42}$$

and therefore the state in $\mathcal{M}_C$ that best approximates $\rho(t+\Delta t)$ fulfills

$$\partial_t \Psi_n(t) = 0\,. \tag{6.43}$$

This forces us to consider the second order in Δt, and therefore the effective equation of motion for $\Psi_n(t)$ is going to be a second order differential equation in time. We then have

$$\partial_t^2 \rho(t) = \sum_n \partial_t^2 \Psi_n(t) |n\rangle\langle n| = -\frac{1}{\hbar^2} \left[\widehat{H}_0, [\widehat{H}_0, \rho(t)]\right] .$$

The dephased state in the position eigenbasis that best approximates $\rho(t + \Delta t)$ can be easily determined by computing the double commutator of the previous equation. It obeys the evolution

$$\begin{aligned} \frac{\hbar^2}{2}\partial_t^2 \Psi_n(t) = &- \left(f_{n,n+1}^2 + f_{n-1,n}^2\right) \Psi_n(t) \\ &+ f_{n-1,n}^2 \Psi_{n-1}(t) + f_{n,n+1}^2 \Psi_{n-1}(t) . \end{aligned} \tag{6.44}$$

In order to rewrite the previous expression in a nicer way, let us add and subtract the quantity $f_{n-1,n}^2(\Psi_{n+1}(t) + \Psi_n(t))$ in the right-hand side, obtaining

$$\begin{aligned} \frac{\hbar^2}{2}\partial_t^2 \Psi_n(t) = &f_{n-1,n}^2 \left(\Psi_{n+1}(t) + \Psi_{n-1}(t) - 2\Psi_n(t)\right) \\ &+ \left(f_{n+1,n}^2 - f_{n-1,n}^2\right) \left(\Psi_{n+1}(t) - \Psi_n(t)\right) . \end{aligned} \tag{6.45}$$

This equation becomes a wave equation in the continuum,

$$\partial_t^2 \Psi(x,t) - \partial_x \left(c^2(x) \partial_x \Psi(x,t)\right) = 0 , \tag{6.46}$$

where

$$\frac{1}{c(x)} = \sqrt{\frac{\hbar^2}{2f^2(x)E_{\text{hop}}^2}} = \frac{\hbar}{E_{\text{hop}}\sqrt{2f^2(x)}}\,, \tag{6.47}$$

and $\Psi(x,t)$ and $f(x)$ are the continuous limit functions of $\Psi_n(t)$ and $f_{n,n-1}$ respectively.

We have shown that the equation of motion of the Bose-Hubbard model, restricted to the convex set formed by classical states, is the wave equation. This is a significant result that establishes a relation between the coupling constants of the Bose-Hubbard model and the speed of propagation of the fields $\Psi(x,t)$. Equation (6.46) has the same form as the equation for propagation of light in media with a space-dependent refraction index, as is also the case in black hole analogue systems [69].

A few comments are in order. In equation (6.46), *the constant of the speed of light is quantized*. It is proportional to the inverse of the number of links between the nodes in this simplified model. This constant depends on the hopping coupling constant of the hamiltonian, E_{hop}. Finally, even though equation (6.46) is for a scalar quantity, the analogy with a Klein-Gordon field can not be pushed too far. The equation refers to the 1-particle density from which we started from, $\Psi_n(t) = \langle n \mid \rho(t) \mid n\rangle$, and so is completely classical. A generalization of equation (6.46) to the case of many distinguishable interacting particles is given in detail in the Appendix, where we analyze also the effect of a local and non-local interaction.

6.3.2 Dispersion relation and continuum limit

Let us consider in more detail the translational invariant case in which $f_{n-1,n} = f$ and $\mu_n = \mu$ for all n. In this case, the continuous wave equation (6.46) becomes

$$\partial_t^2 \Psi(x,t) - c^2 \partial_x^2 \Psi(x,t) = 0\,, \tag{6.48}$$

where c is the speed of propagation.

In order to understand the continuum limit, we evaluate the dispersion relation for the propagation of probability in the translationally invariant case. Let us introduce a discrete Fourier transform in the spatial coordinate and a continuous Fourier transform in the temporal coordinate, given by

$$\Psi_n(t) = \frac{1}{\sqrt{M}} \sum_{k=0}^{M-1} \tilde{\Psi}_k(t) e^{-\mathrm{i}\,\frac{2\pi}{M} nk}\,, \tag{6.49}$$

and $\tilde{\Psi}_k(t) = Ae^{\mathrm{i}\,\omega_k t} + Be^{-\mathrm{i}\,\omega_k t}$. After a straightforward calculation, we find that the relation between ω_k and k is given by

$$\omega_k c = \sqrt{2}\,\sqrt{1 - \cos\left(\frac{2\pi}{M} k\right)}. \tag{6.50}$$

Note that this dispersion relation is different from that of the quantum excitations. In order to see this, we Fourier transform the Hamiltonian in the translational invariant modes. We define the field momentum $\Psi_k(t)$ as $\Psi_k(t) = \langle k \mid \rho(t) \mid k \rangle$, where $\mid k\rangle = \sum_m e^{\mathrm{i}\,2\pi km/M}/\sqrt{M} \mid m\rangle$ are the eigenstates of the translationally invariant Hamiltonian

$\widehat{H}_0 \mid k\rangle = \hbar\omega_k^H \mid k\rangle$, with

$$\hbar\omega_k^H = 2\left(1 - \cos\left(\frac{2\pi k}{M}\right)\right). \tag{6.51}$$

Therefore,

$$\Psi_k(t) = \sum_{n,m} e^{\mathrm{i}\,2\pi k(n-m)/M}\rho_{n,m}(t), \tag{6.52}$$

and, for the classical states $\rho_{n,m}(t) = \delta_{n,m}\Psi_n(t)$,

$$\Psi_k(t) = \frac{1}{M}\sum_{n=0}^{M-1}\Psi_n(t) = \frac{1}{M}. \tag{6.53}$$

Note now that Eq. (6.51) differs from (6.50). In fact, at the quantum level, the continuum limit gives the ordinary galilean invariance, while at the quantum level, the continuum limit gives excitations (time-evolving probability densities) which are Lorentz invariant.

However, the continuum limit is tricky because we have continuous time and discrete space, and no *spatial* scale to send to zero with the inverse of the number of lattice points (the graph is not embedded in any geometry). Thus the continuum limit is in the time scale of the modes. If we rescale $\omega_k \to \tilde{\omega}_k/M$ (or equivalently c), we find that

$$\tilde{\omega}_k\, c = \sqrt{2M}\sqrt{1 - \cos\left(\frac{2\pi}{M}k\right)}, \tag{6.54}$$

and, therefore,

$$\lim_{M\to\infty} \tilde{\omega}_k \approx 2\pi \frac{k}{c}. \tag{6.55}$$

That is, only modes that are slow with respect to the time scale set by c see the continuum. Note that by rescaling the speed of propagation c, the continuum limit can be obtained by a double scaling limit, $E_{\text{hop}} \to E_{\text{hop}} M$ and $M \to \infty$ for lattice size M. In this limit, the probability density has a Lorentz invariant dispersion relation. Another interesting rescaling which gives Lorentz invariant dispersion relations is the rescaling of $\hbar$.

To conclude the discussion, let us note that the speed of propagation of the probability sets the timescale of the interaction: if there are P points with constant speed of light given by c, then the timescale of the propagation of the interaction in the classical limit in that region is given by $t_{\text{dyn}} = P/c$.

An embedding of the graph in space, on the other hand, would mean requiring that $\Psi_n(t)$ depends on a point in space and a length scale a (the lattice spacing): $\Psi_n(t) \equiv \Psi(b_0 + na, t)$, and that the coupling constant scales as $E_{\text{hop}} \to E_{\text{hop}}/a$. In this case the continuum limit $a \to 0$ gives the ordinary dispersion relation.

6.3.3 Lieb-Robinson bound for hopping bosons

A general result, which will now be useful, has been given in [161]. This is strictly related to our result, as it establish a finite speed of propagation for the interacting Bose-Hubbard

model, defined as:

$$\hat{H}_{BH} = -E_{hop} \sum_{j,k} A_{j,k} (\hat{b}_j^\dagger \hat{b}_k + h.c.) + \frac{U}{2} \sum_j \hat{N}_j (\hat{N}_j - 1) - \mu \sum_j \hat{N}_j. \tag{6.56}$$

In the limit $U \to \infty$ we obtain a Bose-Hubbard model with Hard-Core bosons. Here we consider the adjacency matrix being the one of a graph G given by a square lattice, where there exist a natural metric, given by $d(j,k) = |j-k|$. The arguments directly generalize to Hamiltonians of the form

$$\hat{H}_{BH} = -E_{hop} \sum_{j,k} A_{j,k} (\hat{b}_j^\dagger \hat{b}_k + h.c.) + f(\{\hat{N}_{1,j} \cdots \hat{N}_{L,j}\}_{j \in G}). \tag{6.57}$$

The result is similar to ours, since in order to obtain the bound, we focus on particular expectation values, as the local particle density, given by $\psi_j(t) = \text{tr}(\hat{N}_j \hat{\rho}(t))$. Also in this case, the proof of the result that we are going to describe, relies on the time derivative of $\psi_j(t)$. Using standard bounds, one's can prove that:

$$|\dot{\psi}_j(t)| \leq 2E_{hop} \sum_{j,k} A_{j,k} |\text{tr}(\hat{b}_j^\dagger \hat{b}_k \hat{\rho}(t))| \tag{6.58}$$

Using then the operatorial version of the Cauchy-Schwarz inequality, one can show that the following inequality holds

$$|\dot{\psi}_j(t)| \leq E_{hop} \big(D \; \psi_j(t) + \sum_{j,k} A_{j,k} \psi_k(t) \big), \tag{6.59}$$

where D is the degree of the graph. An equality can then be imposed, and integrating the resulting equation, one obtains

$$\psi_i(t) \leq e^{DE_{hop}t}[e^{E_{hop}At}]_{ij}\psi_j(t). \tag{6.60}$$

An analysis on the operator exponential shows that it is possible to bound also the off-diagonal elements, as:

$$[e^{E_{hop}At}]_{ij} \leq Ce^{\bar{v}t-d(i,j)} \tag{6.61}$$

with $\xi \approx 3.59$, and $C \approx 10$. Thus, with the prefactor, the Lieb-Robinson speed becomes $v = \bar{v} + DE_{hop}$.

We notice that the differential equation that we obtained in 6.46 is tighter than this Lieb-Robinson speed, as for us $\bar{v} = 0$. We have implicitly assumed that the particles were Hard-Core bosons, thus $U = \infty$. We would like to stress that $\bar{v} = 0$ is obtained also for the case $U = 0$ [161].

It is usually believed that the Lieb-Robinson bound is associated to a classical light cone, i.e. a classical Doppler effect. Instead, here we have shown that this bound could be related to a relativistic effect. How general is this result is an open question and we believe it should be further investigated.

6.4 Model with parametrized fall-off of connectivity

In this section, we study a graph with a trapped surface (completely connected region) whose boundary is extended and the connectivity of its nodes decreases gradually towards the outer edge of the boundary. We parametrize the fall-off of the parameters of the model and study the localization of a one-particle state. We use the techniques developed in Secs. 6.1 and 6.2 to find the ground state of the system and check its robustness against finite temperature and many interacting particles.

This section summarizes the two main ideas of this chapter: the relation between the connectivity of a graph and the optical parameter, and the analysis of the power of trapping of a completely connected region.

6.4.1 The Model

Let us consider a 2-dimensional rotational invariant graph where the connectivity $f_{r,r+1}$ between two layers r and $r+1$ is not constant ($\mathcal{K}_N$ case), but decreases as

$$-f_{r,r+1} = E_{hop} d_{r,r+1} \sqrt{\frac{N_r}{N_{r+1}}} = \left(1 + \frac{N}{r^\gamma}\right) . \tag{6.62}$$

$d_{r,r+1}$ is the relative degree of a site of the r-th subgraph towards the $r+1$-th subgraph, N_r is the number of vertices in the layer r, and γ is a parameter that controls how fast the connectivity decreases. Note that this choice is consistent because we can always tune E_{hop} to be small enough, $N_r = N$ uniform, and $d_{r,r+1}$ to be such that we can approximate the rhs of Eq. (6.62). The $\mathcal{K}_N$ model corresponds to $\gamma \to \infty$ together with N. We expect

that the larger γ is, the larger is the localization.

6.4.2 Trapped surface

The rotational symmetry allows us to perform the same diagonalization procedure followed in Sec. 6.2. That is, we will diagonalize the Hamiltonian in blocks corresponding to the eigenspaces of the rotation operator $\hat{L}$. Unlike the $\mathcal{K}_N$ graph, the diagonalization in such subspaces must be done numerically. This is not a problem in the single particle sector. We can then determine the ground state and the gap of the system.

In Fig. 6.9, we have found the spectrum of the system. We see that the ground state is protected by a gap that increases linearly with the size of the completely connected region N. By the same argument as in the $\mathcal{K}_N$ model, this gap guarantees that the completely connected region is a trapped surface robust against finite temperature and against adding several interacting particles.

To characterize the ground state of the system, the probability distribution of the position of the particle is plot in Fig. 6.10. We note that, unlike the $\mathcal{K}_N$ model, the particle is not completely localized inside the trapped surface, but localized in a small region in and around the trapping surface.

In Fig. 6.11, the localization of the particle inside the completely connected region is plotted against its size and for three different parameters $\gamma = 1/2, 1$ and 2. Both this plot and Fig. 6.10 illustrate that, the higher the parameter γ, the stronger the localization in the completely connected region.

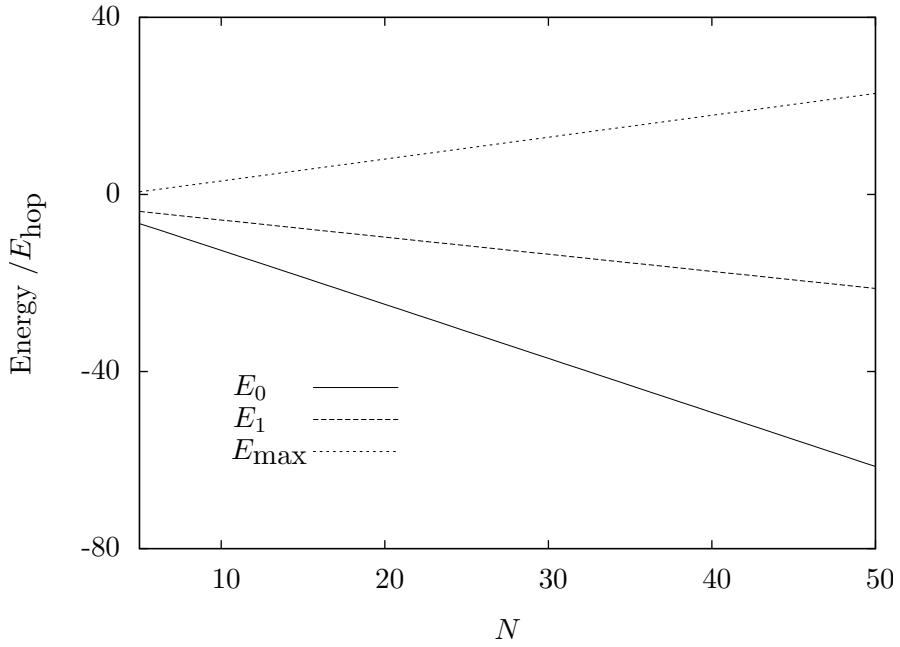

Figure 6.9: Plot of the energies of the ground state E_0, the first excited state E_1, and the state with maximum energy E_{max}, with respect to the size of the trapping surface, N, for a rotational invariant graph with decaying connectivity $(1 + N/r)$, in the single particle sector. Note that the gap $E_1 - E_0$ increases linearly with N.

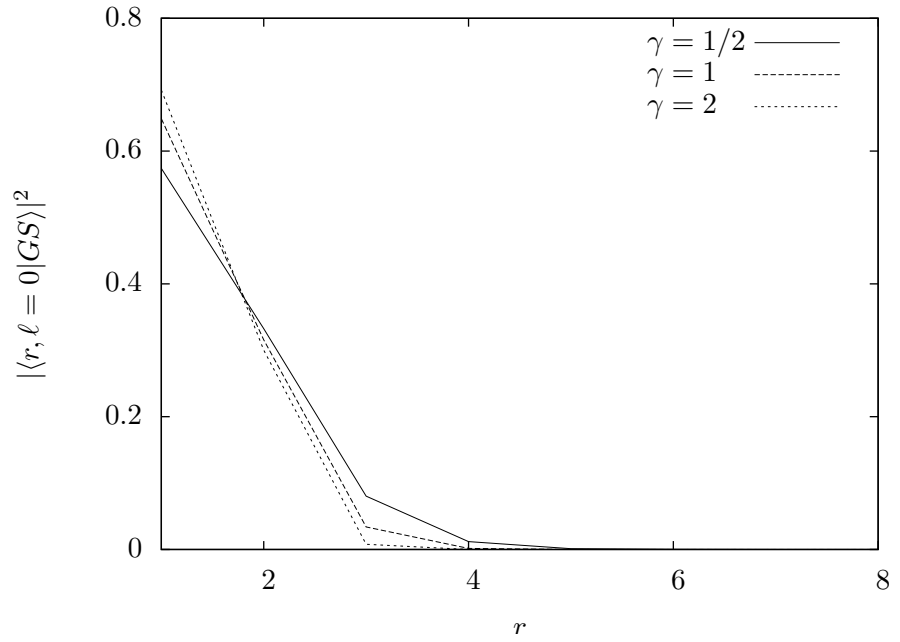

Figure 6.10: Probability distribution of the position of the particle. The particle is completely confined around the trapping surface. The larger the fall-off coefficient γ, the larger the confinement.

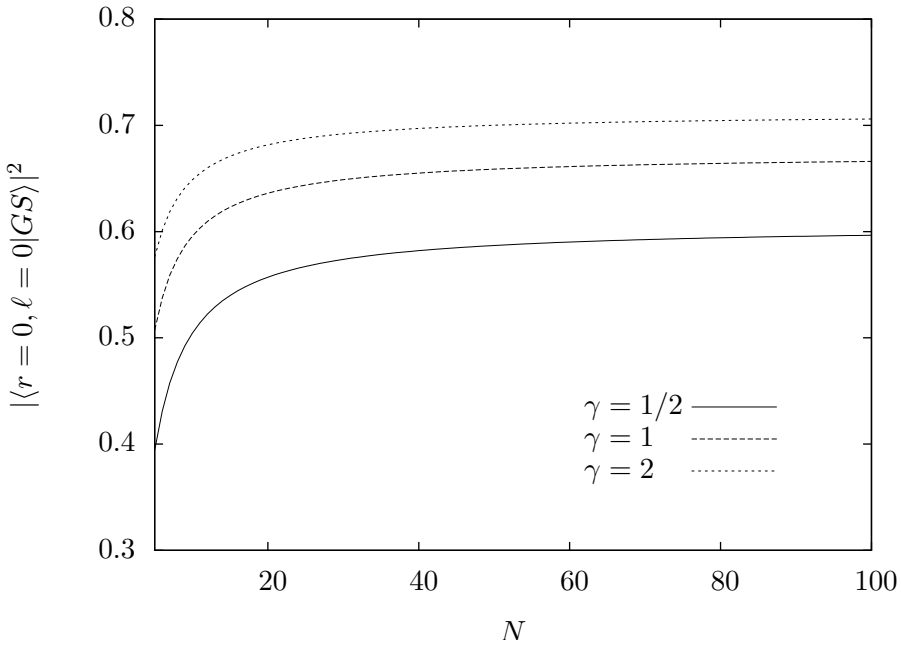

Figure 6.11: Localization of a single particle in a trapped surface vs its size. The localization of the particle increases with the size N and the fall-off coefficient γ (see the definition of γ in Eq. (6.62)).

6.5 Emergence of the mass for the scalar field

As we have seen, the equation of motion for the particle on the graph, is the one of a massless scalar field. Moreover, inserting a chemical potential is useless, as the term cancels when taking a second derivative of the field. We here describe two mechanism to obtain a mass for the field [2].

6.5.1 Emergence of the mass from disordered locality

A fascinating idea proposed by Wheeler in the early years of Quantum Gravity, is that, at the Planck scale, geometry may be bumpy due to quantum fluctuations. This is the *quantum foam* [108]. While intuitively natural, this idea is very complicated to put into

[2]This section is based on the work of [112] and [113]. The role of the author was the derivation of the new effective equation with the correction due to the superposition of graphs, and the calculation of the running of the effective masses.

action. In the present section, we will use the framework of Quantum Graphity [80, 111, 112] to construct a simple model of quantum foam.

A key feature of a quantum foam is its non-local nature. While non-locality is undesirable in quantum field theory, the situation in quantum gravity is open. It is often said that the only way to cure the divergences appearing perturbatively in quantizations of gravity without introducing new physics (i.e., string theory or super-symmetric extensions of gravity), is to introduce some kind of non-locality in the action which smears out Green functions evaluated on one point only. Until now, ghosts in the theory have blocked research in this direction (some progress has been achieved recently in [56]). For the purposes of the present work, it is important to note that there are two possible types of non-locality which contribute in different ways. One, violation of *microlocality*, disappears when the cut-off is taken to zero, while the other, violation of *macrolocality*, or *disordered locality*, does not [15]. Violations of macrolocality amount to the presence of what a relativist would call a *wormhole* [110], a path through spacetime disallowed in a Lorentzian topology. General relativity allows for such paths and, in principle, they should be taken into account in a full quantum theory of gravity. In principle, in order to have traversable wormholes, the common positive-energy conditions and some other conditions on the throats have to be satisfied. In principle, the analogy between links violating macrolocality in graphs and wormholes could be considered far-fetched. However, the effect of the two is the same: particles have the possibility to take shortcuts. Thus we believe that by modeling wormholes with macrolocal links, even though we are not studying wormholes *per se*, we are studying their effect on quantum particles.

Also, in graph-based quantum gravity states, such as in Loop Quantum Gravity [33], Causets [120] or Quantum Graphity [121], spacetimes which are not macrolocal are very natural, and violation of macrolocality appears in the form of non-local links. A first study of the physics of these non-local links was carried out in [15, 122].

We will extend eqn. (6.46) to one which allows the interaction with a static quantum foam. Instead of a classical background state (a single graph), we will consider a state that is a superposition of many graphs. This amounts to a quantum foam with a superposition of Planck scale sized wormholes. In our setting, the intrinsic discreteness of the graph sets the minimum scale. Assuming foliability of the graph, we can define a metric distance as in [112]. We can then study the effect of the *quantumness* of the graph on the dispersion relations. It is natural to construct graph states in which the largest contribution comes from the graph with the Lorentz invariant dispersion relations. The states with non-local links violate macrolocality and give corrections to Lorentz invariance. We will construct states with a distribution of wormholes which is suppressed by their combinatorial length. In addition, the distribution depends on the density of wormholes. We will then calculate the effect on the Lorentz dispersion relations in the continuum limit. The result is, as expected, a non-local differential equation for the evolution of the particle probability density.

It is reasonable to expect that a wormhole will violate local Lorentz invariance. A particle can hop through the wormhole and behave like a superluminal particle. As we will see, the presence of all these shortcuts has an effect on the local speed of propagation of probability density. Also, we will find that the probability density acquires a mass which

depends on the density of wormholes. The overall dispersion relation is thus Lorentz invariant and with a square-positive mass. However, this depends on the distribution of wormholes and thus we will study two particular cases. Using the framework of Quantum Graphity and the techniques developed in [112], we will calculate the emergent mass and the constants appearing in the effective equation.

We will study the model for a particular class of graphs that have been conjectured to be analogues of trapped surfaces. We are interested in the approximation $k \ll E_{hop}$, which can be seen as the equivalent of ignoring the backreaction of the matter on the geometry. As in [112], we will consider an Hamiltonian of the form

$$\widehat{H} = \widehat{H}_v + \widehat{H}_{\text{hop}}. \tag{6.63}$$

In this case, the total number of particles on the graph is a conserved charge. $\widehat{H}_v$ and $\widehat{H}_{links}$ are constants on fixed graphs with fixed number of particles. The Hamiltonian is the ordinary Bose-Hubbard model on a fixed graph, but that graph can be unusual, with sites of varying connectivity and with more than one edge connecting two sites. Our aim will then be to study the non-local and quantum corrections to the effective geometry which can be encoded in the graph, as shown in [112]. Even on a fixed lattice, the Hubbard model is difficult to analyze, with few results in higher dimensions. It would seem that our problem, propagation on a lattice with connectivity which varies from site to site is also very difficult. Fortunately, it turns out that for our purposes it is sufficient to restrict attention to lattices with certain symmetries and then to restrict to an effective

1+1 dimensional model.

A non-local state distribution

In this section, we show the effect of having a quantum superposition of graph in (6.67) on the equation (6.45). *The effect of a quantum superposition of graphs.* In order to do the explicit calculation, we will modify the Bose-Hubbard interaction. Let us consider a one-dimensional Bose-Hubbard of the form,

$$\widehat{H} = \sum_i A_{i,i-1}(\hat{a}_i^\dagger \hat{a}_i + h.c.) \tag{6.64}$$

and then consider its generalization, from $A_{i,j} = \delta_{j,i-1} + \delta_{j,i+1}$, to $\widehat{A}_{i,j} = \widehat{N}_{ij}$, with $\widehat{N}_{ij} = \hat{b}_{ij}^\dagger \hat{b}_{ij}$ and $\hat{b}_{ij}$,$\hat{b}_{ij}^\dagger$ the ladder operators on the Hilbert space of the link ij. $\widehat{N}_{ij}$ is then the number operator on the Hilbert space of the graph, as usually considered in Quantum Graphity. This allows, instead of using fixed *classical* graphs, fixed *quantum* graphs, where the state $|\psi_{graph}\rangle$ is superposition of different graphs. The full quantum Hamiltonian for the system is, as usual, on an Hilbert space of the form

$$|\psi_{total}\rangle = Span\{|\psi_{graph}\rangle \otimes |\psi_{bosons}\rangle\}. \tag{6.65}$$

Using this, we want now to repeat the same calculation we performed in the previous sections, i.e. compute:

$$\partial_t^2 \psi_z(t) = -i\, Tr\{[\widehat{H}, [\widehat{H}, \widehat{\rho}(t)]]\widehat{N}_z'\}, \tag{6.66}$$

with $\psi_n = \langle \widehat{N}'_n \rangle$, $\widehat{N}'_n$ number operator on the bosons defined on the node n, and $\widehat{\rho}$ the density matrix on the total system. Let us assume that the graph is not dynamical. We will also to use the Born approximation, that is,

$$\widehat{\rho}(t) \approx \widehat{\rho}_g \otimes \widehat{\rho}_b(t), \tag{6.67}$$

with $\widehat{\rho}_g$ the density matrix of the graph and $\widehat{\rho}_b(t)$ the density matrix of the bosons. This approximation allows us to consider a particle disentangled enough from the graph to be "followed" using the equation (6.46). It is also a physical requirement, which accounts for the existence of the particle on its own. In general, we expect that at long times the full Hamiltonian thermalizes to a specific graph, depending on the parameter of the Hamiltonian which defines the metastable state. Later on, we will rescale the coupling constant of the hopping Hamiltonian in order to obtain the continuum limit. Thus, one could think that this rescaling affects the state of the graph at infinity. However, the hopping of the bosons allows the graph to thermalize, as it has been shown in [111]. Rescaling this constant, just changes the time it takes for the system to thermalize, but not the asymptotic state of the graph. As a matter of fact, we do not know yet a Hamiltonian which gives a specific graph state asymptotically. However, the results of [123] in two dimensions and those of [80], support the conjecture that, in general, such a Hamiltonian exists.

Based on these considerations, we conjecture the following graph state, $|\psi_{graph}\rangle = |\psi_{cl}\rangle + |\psi_{nl}\rangle$ with $\langle \psi_{cl} | \psi_{nl} \rangle = 0$. $|\psi_{nl}\rangle$ is a correction to the classical graph state $|\psi_{cl}\rangle$ considered in [112] that we will discuss (and construct) in the next section. For the time being,

let us consider the effect of this correction on eqn. (6.45). We have $\widehat{\rho}_g = |\psi_{graph}\rangle\langle\psi_{graph}|$. Thus:

$$\widehat{\rho}_g = |\psi_{cl}\rangle\langle\psi_{cl}| + |\psi_{nl}\rangle\langle\psi_{nl}| + (|\psi_{nl}\rangle\langle\psi_{cl}| + |\psi_{cl}\rangle\langle\psi_{nl}|). \tag{6.68}$$

Let us now evaluate these traces. A straightforward calculation shows that,

$$\begin{aligned} -\frac{E_{hop}^2}{\hbar^2}\partial_t^2\psi_n &= Tr\ \{(\widehat{H}^2\widehat{\rho} + \widehat{\rho}\widehat{H}^2 - 2\widehat{H}\widehat{\rho}\widehat{H})\widehat{N}_z\} \\ &= 2\sum_{ij,mn}\big[Tr\{\widehat{A}_{ij}\widehat{A}_{mn}\widehat{\rho}_g\}Tr\{\hat{a}_i^\dagger\hat{a}_j\hat{a}_m^\dagger\hat{a}_n\widehat{\rho}_b\widehat{N}_z\} \\ &- Tr\{\widehat{A}_{ij}\widehat{\rho}_g\widehat{A}_{mn}\}Tr\{\hat{a}_i^\dagger\hat{a}_j\widehat{\rho}_b\hat{a}_m^\dagger\hat{a}_n\widehat{N}_z\}\big]. \end{aligned} \tag{6.69}$$

We now substitute the equation for $\widehat{\rho}_g$, and obtain:

$$-\frac{E_{hop}^2}{\hbar^2}\partial_t^2\psi_n = \tilde{\triangle}\psi_n(t) + C_n(t), \tag{6.70}$$

with $\tilde{\triangle}\psi_n(t)$ is the discrete second derivative and $C_n(t)$ is:

$$C_n(t) = 2\sum_{ij,mn}\big[P_{ijmn}Tr\{\hat{a}_i^\dagger\hat{a}_j\hat{a}_m^\dagger\hat{a}_n\widehat{\rho}_b\widehat{N}_z\} - Q_{ij}Q_{mn}Tr\{\hat{a}_i^\dagger\hat{a}_j\widehat{\rho}_b\hat{a}_m^\dagger\hat{a}_n\widehat{N}_z\}\big], \tag{6.71}$$

with:

$$P_{ijmn} = \langle\psi_{nl}|\widehat{A}_{ij}\widehat{A}_{mn}|\psi_{nl}\rangle, \tag{6.72}$$

$$Q_{ij} = \langle\psi_{nl}|\widehat{A}_{ij}|\psi_{nl}\rangle, \tag{6.73}$$

Figure 6.12: The intuitive picture of non-local links inserted in the graph.

where we used the orthogonality condition $\langle \psi_{nl} | \psi_{cl} \rangle = 0$.

Our task now is to evaluate these two quantities on different classes of interesting states.

The choice of the quantum state for the graph

Let us now introduce the states on which we will evaluate the quantities defined in the previous section, P_{ijmn} and Q_{ij}. Motivated by the fact that we can reduce using the translationally symmetric graphs to one line, we will restrict our attention to a one-dimensional lattices.

Let us consider first a metric on the classical graph, with $d(i,j)$ the distance between the nodes of the classical graph $|\psi_{cl}\rangle$, with all the ordinary properties of distances. On a one-dimensional line this distance could be, for instance, given by $|i-j|$. Let us then construct states with non-local links on top. We want to penalize states with too long non-local links. We then introduce a factor $\rho(i,j)$, which depends on a distance $d(i,j)$ evaluated on the base graph, assuming that $d(i,j) \geq 0$, and a parameter l describing how non-local the links are w.r.t. the length of the graph. Then we define the operator:

$$\widehat{T_l} = \sum_{i<j} \rho(i,j)\ \hat{a}^{\dagger}_{ij}, \tag{6.74}$$

with

$$\sum_{i<j} \rho(i,j)^2 = 1, \tag{6.75}$$

which ensures that $\rho(i,j)^2$ can be interpreted as a classical probability distribution. When applied to $|\psi_{cl}\rangle$ this operator generates a superposition of all the possible non-local links which can be created on $|\psi_{cl}\rangle$, with a factor that with the distance of the links,

$$|\psi^1_{nl}\rangle = \widehat{T}_l|\psi_{cl}\rangle, \tag{6.76}$$

and we can imagine to apply this operator several times to create more non-local links,

$$|\psi^R_{nl}\rangle = \frac{\widehat{T}^R_l}{R!}|\psi_{cl}\rangle. \tag{6.77}$$

The meaning to give to l is thus that of a cut-off in the length of these non-local links. Note that we can bias the number of links on which we want to peak the quantum non-local state the same way,

$$\widehat{\mathfrak{T}}^K_l = \sum_{s=1}^{\infty} \frac{K^s}{s!}\widehat{T}^s_l = e^{K\widehat{T}_l} - 1. \tag{6.78}$$

We see then that we can write the quantum state for the graph in the convenient form:

$$|\psi_{nl}\rangle = \left[1 + e^{K\widehat{T}_l}\right]|\psi_{cl}\rangle. \tag{6.79}$$

This state depends explicitly on two parameters, l and K, and on the classical graph together with its distance. On this state we now want to evaluate:

$$P_{ijmn} = \langle \psi_{nl} | \widehat{A}_{ij} \widehat{A}_{mn} | \psi_{nl} \rangle = \langle \psi_{cl} | \widehat{\mathfrak{T}}_l^{K\dagger} \widehat{A}_{ij} \widehat{A}_{mn} \widehat{\mathfrak{T}}_l^K | \psi_{cl} \rangle, \tag{6.80}$$

and

$$Q_{ij} = \langle \psi_{nl} | \widehat{A}_{ij} | \psi_{nl} \rangle = \langle \psi_{cl} | \widehat{\mathfrak{T}}_l^{K\dagger} \widehat{A}_{ij} \widehat{\mathfrak{T}}_l^K | \psi_{cl} \rangle. \tag{6.81}$$

Let us then consider first the average. We note that, since $\widehat{A}_{ij}$ acts like a projector, and states with different powers of the $\widehat{T}_l$ operators are orthogonal, we can write:

$$Q_{ij} = \sum_{s=1}^{\infty} \frac{K^{2s}}{s!^2} \langle \psi_{cl} | T_l^{\dagger s} \widehat{A}_{ij} T_l^s | \psi_{cl} \rangle. \tag{6.82}$$

To clarify the idea, let us consider the case in which we add just a link. In this case, the state is the sum over all possible links which can be created, with a factor $\rho^2(i,j)$.This link can be created in one way only, and so $\widehat{A}_{ij}$ projects on the only state which can be non-zero. A very straightforward calculation shows that

$$\langle \psi_{cl} | T_l^{\dagger 1} \widehat{A}_{ij} T_l^1 | \psi_{cl} \rangle = 2\ \rho^2(i,j). \tag{6.83}$$

For the higher order term, we instead have:

$$\langle\psi_{cl}|T_l^{\dagger s}\widehat{A}_{ij}T_l^s|\psi_{cl}\rangle = \rho^2(i,j)\sum_{i_1,j_1,\cdots,i_{s-1},j_{s-1}}\prod_{l=1}^{s-1}\rho^2(i_l,j_l). \tag{6.84}$$

It is easy to see that

$$\sum_{i_1,j_1,\cdots,i_{s-1},j_{s-1}}\prod_{l=1}^{s}\rho^2(i_l,j_l) \approx 2^s\ s\ (l\ L)^s, \tag{6.85}$$

due to the fact that the integration is over the line, while the distribution has an extension of *circa* l combinatorial points. The factor 2^s comes from the fact that there are 2 points we are summing over and the s factor from the s sums appearing in T_l^s. Thus, we can write:

$$\langle\psi_{cl}|T_l^{\dagger s}\widehat{A}_{ij}T_l^s|\psi_{cl}\rangle = c_s\ \rho^2(i,j)\ 2^s\ s\ (L\ l)^{s-1}. \tag{6.86}$$

In principle, given a distribution, we can calculate this factor from eq. (6.85). We will calculate these factors later for two particular distributions. Plugging eqn. (6.86) into Q_{ij}, we obtain

$$Q_{ij} = \sum_{s=1}^{\infty}\frac{K^{2s}}{s!^2}\ 2^s\ s\ (L\ l)^{s-1}\rho^2(i,j)c_s = \rho^2(i,j)R(K,l\ L), \tag{6.87}$$

with:

$$R(K,l\ L) = \sum_{s=1}^{\infty}\frac{K^{2s}}{s!^2}\ c_s\ 2^s\ s\ (l\ L)^{s-1}, \tag{6.88}$$

and, therefore,

$$Q_{ij}Q_{mn} = \rho^2(i,j)\rho^2(m,n)R(K,l\ L)^2. \tag{6.89}$$

We can, in fact, do an analogous calculation for P_{ijmn} and find that:

$$P_{ijmn} = \rho^2(i,j)\rho^2(m,n)L(K,l\ L), \tag{6.90}$$

with:

$$L(K,l\ L) = \sum_{s=1}^{\infty} \frac{K^{2s}}{s!^2} c_s (l\ L)^{s-2}\ 2^s\ s. \tag{6.91}$$

Going back to the original problem, we find that the correction to the discrete Lorentz equation is:

$$C_z = 2\sum_{ij,mn} \rho^2(i,j)\rho^2(m,n)\big[L(K,l\ L)Tr\{\hat{a}_i^\dagger \hat{a}_j \hat{a}_m^\dagger \hat{a}_n \widehat{\rho}_b \widehat{N}_z\} - R(K,l\ L)^2 Tr\{\hat{a}_i^\dagger \hat{a}_j \widehat{\rho}_b \hat{a}_m^\dagger \hat{a}_n \widehat{N}_z\}\big]. \tag{6.92}$$

If we define:

$$S(K,l\ L) = (l\ L)\ R(K,l\ L) = (l\ L)^2\ L(K,l\ L), \tag{6.93}$$

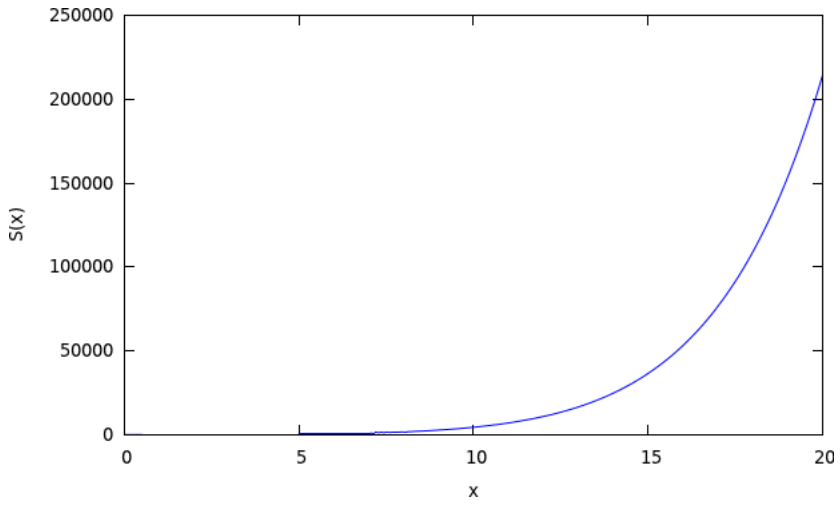

Figure 6.13: A plot of the function $S(x)$ which appears in eq. (6.94).

with $S(K, l\ L) = \sum_{s=1}^{\infty} \frac{K^{2s}}{s!^2}\ c_s\ (l\ L)^s\ 2^s\ s$, then we obtain:

$$C_z(t) = 2 \sum_{ij,mn} \rho^2(i,j)\rho^2(m,n) S(K, l\ L) \big[Tr\{\hat{a}_i^\dagger \hat{a}_j \hat{a}_m^\dagger \hat{a}_n \widehat{\rho}_b \widehat{N}_z\} - S(K, l\ L) Tr\{\hat{a}_i^\dagger \hat{a}_j \widehat{\rho}_b \hat{a}_m^\dagger \hat{a}_n \widehat{N}_z\} \big]. \tag{6.94}$$

We see that the function $S(K, l\ L)$ depends, as a matter of fact, on $\xi = K\sqrt{l\ L}$, $S(K, l\ L) \equiv S(\xi) = \sum_{s=1}^{\infty}\ c_s\ [\frac{\xi^s}{s!}]^2\ 2^s\ s$. A plot of the function $S(K, lL)$ can be found in Fig. 6.13. The traces can be evaluated, as done in ([112]), and the result is:

$$C_z(t) = 2 \frac{1}{(l\ L)^2} \sum_j \rho^4(z,j) S(K, l\ L)(\psi_z - S(K, l\ L)\psi_j). \tag{6.95}$$

Some comments are now in order. First of all, note that the equation has the shape of a second derivative. To understand this, we can look at a term of the form $\sum_{|k|\geq 2} J(k)(\psi_z -$

ψ_{z+k}). This term can be written as:

$$\sum_k J(k)\cdots = -J(2)\big(\psi_{z+2}-2\psi_z+\psi_{z-2}\big) - J(3)\big(\psi_{z+3}-2\psi_z+\psi_{z-3}\big) - J(4)\cdots . \quad (6.96)$$

This is a sum of discrete second derivatives with a non-local mass,

$$J(k)\big(\psi_{z+k}-2\psi_z+\psi_{z-k}\big) = -J(k)\big(\psi_{z+k-1}+\psi_{z-k+1}\big) - J(k)\sum_{i=2}^{k-1}\big(\psi_{z+i+1}-2\psi_{z+i}+\psi_{z+i-1}\big), \quad (6.97)$$

so we expect, in the end, to obtain a mass term out of this equation and, when we will have rearranged all the terms, we will.

Note that, for the case $c_s = 1$, $S(\xi) = 1$ for $\xi = 0.903$, and so $K = \frac{0.903}{\sqrt{l\ L}}$. We then see that K^2 plays the role of the density of non-local links per units of $l\ L$.

To end this section, we have to calculate the norm of this state. This can be written as:

$$|\langle\psi_{nl}|\psi_{nl}\rangle| = \sqrt{1+\langle\psi_{cl}|e^{K\widehat{T}_l^\dagger}e^{K\widehat{T}_l}|\psi_{cl}\rangle^2 + 2\mathfrak{Re}\{\langle\psi_{cl}|e^{K\widehat{T}_l}|\psi_{cl}\rangle\}}, \quad (6.98)$$

which reads,

$$|\langle\psi_{nl}|\psi_{nl}\rangle| = \sqrt{1+\big(\langle\psi_{cl}|e^{K\widehat{T}_l^\dagger}e^{K\widehat{T}_l}|\psi_{cl}\rangle^2 - 1\big)\}} \quad (6.99)$$

and substituting for the $\mathcal{T}$ operators, we finally find

$$\mathcal{N} = |\langle\psi_{nl}|\psi_{nl}\rangle| = \sqrt{1 + \big(\sum_{s=1} \frac{K^{2s}}{(s!)^2} \sum_{i<j} \rho(i,j)^2\big)^2} = \sqrt{1 + \big(\sum_{s=1} \frac{K^{2s}}{(s!)^2} 2^s s\big)^2} = \sqrt{1 + S^2(K, l\ L)}. \tag{6.100}$$

We can thus normalize the graph state by dividing by a factor of $\mathcal{N}$.

The modified dispersion relation due to disordered locality

The general case. We will now discuss the continuum limit. As we have seen, the continuum limit is obtained by rescaling $E_{hop} \to \tilde{E}_{hop} L$ and then sending $L \to \infty$. Please note that E_{hop} appears whenever we hop with a particle, so in these calculations it appears everywhere but in the ∂_t^2 term. In order to perform the continuum limit, first we have to make sense of the quantity $(\psi_z - S(K, l\ L)\psi_j)$ at least for the *flat* case, which we know correspond to Lorentz from [112]. We can add and subtract,

$$\begin{aligned} &(S(K, l\ L) - 1)\psi_z + (S(K, l\ L)\psi_z - S(K, l\ L)\psi_j) = \\ &= (S(K, l\ L) - 1)\psi_z + S(K, l\ L)(\psi_z - \psi_{z-1} + \psi_{z-1} + \psi_{z-2} - \cdots - \psi_j). \end{aligned} \tag{6.101}$$

In the continuum limit this becomes $(S(K, l\ L) - 1)\psi(z,t) + S(K, l\ L) \int_j^z \partial_\xi \psi(\xi, t) d\xi$, and thus $C_z(t)$ reads:

$$C_z(t) = \int_L dx\ \rho^4(z,x)[\frac{(S(K, l\ L) - 1)S(K, l\ L)}{(l\ L)^2}\psi(z,t) + \frac{S^2(K, l\ L)}{(l\ L)^2} \int_x^z \partial_\xi \psi(\xi, t) d\xi], \tag{6.102}$$

which is:

$$C_z(t) = \psi(z,t) \int_L dx\, \rho^4(z,x) \frac{(S(K,l\ L)-1)S(K,l\ L)}{(l\ L)^2} + \frac{S^2(K,l\ L)}{(l\ L)^2} \int_L \rho^4(z,x) \int_x^z \partial_\xi \psi(\xi,t)\, d\xi\, dx. \tag{6.103}$$

This can be written as:

$$C_z(t) = \psi(z,t) F(K,l\ L) + O(K,l\ L) \int_L \rho^4(z,x) \int_x^z \partial_\xi \psi(\xi,t)\, d\xi\, dx, \tag{6.104}$$

with $F(K,l\ L) = \int_L dx \rho^4(z,x) \frac{(S(K,l\ L)-1)S(K,l\ L)}{(l\ L)^2}$,$O(K,l\ L) = \frac{S^2(K,l\ L)}{(l\ L)^2}$. Please note here that these steps have been performed naively, though we have an explicit dependence on L in S. It is important to point out that the only way to keep the function $S(l\ L, K)$ finite is to rescale the quantity $K^2 l \approx \frac{\tilde{K}^2 \tilde{l}}{L}$. To keep the discussion simple, let us discuss this point at the end of the section. L is the combinatorial length of the 1-d lattice we are considering, and over which $\psi(x,t)$ is defined. Thus the equation of motion for the flat case is given, in the continuum, by:

$$[\partial_t^2 - c^2\big(1 + S^2(K,l\ L)\big)\partial_z^2 - F(K,l\ L)]\psi(z,t) = O(K,l\ L) \int_L \rho^4(z,x) \int_x^z \partial_\xi \psi(\xi,t)\, d\xi\, dx, \tag{6.105}$$

which is an integro-differential equation for the field integrated over the line, which shows the strong non-local character of the equation.

We note that there is a contribution to the speed of propagation of the signal, due to the

fact that particle can hop on many more graphs than the single classical one. This factor contributes with a $c^2 S^2(K, l\ L)$ added to the effective speed c^2. Let us stress that this contribution is merely due to the fact that there are many more graphs in the superposition, and not due to the fact that the particle can hop further: this is kept track of in the $C_z(t)$ term of the equation. Also, we see that $F(l, K)$ becomes a mass, due to non-locality, while on the r.h.s. there a new term appears. We can further reduce the equation by evaluating the integrals. It is clear that in order to have a finite result, which is physically expected, we have to rescale at this point only $l \approx \tilde{l}/L$, keeping K^2 independent from L. Said this, we see that the distribution itself, when is well chosen, becomes a δ function and therefore the models becomes local again.

Let us now calculate the terms at the leading order in $1/L$, since that is what we are interested in. The discrete differential equation becomes:

$$[\partial_t^2 - c^2\big(1 + S^2(K, l\ L)\big)\tilde{\partial}_z^2 - \tilde{F}(K, l\ L)]\psi_z(t) = -O(K, l\ L)\sum_{x=0}^{L}\rho^4(z, x)\psi_z(t), \qquad (6.106)$$

where $\tilde{\partial}_z^2$ is the discrete spatial second derivative. Using now (6.50), we see that the dispersion relation for the field becomes:

$$\omega_k c\big(1 + S^2(K, l\ L)\big) = \sqrt{2}\sqrt{1 - \cos\big(\frac{2\pi}{L}k\big) + \tilde{F}(K, l\ L) + \tilde{\rho}^4(k)O(K, l\ L)} \qquad (6.107)$$

Please note that with this rescaling of K, we have that $S(K, l\ L)$ can be expanded in even

powers of $1/L$:

$$S(K, l\ L) = 2\frac{\tilde{K}^2\ l\ L}{L^2} + 8\frac{\tilde{K}^2(l\ L)^2}{L^4} + \cdots . \tag{6.108}$$

Thus, we see that the superluminal effect, which is, the factor $1 + S^2(K, l\ L)$, becomes one in the limit $L \to \infty$; also, in the same limit, only the part quadratic in K survives. At this point the equation would become, in the continuum:

$$[\partial_t^2 - c^2\partial_z^2 - \tilde{F}(K, l\ L)]\psi(z,t) = -O(K, l\ L)\int_L \rho^4(z,x)\psi(z,t)\ dz \tag{6.109}$$

with $\tilde{F}(k, l\ L) = F(K, l\ L) + O(K, l\ L)\int_L \rho^4(z,x)\ dx$. Note that, while $\tilde{F}$ might seem to be dependent on the point z, being $\tilde{F}$ dependent on $z - x$ and integrated over x, it is indeed independent from it. In particular, if we define $l\ L \equiv \xi$, in the limit $L \to \infty$ and with the rescaling of K and l, $S(K, l\ L) \to 2\tilde{K}^2\xi$. We see now that the only way to obtain the continuum dispersion relation by rescaling $c \to \tilde{c}/L$, as done for the single-graph state, is to rescale also K, with $K \to \tilde{K}/L$.

Just as an exercise, we can insert a trivial spatially-constant solution, which then becomes of the form $\partial_t^2\psi(t) = R(K, l\ L)\psi(t)$. where $R(K, l\ L) = F(K, l\ L) + 2\ O(K, l\ L)\ \int_L \rho^4(z,x)\ dx$. Note that this quantity is always positive, so constant solutions are stable. Let us try to find a generic solution, instead. Let's do it for the equation:

$$[\partial_t^2 - \tilde{c}^2\partial_x^2 + \tilde{c}^2 q]\psi(x,t) = -\tilde{c}^2\int_L \sigma(z,x)\psi(y,t)\ dy. \tag{6.110}$$

Since the equation is linear in the field ψ, we can solve it by means of a Fourier transform. We then look at the dispersion relation for the function $\psi(x,t)$, with q and P generic functions. We can do it by Fourier transform. In this case, the integral on the right, being a convolution, becomes just the product of the Fourier transform of the single functions. Thus we have:

$$-\omega^2 + k^2\tilde{c}^2 + \tilde{c}^2 q = -\tilde{c}^2\sigma(k), \tag{6.111}$$

and we have that:

$$\omega = \pm c\sqrt{\tilde{k}^2 + q + \tilde{\sigma}(k)}. \tag{6.112}$$

Now, of course $\tilde{\sigma}(k)$ depends on the distribution of non-local links that we inserted in the wavefunction of the graph.

Two specific distributions. Let us consider two specific cases:

- $\rho_1(x-y) = \pi^{\frac{1}{4}}\,\sqrt{l}\,e^{-\frac{(x-y)^2}{2l^2}}$;
- $\rho_2(x-y) = \sqrt{2\,l}\,e^{-\frac{|x-y|}{2l}}$.

In these cases we find, using standard tables of Fourier transforms:

- $\tilde{\sigma}_1(k) = e^{-\frac{k^2}{a}}$;
- $\tilde{\sigma}_2(k) = \frac{a}{a^2+k^2}$.

and thus, keeping track of all the factors, we obtain:

$$\omega_1 = \pm\frac{1}{c}\sqrt{\frac{k^2}{1+S^2(K,l\ L)} + \tilde{F}_1(K,l\ L) + O(K,l\ L)e^{-\frac{k^2l^2}{8}}}, \tag{6.113}$$

and

$$\omega_2 = \pm\frac{1}{c}\sqrt{\frac{k^2}{1+S^2(K,l\ L)} + \tilde{F}_2(K,l\ L) + \frac{2O(K,l\ L)}{\pi}\frac{l^2}{l^2+k^2}}, \tag{6.114}$$

with $\tilde{F}_1(K,l\ L) = \sqrt{2}\ O^2(K,l\ L)$ and $\tilde{F}_2(K,l\ L) = O^2(K,l\ L)$, which can be calculated by evaluating $\int_L \rho_i^4(x-y)dx$. We have that $S^2(K,l\ L) = 4\tilde{K}^4\xi^2/L^4$ and thus can be neglected with respect to 1. Also, since the c contribute with a factor of L^2 within the square root, also S^2 can be neglected, and it contributes only the mass term in the L. Now we note a nice property: both the two distributions go to 0 for $k \to \infty$, that is, at high energy the dispersion relations become Lorentz again. We see then that the total effect the one of having an effective scale-dependent mass, which runs from one mass to another one, in both cases:

$$m_1(k) = \frac{1}{l\ L}\sqrt{S^2(K,l\ L) + S(K,l\ L)e^{-\frac{k^2l^2}{8}}}, \tag{6.115}$$

$$m_2(k) = \frac{1}{l\ L}\sqrt{S^2(K,l\ L) + S(K,l\ L)\frac{2}{\pi}\frac{l^2}{l^2+k^2}}. \tag{6.116}$$

The masses which are intertwined are given by

$$m_1(0) = \frac{1}{l\ L}\sqrt{S^2(K, l\ L) + S(K, l\ L)}, \quad m_1(\infty) = \frac{S(K, l\ L)}{l\ L}, \tag{6.117}$$

$$m_2(0) = \frac{1}{l\ L}\sqrt{S^2(K, l\ L) + \frac{2}{\pi}S(K, l\ L)}, \quad m_2(\infty) = \frac{S(K, l\ L)}{l\ L}. \tag{6.118}$$

This property, of intertwining two different masses between $k = 0$ and $k = \infty$ is shared by any function which is at least $\mathcal{C}^1$. It is remarkable, instead, that the mass at $k = \infty$ does not depend on the distribution we inserted at hand. In fact, any $\mathcal{C}^r$ distribution will lead to a Fourier transformed distribution which goes to zero at $k = \infty$ as $1/k^r$ and thus tend to a finite value for the mass. Note that, if we send $l \to 0$, as required to have S finite, the dependence on the scale seems to disappear, leaving a Lorentz dispersion relation with a mass which depends on the function S. However, we have to remember that, in fact these Fourier distributions come from the discrete dispersion relation. There, the distributions depend on $2\pi k/L$. If we define $\tilde{k}L = k$, then we have that the distributions cancel out the dependence on L, leaving exactly (6.117) and (6.118) but dependent on this new momentum $\tilde{k}$. Still, this mass depends on the distribution we have chosen through $\tilde{\sigma}_i(\tilde{k} = 0)$ and so it has a valuable effect. We plot the running of $(l\ L)m_i(\tilde{k})$ as a function of $x = K^2\ l\ L$, for the case $L = 1$ in Fig. (6.14) and $L = \infty$ in Fig. (6.15).

We would like to point out that the appearance of a mass which is square-positive is rather surprising. The physical reason is that, before starting the calculation, we would

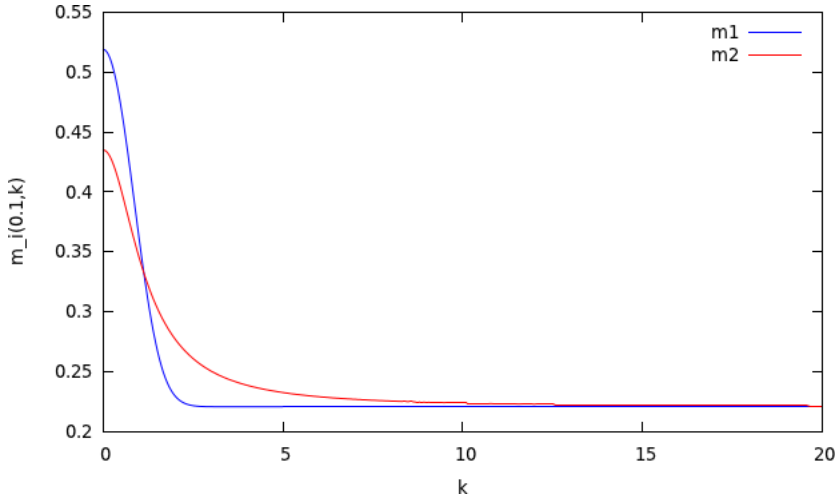

Figure 6.14: The running of $m_i(\tilde{k})$ for $x = 0.1$, $l = 1$ and $L = 1$.

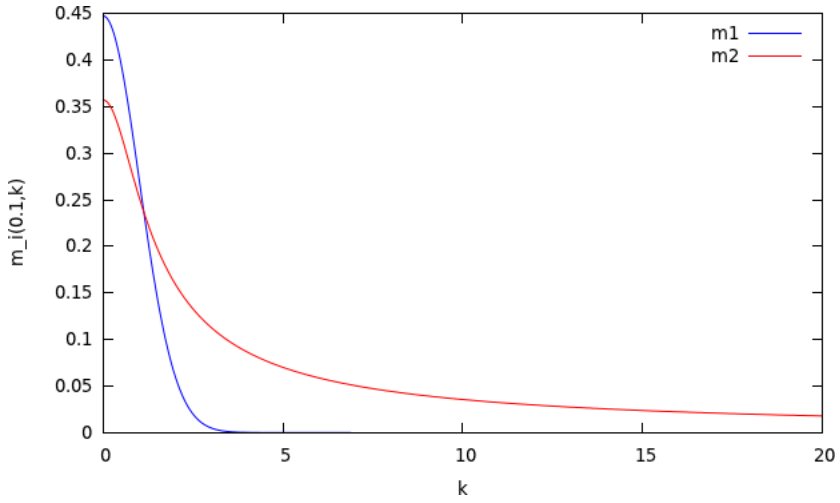

Figure 6.15: The running of $m_i(\tilde{k})$ for $x = 0.1$, $l = 1$ and $L = \infty$.

have expected that the presence of these non-local links would have shown a superluminal effect due to the non-local links themselves. However, the effective speed of propagation is higher because of the *superposition* of the graphs and not the non-local links. Indeed, the non-local links contributed *only* in the mass, thus the term $C_z(t)$ additional to the differential equation we obtained. Besides, this mass is square-positive, thus it is an effective mass and not a tachyonic one, which we would have expected from the presence of wormholes on physical grounds. The fact that it is square positive comes merely from the fact that the equation comes from a quantum mechanical average, and thus the terms appear squared.

6.5.2 Emergence of the mass from multi-particles interactions

In this section, we generalize the results of Section 6.3 to the case of multiple particles hopping on the graph. As we will see, the interaction of the particles will allow the field to acquire a mass.

Free motion. Let us first consider K distinguishable particles in states which are tensor products of delocalized states. This will allow us to track every single particle using a number operator.

Since the particles are distinguishable, we cannot use the standard second quantization formalism. Instead, a quantum state of the system must be described by

$$| \Phi_K\rangle = \sum_{m_1,\dots,m_K=1}^{\tilde{N}} c_{m_1,\dots,m_K} |m_1\rangle \otimes \cdots \otimes |m_K\rangle \,, \tag{6.119}$$

where $\mid m_i\rangle$ is the state of the i-th particle at the site m_i, and $\widetilde{N}$ is the total number of sites of the lattice. Note that the dimension of the Hilbert space is $\widetilde{N}^K$.

Let us also introduce a number operators $\widehat{N}_i$, defined as the tensor product of the number operator on the site of the particle i with identity operators on all sites except i so that the total number operator is $\widehat{N} = \sum_{i=1}^{K} \widehat{N}_i$. This number operator counts the total number of particles on the graph. To see how to go from the 1-particle case to this number operator, let us define $\widehat{N}_i^k$ as the number operator on the vertex k for the particle i. In this case we can write $\widehat{N} = \sum_{i,k} \widehat{N}_i^k$, and define a number operator for a region A of the graph as $\widehat{N}_A = \sum_{k\in A,i} \widehat{N}_i^k$. This consistently measures the number of particles in a region A of the graph.

It is easiest to start with the 2-particle case and then extend the analysis to K particles. The main complication compared to the 1-particle case is that we now have a density matrix with 4 indices. In the non-diagonal case, we have

$$\rho = \sum_{k_1,k_2,k_1\prime,k_2\prime} U_{k_1,k_2,k_1\prime,k_2\prime}(t)|k_1\rangle\langle k_2| \otimes |k_1'\rangle\langle k_2'|. \tag{6.120}$$

Fortunately, we also have $\widehat{H} = \widehat{H}_1 + \widehat{H}_2$, with $[\widehat{H}_1, \widehat{H}_2] = 0$. A straightforward calculation shows that we can use the result from the 1-particle case:

$$\Big[\widehat{H}, [\widehat{H}, \rho]\Big] = \Big[\widehat{H}_1, [\widehat{H}_1, \rho]\Big] + \Big[\widehat{H}_2, [\widehat{H}_2, \rho]\Big] + \widehat{R}, \tag{6.121}$$

where the mixed term is

$$\widehat{R} = 2\left(\widehat{H}_1\widehat{H}_2\rho + \rho\widehat{H}_1\widehat{H}_2 - \widehat{H}_1\rho\widehat{H}_2 - \widehat{H}_2\rho\widehat{H}_1\right). \tag{6.122}$$

We follow the same steps as in the 1-particle case and evaluate the second derivative of the expectation value of the two number operators to find

$$\begin{aligned}\partial_t^2\alpha_k^1 + \partial_t^2\alpha_k^2 = -\frac{1}{\hbar^2}\Big(&\text{Tr}\left[[\widehat{H}_1,[\widehat{H}_1,\rho]]\widehat{N}_k^1\right] + \text{Tr}\left[[\widehat{H}_2,[\widehat{H}_2,\rho]]\widehat{N}_k^2\right] \\ &+ \text{Tr}\left[\widehat{R}\rho(\widehat{N}_k^1 + \widehat{N}_k^2)\right]\Big).\end{aligned} \tag{6.123}$$

It is easy to understand what happens when $\rho = \rho_1 \otimes \rho_2$. In this case we have

$$U_{k_1,k_2,k_1\prime,k_2\prime}(t) = U_{k_1,k_2}(t)\tilde{U}_{k_1\prime,k_2\prime}(t), \tag{6.124}$$

and the first and second terms on the r.h.s. of Eq. (6.123) reduce to discrete second-order derivatives, as in the 1-particle case. We therefore only have to deal with the $\text{Tr}\big[\widehat{R}\rho(\widehat{N}_k^1 + \widehat{N}_k^2)\big]$ term.

Another way to see this is by noticing that $\widehat{N}_j$ acts as a projector on the one-particle states. We have $\text{Tr}[\widehat{H}_1\rho\widehat{H}_2] = \text{Tr}[\widehat{H}_2\widehat{H}_1\rho]$, using the properties of the trace. Term by term, we can show that, for each $\widehat{H}_i$ and $\widehat{H}_j$, the mixed term vanishes for any number of particles. Defining $\widehat{R}_{ij} = \widehat{H}_i\widehat{H}_j\rho + \rho\widehat{H}_i\widehat{H}_j - \widehat{H}_i\rho\widehat{H}_j - \widehat{H}_j\rho\widehat{H}_i$, we find that the many-particle

equation becomes,

$$\sum_i \partial_t^2 \alpha_k^i(t) = \sum_i \nabla \alpha_k^i + 2\text{Tr}\left[\left[\sum_{<ij>} \widehat{R}_{ij}\right] \sum_i \widehat{N}_k^i\right], \tag{6.125}$$

where $\nabla \alpha_k^i$ is the second order discrete derivative $\partial_x(c\partial_x(\cdot))$.

We can now use the same argument as in the 2-particle case to show that all the terms $\widehat{R}_{ij}$ vanish independently. We define $\alpha_k := \frac{1}{2}\sum_i \alpha_k^i$ to be the probability of finding a particle at k. This quantity satisfies the same equation as the one-particle sector probability:

$$\sum_i \partial_t^2 \alpha_k^i(t) = \sum_i \nabla \alpha_k^i. \tag{6.126}$$

That is, particles are independent from each other and each follows its own equation (6.126).

Interaction. Including interaction, in general, the Hamiltonian of the system can be written as

$$\widehat{H} = \sum_{i=1}^{K} \widehat{H}_i + \sum_{i<j} \widehat{H}_{ij}\,, \tag{6.127}$$

where $\widehat{H}_i = \underbrace{\hat{1}\otimes\cdots\hat{1}}_{i-1 \text{ times}} \otimes \widehat{H} \otimes \underbrace{\hat{1}\otimes\cdots\otimes\hat{1}}_{K-i-1 \text{ times}}$. For what follows, again we first check the case of two particles, and calculate what happens to Eq. (6.126) when we add an interaction term. The most general interaction Hamiltonian is of the form $\widehat{H}_{int} = \sum_{ijkl} \widetilde{U}_{ijkl}\, \widehat{a}_i^{1\dagger}\widehat{a}_j^1 \otimes$

$\widehat{a}_k^{2\dagger}\widehat{a}_l^2$. We make a simplifying assumption which is natural for delocalized states, and require that the potential respects their symmetries. The simplest such local potential is of the form

$$\widehat{H}_{int} = \sum_k I_k |k\rangle\langle k| \otimes |k\rangle\langle k|. \tag{6.128}$$

If we add this Hamiltonian to the free one, additional terms appear on the rhs in Eq. (6.126). These can be traced back to the additional commutators in the expansion of the full Hamiltonian,

$$\begin{aligned}\widehat{C} := &\left[\widehat{H}_1, [\widehat{H}_{int}, \rho]\right] + \left[\widehat{H}_{int}, [\widehat{H}_1, \rho]\right] \\ &+ (1 \to 2) + \left[\widehat{H}_{int}, [\widehat{H}_{int}, \rho]\right],\end{aligned} \tag{6.129}$$

that come from expanding the full hamiltonian $\widehat{H}_T = \widehat{H}_1 + \widehat{H}_2 + \widehat{H}_{int}$ in the double commutators and keeping only the terms involving free Hamiltonians. Since we want to distinguish the single particles in the continuum limit, we consider the approximation $\|\widehat{H}_{int}\| \ll \|\widehat{H}_{1/2}\|$, with $\|\widehat{T}\| = \sup_v \frac{\|\widehat{T}v\|}{|v|}$. This gives a product of the density matrices of the single particles.

A lengthy but straightforward calculation shows that, when we restrict to diagonal density matrices in the subspace of the single particles, we find:

$$\mathrm{Tr}[\widehat{C}\widehat{N}_k^1] = \mathrm{Tr}[\widehat{C}\widehat{N}_k^2] = 0. \tag{6.130}$$

This means that, surprisingly, in the continuum limit, the wave equations for the fields are decoupled if we use a local potential of the form (6.128).

The next generalization is a potential which is slightly non-local. The simplest such potential is given by

$$\widehat{H}_{int} = \sum_k I_k \, |k+1\rangle\langle k+1| \otimes |k\rangle\langle k| \tag{6.131}$$

for the case of 2-particles. In this case, an even longer but still straightforward evaluation of Tr$[\widehat{C}N_k^1]$ or Tr$[\widehat{C}N_k^2]$ shows that these traces are nonzero. They take the form

$$\text{Tr}[\widehat{C}N_k^1] = f_{k,k}U_{k,k}(t)\tilde{U}_{k+1,k+1}(t)(I_{k+1} - I_k), \tag{6.132}$$

and

$$\text{Tr}[\widehat{C}N_k^2] = f_{k,k}U_{k+1,k+1}(t)\tilde{U}_{k,k}(t)(I_{k+1} - I_k). \tag{6.133}$$

That is, in the continuum limit, the equations for the two probability fields are coupled. If we define $\alpha_k(t) := U_{k,k}(t)$ and $\beta_k(t) := \tilde{U}_{k,k}$ the probability fields obey

$$\partial_t^2\alpha_k - \nabla\alpha_k = \alpha_k\beta_{k+1}f_{k,k}(I_{k+1} - I_k) \tag{6.134}$$

$$\partial_t^2\beta_k - \nabla\beta_k = \beta_k\alpha_{k+1}f_{k,k}(I_{k+1} - I_k) \tag{6.135}$$

If we define $\mu(x)$ to be the continuum equivalent of $f_{k,k}$ and $I(x)$ the continuum equivalent

of I_k, we have

$$\Box\alpha(x,t) = \alpha(x,t)\beta(x,t)\mu(x)I'(x) \tag{6.136}$$

$$\Box\beta(x,t) = \beta(x,t)\alpha(x,t)\mu(x)I'(x). \tag{6.137}$$

These equations can be straightforwardly generalized to the case of more than two particles if the potential is the sum of a 2-body interaction for each pair of particles of the type $\sum_{\langle ij\rangle}\widehat{H}^{ij}_{int}$, with

$$\widehat{H}^{ij}_{int} = \sum_k \hat{1}\otimes\cdots\hat{1}\otimes\underbrace{|k\rangle\langle k|}_{i-\text{th}}\otimes\hat{1}\otimes\cdots\otimes\hat{1}\otimes\underbrace{|k-1\rangle\langle k-1|}_{j-\text{th}}\otimes\hat{1}\cdots\otimes\hat{1}\; I^{ij}_k. \tag{6.138}$$

The sum $\langle ij\rangle$ is over all pairs of particles. If $\alpha^i(x,t)$ is the probability field for particle i, we obtain, for each particle, the following coupled differential equations:

$$\Box\alpha^i = \alpha^i(\sum_{j\neq i}\partial I^{ij}\alpha^j)\mu. \tag{6.139}$$

We can now define $m_i^2 = (\sum_{j\neq i}\partial I^{ij}\alpha^j)\mu$. The EOM becomes,

$$\Box\alpha^i - m_i^2(x,t)\alpha^i = 0 \tag{6.140}$$

The effective mass m_i^2 is determined by the interaction with the other particles. The study of the interaction is important to understand, but beyond of the scope of the present discussion.

CONCLUSIONS

In this thesis we described a journey through graphs and quantum mechanics, motivated by the necessity of obtaining a pre-geometric model of emergent gravity. Along these lines, in previous works [80, 54], *quantum graphity* was proposed and analyzed: it is a background independent spin system for emergent locality, geometry and matter. We discussed how such simple models could say something about general relativity and cosmology. After having described the generic troublesome properties of classical and quantum general relativity, we introduced the first model of Quantum Graphity, aimed to understand alternatives to inflation, Variable Speed of Light theories, as a Quantum Mechanical effect of a time-varying graph.

Simplifications along the route allowed a treatment of an otherwise intractable problem. We collected many results, all of them useful for a better understanding of the phenomenology of the models.

In the first Quantum Graphity model, we introduced a technique to map the Quantum Graphity Hamiltonian on the line graph of a complete graph. This procedure required the introduction of the Kirchhoff matrix of a graph and the n-string matrices related to these. This mapping was general and not specific to Quantum Graphity. Using this mapping in

a weak coupling approximation of the first model, the mean field theory approximation and the low temperature expansion, we studied the properties of the model near zero temperature, not before having identified the average degree as a order parameter. We found that the model is dual to an Ising model with external nonzero magnetic field if we neglected the interaction terms due to loops. In particular, we showed that the average degree is naturally a good order parameter for the mean field theory approximation and we found, implicitly, its average distribution using the mapped Hamiltonian and the mean field theory approximation for the 3-loop term. We then studied the susceptibility function and showed how the duality with the Ising model can help to interpret the results. We have shown that the model possesses a phase transition and at $T = 0$ the system goes to the ground state as expected. While this result was expected on general grounds, the mapping we used simplified the problem and allowed a quantitative analysis. In particular, the transition point was not known, nor the corrections to the mean degree due to the loop terms. More into the specific, what emerged from the study of the average distribution for the degree is that, if the vertex degree term dominates ($g_V \gg g_L$), the loop term corrections to the average degree of the ground state are suppressed at $T = 0$. We found the dependence on the coupling constants explicitly and this result is confirmed by the study of the susceptibility. Thanks to the mean field theory approximation, we found the contribution of all loops to the susceptibility and showed that the susceptibility function tends to the Ising one when T approaches zero. We then applied this procedure to the degenerate case, and showed that the degeneracy does not change the average degree at low temperature, but only the speed with which this ground state is reached. As a final

remark, we stress that the vertex degree is an important quantity in the model. In fact, as shown in [54] using the Lieb-Robinson bound, the speed with which information can propagate on graphs is bounded by a degree-dependent quantity.

As the temperature drops, the speed of the emergent light, hobbyhorse of the Quantum Graphity model, must drop with the degree. This gives a profile of the speed of propagation of signals when the temperature is slowly decreased in the model, and thus as a function of time. Of course, this can be considered as a theory with Variable Speed of Light.

The second model we introduced, was a modification of the first one. Motivated by the problematic appearance of an external temperature, the quantum states of this new system were dynamical graphs whose connectivity represents the locality of space. The Hamiltonian of [80] is not unitary: the universe starts at a high energy configuration (non-local) and evolves to a low energy one (local). This has clear limitations when applied to a cosmological context. The second model was originally intended as an energy-conserving version of [80], in which graph edges can be deleted, matter created and viceversa. The Hamiltonian we was is essentially an extension of the Hubbard model to a dynamical lattice. In this system, the basic building blocks of the theory are not events, but quantum physical systems S_i, represented by a finite-dimensional Hilbert space $\mathcal{H}_i$ and a Hamiltonian H_i. That is, instead of an event, we have the space of all possible states of S_i and the dynamical rules for the time evolution of these. The aim is to study the relationships among the S_i and find geometry as the emerging structure imposed by these relationships, independently of their state. In fact, what we have can be considered as a

unification of matter and geometry to matter only. Certain configurations (bound states) of matter play the role of spatial adjacency in the dynamical sense that they will determine whether interaction of other particles is allowed or not. In that sense, geometry is not fundamental but rather a convenient way to simplify the fundamental evolution of matter. From the condensed matter point of view, we have presented a Hubbard model in which the particles hop on a graph whose shape is determined by the motion of the particles and it is itself a quantum variable.

In order to get an intuition on the behavior of the system, we simulated the quantum system for a complete graph with 4 vertices and hard core bosons and we analyzed the entanglement dynamics of the system, including the one between the particle and edge degrees of freedom. We argued that for the weakly interacting system, entanglement and loss of unitarity for the reduced system can be seen in presence of very high curvature. Moreover, the eigenstate thermalization of the model is studied under two different sets of parameters. Thermalization occurs when potential energy dominates over kinetic energy.

The model with bosons has some features of other models studied in a diversity of contexts and with different purposes. The first central aspect is a quantum dynamics involving a set of graphs. Quantum evolution on graphs is a subject of study related to spin systems, as a generalization of spin chains (see the review by Bose [24]), and quantum walks on graphs, where a particle undergoes a Schrödinger dynamics hopping between the vertices (see the review by Kempe [28]) where, at each time step, a particle is in a superposition of different vertices. Of course, the main difference with respect to our model

is in the fact that in our model the graph is evolving in time as part of the system's evolution. Focusing on another area, it may be interesting to highlight a parallel with the work of Gudder [27], who studied discrete-space time building on ideas of Bohm [23]. In the model described by Gudder, the graph is interpreted as a discrete phase-space in which the vertices represent discrete positions which a particle can occupy, and the edges represent discrete directions that a particle can propagate. This setting was primarily introduced to describe the internal dynamics of elementary particles. From this perspective, each particle is associated to a graph: vertices represent quark-like constituents of a particle and edges represent interaction paths for gluons which are emitted and absorbed by the vertices. Another aspect of this model is that we have many particles evolving at the same time. In the mathematical literature there is a growing number of examples of random walks with multiple particles/agents [25, 22, 26].

In a unitary system for cosmological evolution, the interesting question to ask is whether the system has long-lived metastable states. We studied this question rigorously, using analysis in terms of Markov chains, and also gave an intuitive argument, in both cases finding that dynamical equilibrium is reached when, starting from zero initial particles, half the initial number of edges are destroyed.

An important issue to emphasize is that these models assumes the existence of a notion of time and of time evolution as given by a Hamiltonian, as opposed to the constrained evolution of canonical pure gravity. It is a general question for all condensed matter approaches to quantum gravity whether such evolution is consistent with the diffeomorphism invariance of general relativity. While it is not possible to settle this question

without first knowing whether the condensed matter microscopic system has a low energy phase which is general relativity, we can make a few comments, as well as point the reader to more extensive discussion of this issue elsewhere [42, 32]. In general, there are two possible notions of time: the time related to the g_{00} component of the metric describing the geometry at low energy and the time parameter in the fundamental microscopic Hamiltonian. Let us call the first *geometric time* and the second *fundamental time*. In a geometrogenesis context, it is clear that the geometric time will only appear at low energy, when geometry appears. The problem of the emergence of geometric time is the same as the problem of the emergence of space, of geometry. The constrained evolution of general relativity, often called "time does not exist", refers to geometric time. By making the geometry not fundamental, we are able to make a distinction between the geometric and the fundamental time, which opens up the possibility that, while the geometric time is a symmetry, the fundamental time is real. It is important to note that the relation between geometric and fundamental time is non-trivial and that the existence of a fundamental time does not necessarily imply a preferred geometric time. We also note that, in the presence of matter in general relativity, a proper time can be identified. The particular system studied here has matter and in that sense it is perhaps more natural that it also has a straightforward notion of time.

We expect that several features of this model has still some potentials. For instance, there is nothing in the Hamiltonian to encourage the system to settle in metastable states that are regular graphs. Emergence of geometric symmetries such as Friedman-Robertson-Walker symmetries was not a goal at this stage but can be incorporated in future work by

additional terms in the Hamiltonian as in [80], or possibly also by introducing causality restrictions as in [1]. Finally, we believe that this model is interesting from the condensed matter point of view. Condensed matter systems are always defined on a given lattice. In this model, the lattice itself is a quantum variable.

Using still the second model with bosons, but neglecting the dynamics of the graph, we discussed in the specific what is the role that the connectivity possesses and connected with the Lieb-Robinson bounds. As it is well known, Quantum mechanics drastically deviates from the ordinary intuition because of its nonlocality, or action-at-distance. We do, however, know that in condensed matter systems we observe excitations with relativistic dispersion relations. Why is this? An analogue of this problem is sound in classical systems. Newtonian mechanics is nonlocal but Newton himself evaluated the speed of propagation of sound in gases.

It is now fairly well-understood that theories with nonlocal action but local interactions have excitations that are locally covariant in certain limits. The amount of nonlocality can be bounded using the Lieb-Robinson bounds [70], as we discussed in the first model. In the third part of the thesis we explored this notion of locality in the Hubbard model.

We found that the vertex degree plays a central role as it is related to the local speed of propagation of the classical probability distribution of matter on the lattice. Our analysis is relevant for the idea that relativity, general and special, may be emergent from an underlying theory which is local and quantum. Going further than the analysis of the Lieb-Robinson bounds in [54], we looked at emergence of an effective curved geometry in

the Hubbard model. The quantum Hamiltonian evolution of the one-particle density for a particular set of states leads to an equation of motion that approximates the wave equation for a scalar particle in curved space. The same equation appears in optical systems with a varying refraction index and is thus connected with Analogue Models.

It is widely known that this equation can be cast in the domain of general relativity by noticing that it is the same as evolution in Gordon's space-time. This connection cannot be made in 1+1-dimensions, the case we considered, but equation (6.46) can be extended to more than one spatial dimension by considering graphs which can be foliated in more than one directions.

We should stress also that this has been achieved on a Bose-Hubbard model on graphs with varying vertex degree and multiple edges between sites. The important picture to keep in mind to understand this mechanism is Fig. 6.1. The graph modifies the strength of the interaction of the original Bose-Hubbard model and, for the particular states we are interested in, we can obtain Eq. (6.46) for the particle localization.

As with the emergent wave equation, this result is reminiscent of the physics of analogue gravity systems . It is then interesting to consider the model of [111] as a rather unusual analogue gravity model.

Also, we have investigated physical models related to Quantum Gravity which had been suggested in the literature as models of non-locality. One of the most striking theoretical consequences of General Relativity is the existence of wormholes and black holes. In the present thesis we considered such a possibility in a toy model constructed using the framework Quantum Graphity. In order to do so, we had to extend the results of

[112] to a case in which the quantum state of the background is a superposition of many graph states. The superposition of this graphs has been chosen such that it is dominated by a graph on which, as we showed in earlier works, the expectation values of number operators of the bosons hopping on it satisfy a closed equation for probability density in the classical regime, i.e. a wave equation. We extended the formula previously obtained and studied a particular case, which is, graphs which violate micro- and macro- locality. As discussed, a violation of macro-locality can be interpreted, within the model, as the presence of non-local links in the background spacetime. This is a concrete example of a quantum foam within the framework of Quantum Graphity [80, 111]. The graph state was chosen on the basis of what we know from low energy physics, which is, Lorentz invariance is satisfied up and above the Planck scale [132]. We thus constructed the states which represent corrections to the low-energy physics. We assumed that the non-local links (i.e. the wormholes) are suppressed by a length according to a certain distribution. The length is measured by a combinatorial distance based on the *low energy* graph and which defines the state and the distance. We chosen two natural distances, given by the cases $d(x,y) = (x-y)^2$ and $d(x,y) = |x-y|$. We found that, in the continuum limit, there is no superluminal effect on the low-energy physics, i.e. the speed of propagation is unaffected. However, there is an appearance of momentum dependent masses for the scalar field that can be calculated within the model. These masses are surprisingly square-positive and thus do not violate the physics of the restricted Lorentz group, i.e., are not tachyonic and a simple analysis showed that this mass runs with the energy scale and, in particular, runs to zero at high energy. We ask ourselves if a similar phenomenon hap-

pens for the other fields. This analysis suggested the possibility that a quantum foam could contribute, in principle, to the mass of a quantum field. As suggested in [15] and [122], the possibility of having non-local link states within Loop Quantum Gravity is very natural. Also, it has been suggested that these states could add something to the dark energy puzzle discussion. We suggested also a second mechanism for the generation of the mass of the hopping particle, due to the interaction with different particles on the graph. We found that a local interaction is not able to give a mass to the field. We thus extended our search to different type of interactions, and found that the mass emerges from non-local ones in the continuous limit. These particles might well be in a multiplet, but an interaction able to assign a pseudo-spin to it has to be found.

In summary, we explored not only technical points, but also fundamental facts of a relational approach to quantum gravity. The notion of time, given since the very beginning as an external parameter, changed through the thesis. At the end we have shown that a Lorentzian metric emerges and that curvature can be encoded in the graph. We hope that our work can at least instill the doubt that phenomena given for granted can have an origin which is very different from the standard description. Variable Speed of Light theories were our hobbyhorse in the beginning, but we are quite confident that other interesting phenomena can be studied in simple models like the ones we have discussed in this thesis.

Appendix A

Random Walk

The following general result is useful to study the random walks described in the thesis:

Theorem A.0.1. *Let G be a graph drawn from* any *random walk on $\mathcal{G}_N$ with stationary distribution π. Assume that there exists $\alpha < 2$ such that*

$$g(\pi) = \max_{G,H \in V(\mathcal{G}_N)} \frac{[\pi]_G}{[\pi]_H} < e^{N^\alpha}. \tag{A.1}$$

Then

1. $E\left(|E(G)|\right) = \frac{1}{2}\binom{N}{2} + o(1)$;
2. *For* $t \geq \sqrt{N^\alpha \binom{N}{2}}$,

$$\textit{Prob}\left[\left||E(G)| - \frac{1}{2}\binom{N}{2}\right| > t\right] \leq 8\exp(-N^\alpha).$$

Proof. We will prove the theorem by proving a deviation bound for $\text{Prob}\left[\left||E(G)| - \frac{1}{2}\binom{N}{2}\right| > t\right]$ in terms of t.

Let

$$A_t = \left\{ G : \left| |E(G)| - \frac{1}{2}\binom{N}{2} \right| \leq t \right\}.$$

Note that A_t contains both connected and disconnected graphs.

Let C be a function from the set of all graphs on N vertices to the set $\{0, 1\}$. Specifically, let

$$C(G) := \begin{cases} 1 & \text{if } G \text{ is connected;} \\ 0 & \text{otherwise.} \end{cases}$$

Let $C(N, t)$ denote the probability that a graph drawn uniformly at random from A_t is connected. The probability that a graph drawn from the random walk belongs to A_t is $\sum_{G \in A_t} C(G)[\pi]_G$; likewise for $G \notin A_t$. We will now bound the quotient between these two probabilities. It is well known, see *e.g.* [18], that

$$C(N, t) = 1 + o(1)$$

for, *e.g.*, $t < N/2$. Then

$$\begin{aligned}\frac{\sum_{H\notin A_t} C(H)[\pi]_H}{\sum_{G\in A_t} C(G)[\pi]_G} &\leq g(\pi)\frac{\sum_{H\notin A_t} C(H)}{\sum_{G\in A_t} C(G)} \\ &\leq g(\pi)\frac{|\overline{A_t}|}{|A_t|C(N,t)} \\ &\leq g(\pi)\frac{|\overline{A_t}|}{|A_t|(1+o(1))} \\ &\leq 2g(\pi)\frac{|\overline{A_t}|}{|A_t|}\end{aligned} \tag{A.2}$$

This can be written as

$$2g(\pi)\frac{P_{N,t}}{1-P_{N,t}}, \tag{A.3}$$

where

$$P_{N,t} = |\overline{A_t}|/2^{\binom{N}{2}}$$

is the probability that a binomial random variable with distribution $\mathrm{Bin}(\binom{N}{2}, \frac{1}{2})$ deviates more than t from its expectation. Using the Chernoff bound we have then

$$P_{N,t} \leq 2\exp\left(\frac{-2t^2}{\binom{N}{2}}\right)$$

If $t = \sqrt{N^\alpha \binom{N}{2}}$ we can thus bound (A.3) as

$$2g(\pi)\frac{P_{N,t}}{1-P_{N,t}} \leq 2g(\pi)4\exp(\frac{-2t^2}{\binom{N}{2}}) \tag{A.4}$$
$$= 8g(\pi)\exp(-2n^\alpha)$$
$$= 8\exp(-N^\alpha)$$

Since the denominator in the first step of Eq. (A.2) is less than 1 we have the following bound for our walk

$$\text{Prob}\left[H \notin A_t\right] \leq \sum_{H \notin A_t} C(H)[\pi]_H \leq 8\exp(-N^\alpha) \tag{A.5}$$

For our range of α the value of t is $o\left(\binom{N}{2}\right)$ which means that for a graph from A_t the number of edges is $\frac{1}{2}\binom{N}{2} + o(1)$ and the contribution to the expected number of edges from graphs not in A_t is between zero and $\binom{N}{2}8\exp(-N^\alpha)$. This is $o(1)$. Thus the total expectation is $\frac{1}{2}\binom{N}{2} + o(1)$. □

Corollary A.0.2. *Let G be a graph drawn from a simple random walk on $\mathcal{G}_N$. Then*

$$E(|E(G)|) = \frac{1}{2}\binom{N}{2} + o(1)$$

Proof. We know that the underlying graph of this random walk is bipartite and that in the asymptotic limit the stationary distribution oscillates between π_{even} and π_{odd} depending on whether we have taken an even or an odd number of steps. However if we start a

new walk by not changing the graph in the first time step with probability $1/2$, the new stationary distribution will be

$$\pi = \frac{1}{2}(\pi_{even} + \pi_{odd}). \tag{A.6}$$

Since we are looking at graphs with N vertices, $d(i)$ is at most $\binom{N}{2}$ and not less than $N-2$. Hence,

$$g(\pi) \leq \frac{N^2 - N}{2n - 4}.$$

and the corollary follows from Theorem A.0.1. □

Note that here we only used the fact the walk converges towards a stationary distribution on $\mathcal{G}_N$ and that $g(\pi)$ is bounded by a polynomial in N for this walk. The same result holds for any form of walk on $\mathcal{G}_N$ for which $g(\pi)$ is not exponential in N.

Let us recall that a random event happens *asymptotically almost surely*, or *a.a.s*, if the probability for the event is $1 - o(1)$. A *clique* in a graph is a subgraph isomorphic to the complete graph. The *clique number* of a graph G, denoted by $\omega(G)$, is the number of vertices of the largest clique in G.

Theorem A.0.3. *Let G be a graph drawn from a simple random walk on $\mathcal{G}_N$. Then there exist constants $c_1 < c_2$ such that a.a.s the clique number $\omega(G)$ satisfies*

$$c_0 \log(N) - c_1 \leq \omega(G) \leq c_0 \log(N) + c_2.$$

Proof. It is well known, see, *e.g.*, Chapter 11 of [18], that the expected clique number of a uniform random graph with edge probability $\frac{1}{2}$ is

$$\frac{2}{\log 2}\log(N) = c_0 \log N$$

and that the following concentration bounds hold

$$\text{Prob}\left[\omega(G) - c_0 \log N \geq r\right] < N^{-r}, \tag{A.7}$$

$$\text{Prob}\left[c_0 \log N - \omega(G) \geq r\right] < N^{-\lfloor 2^{\frac{r-2}{2}} \rfloor} \tag{A.8}$$

We can now proceed in the same way as in the proof of Theorem A.0.1 using the set

$$B_t^u = \{G|\omega(G) - c_0 \log N\}| \leq t\}$$

to give a bound on the upper tail probability and

$$B_t^l = \{G|c_0 \log N - \omega(G)\}| \leq t\}$$

for the lower tail probability, together with the bound on $g(\pi)$ from the proof of Corollary A.0.2 and the concentration bounds from the inequalities (A.7) and (A.8). This gives the

following inequalities:

$$\text{Prob}\left[\omega(G) - c_0 \log N \geq r\right] < c_1 \frac{N(N-1)}{N-2} N^{-r} \tag{A.9}$$

$$\text{Prob}\left[c_0 \log N - \omega(G) \geq r\right] < \frac{N(N-1)}{N-2} N^{-\left\lfloor 2^{\frac{t-2}{2}} \right\rfloor} \tag{A.10}$$

We can now use these inequalities to bound the contributions to the expected clique number. A clear but lengthy calculation can show that the contributions from the two tails are asymptotically bounded by two constants, giving us the bound stated in the theorem. □

A rigorous analysis of the expected number of edges when we consider particles will be more difficult, since the model corresponds to a random walk on a directed graph, *i.e.*, a graph in which edges have a direction. This is associated to an adjacency matrix which is not necessarily symmetric. There are transitions where, *e.g.*, an edge is deleted and the particle distribution changes so that the endpoint of the edge do not have any particles on them, thus making the re-addition of the edge impossible in the next step. However, for states with a large number of particles, such as any graph with less than $\frac{1}{2}\binom{n}{2}$ edges, the vast majority of transitions will be reversible, as it is in the case without particles.

Let us consider the number of possible transitions from a state $(G, \mathbf{x})$ defined as follows: here G has n vertices, t edges which are part of triangles, s edges with endpoints

at distance 2, and p indistinguishable particles. If we assume that there are particles at all vertices we have three types of transitions which can be explicitly enumerated:

1. There are $\binom{n+p-1}{p}$ transitions which correspond to redistributing the particles without changing G.

2. There are $t\binom{n+p}{p+1}$ transitions which correspond to deleting an edge and redistributing the $p+1$ particles.

3. There are $s\binom{n+p-2}{p-1}$ transitions which correspond to adding an edge and redistributing the $p-1$ particles.

Only the number of transitions of the last type is affected by the assumption that there are particles at all vertices.

If $p \approx c\frac{1}{2}\binom{n}{2}$ we can estimate $\binom{n+p-1}{p}$ as

$$\begin{aligned}
\binom{n+p-1}{p} &\approx \frac{p^{n-1}}{n!}\left(1+\frac{n(n-1)}{2p}+\mathcal{O}(p^{-2})\right) \\
&\approx \frac{p^{n-1}}{(n/e)^n}(1+\frac{1}{c}+\mathcal{O}(p^{-2})) \\
&\approx \frac{e^n}{n}\left(\frac{p}{n}\right)^{n-1}(1+\frac{1}{c}+\mathcal{O}(p^{-2})) \\
&\approx \frac{e^n}{n}\left(c\frac{n-1}{2n}\right)^{n-1}(1+\frac{1}{c}+\mathcal{O}(p^{-2})) \\
&\approx \mathcal{O}\left(\frac{(ce)^n}{n}\right)
\end{aligned}$$

Inserting this into the numbers of transitions given above, shows that for this model the maximum degree of the transition graph is bounded from above by a simple exponential, and the minimum degree is of course still greater than a multiple of n. According to

Theorem 1 this is not sufficient to change the expected number of edges from being $\frac{1}{2}\binom{n}{2}$. In order to make this analysis fully rigorous it is also necessary to show that the states with unoccupied vertices do not make a significant contribution, which will be lengthy but mostly a technical issue.

The discussion for a case with distinguishable particles will be very similar but $\binom{n+p-1}{p}$ will be replaced by n^p which is large enough to escape Theorem 1. These counts also give an easy way to implement a simulation algorithm for both models. Just pick uniformly among all the possible transitions from the current state. If we do not consider particles or consider indistinguishable particles, the degrees of the vertices in the graphs will be close to those of random graphs with probability 1/2. This is more or less for the same reason that Theorem 1 works. The number of "typical" graphs in $G(n, \frac{1}{2})$ is so large that their behavior will still control these models.

BIBLIOGRAPHY

[1] J. Ambjorn, R. Loll, Nucl. Phys. B (1998), 536-407, hep-th/9805108; J. Ambjorn, J. Jurkiewicz, R. Loll, Phys. Rev. Lett. 93, 131301, (2004), hep-th/0404156

[2] L. Freidel, Int.J.Theor.Phys. 44, 1769 (2005), hep-th/0607032.

[3] D. Oriti, In: Quantum Gravity, Eds. B. Fauser, J. Tolksdorf and E. Zeidler, Birkhauser, Basel (2007), gr-qc/0512103.

[4] C. Rovelli, L. Smolin, Nucl Phys B 442 (1995) 593; A. Ashtekar, J. Lewandowski, Class. Quant. Grav. 14 (1997) A55; J. Lewandowski, Class. Quant. Grav. 14 (1997) 71.

[5] R. Penrose (unpublished); in Quantum Theory and Beyond, edited by T. Bastin, Cambridge University Press, Cambridge, United Kingdom (1971)

[6] D. Oriti, arXiv:gr-qc/0607032 (2006); arXiv:1110.5606 (2011)

[7] B. Hasslacher, M.J. Perry, Phys. Lett. 103B 21 (1981)

[8] J. Ambjorn, J. Jurkiewicz, R. Loll, Int.J.Mod.Phys.D17:2515-2520 (2009), arXiv:0806.0397.

[9] D. Oriti, arXiv:0710.3276 (2007)

[10] W. G. Unruh, Phys. Rev. D 51, 2827-2838 (1995), arXiv:gr-qc/9409008; M. Visser, S. Weinfurtner, PoSQG-Ph:042 (2007) arXiv:0712.0427.

[11] B. L. Hu, arXiv:gr-qc/0503067 (2005)

[12] Z. C. Gu, X.-G. Wen, arXiv:0907.1203 (2009)

[13] H. Tasaki, J. Phys.: Condens. Matter 10, 4353 (1998).

[14] T. Konopka, Phys. Rev. D 78 044032 (2008), arXiv:0805.2283.

[15] F. Markopoulou, L. Smolin, Class. Quant. Grav. 24, 3813-3824 (2007), arXiv:gr-qc/0702044.

[16] E. H. Lieb, D. W.Robinson, Comm. Math. Phys. 28, 251 (1972).

[17] H. S. , H.S. Wilf, generatingfunctionology, A.K. Peters,San Diego California (2006)

[18] B. Bollobas, Random Graphs, Cambridge University Press, Cambridge, United Kingdom (2004)

[19] L. Lovasz,, in "Combinatorics, Paul Erdös is Eighty", Vol. II, ed. by D. Miklos, V.T. Sos and T. Szonyi, Bolyai Soc. Math. Stud.,Budapest (1994)

[20] W.K. Wootters, Phys. Rev. Lett. 80, 2245 (1998).

[21] N. Alon, C. Avin, M. Koucky,G. Kozma, Z. Lotker, M. R. Tuttle, 20th ACM Symposium on Parallelism in Algorithms and Architectures (2008)

[22] C. Avin, M. Koucký, Z. Lotker, Proceedings of the Conference ICALP, 121, (2008).

[23] D. Bohm, The Scientist Speculates, I. J. Good, ed. Basic Books, New York (1962), pp. 302-314.

[24] S. Bose, Contemp. Phys., Vol. 48 1, 13-30 (2007)

[25] C. Cooper, A. M. Frieze, T. Radzik, Multiple Random Walks and Interacting Particles Systems, Lecture notes in Computer Science, Springer Berlin, Volume 5556 (2009), pp. 388-410

[26] C. Cooper, A. M. Frieze, Internet Mathematics 1, 57-90 (2003)

[27] S. P. Gudder, Found. Phys. 18 7, 751-776 (1988)

[28] J. Kempe, Contemp. Physics, Vol. 44 4, pp.307-327 (2003)

[29] S. Popescu, A. J. Short, A. Winter, Nature Physics 754 (2006); N. Linden, S. Popescu, A. J. Short, A.Winter, arXiv:0812.2385 (2008)

[30] L. Campos Venuti, P. Zanardi, arXiv:0907.0683 (2009)

[31] X. G. Wen, Phys. Rev. D 68, 065003 (2003); Phys. Rev. B 68, 115413 (2003)

[32] F. Markopoulou, "Space does not exist, so time can", http://www.fqxi.org/community/essay/winners (2008)

[33] R. Gambini, J. Pullin, Loops, Knots, Gauge Theories and Quantum Gravity, Cambridge U. Press, New York (2000); C. Rovelli, Quantum Gravity, Cambridge U.

Press, New York (2004); T. Thiemann, arXiv:gr-qc/0110034. (2001); A. Ashtekar, J. Lewandowski, Class. Quant. Grav. 21, R53 (2004), arXiv:gr-qc/0404018

[34] J. D. Bekenstein Phys. Rev. D 7 (8): 2333–2346 (1973)

[35] J. M. Bardeen, B. Carter, S. W. Hawking, Comm. in Math. Phys. 31 (2): 161–170 (1973)

[36] V. E. Hubeny, S. Minwalla, M. Rangamani, Contribution to "Black Holes in Higher Dimensions", Cambridge Press, edited by G. Horowitz, arXiv:1107.5780 (2011)

[37] F. Markopoulou, arXiv:hep-th/0604120. (2006)

[38] D. W. Kribs, F. Markopoulou, arXiv:gr-qc/0510052 (2005)

[39] Z. C. Gu and X. G. Wen, arXiv:gr-qc/0606100 (2006)

[40] S. S. Lee, arXiv:gr-qc/0609107 (2006)

[41] G. Volovik, The Universe in a Helium Droplet, Oxford University Press (2009)

[42] F. Markopoulou, in Approaches to Quantum Gravity - towards a new understanding of space, time and matter, edited by D. Oriti, Cambridge Univ. Press (2009)

[43] P. Gibbs, Int.J.Theor.Phys.35:1037–1062, (1996)

[44] M.Levin , X. G. Wen, "Fermions, strings, and gauge fields in lattice spin models," Phys. Rev. B **67**, 245316 (2003) [arXiv:cond-mat/0302460]; M.A.Levin , X.G. Wen, "String-net condensation: A physical mechanism for topological phases," Phys. Rev. B **71**, 045110 (2005) arXiv:cond-mat/0404617; M.Levin, X.G.Wen, arXiv:hep-th/0507118 (2005);

[45] E. Curiel, Phyl. of Sci. 68 (Proceedings) pp. 424-441 0031-8248/2001/68supp-0034;

[46] C. Rovelli, Phys. Rev. Lett., 14, 3288-3291, (1996) arXiv:gr-qc/9603063; A. Ghosh, A. Perez, Phys. Rev. Lett. 107, 241301 (2011), arXiv:1107.1320v3; E. Bianchi, arXiv:1204.5122 ;

[47] C. Rovelli, L. Smolin, Nucl.Phys. B442 (1995) 593-622; Erratum-ibid. B456 (1995) 753;

[48] T. Padmanabhan , Rep. Prog. Phys. 73 : 6901 (2010). arXiv:0911.5004;

[49] Beineke, L. W., "Derived graphs of digraphs", in Sachs, H.; Voss, H.-J.; Walter, H.-J., Beiträge zur Graphentheorie, Leipzig: Teubner, pp. 17–33 (1968)

[50] J. Amborn, A. Gorlich, J. Jurkiewicz, R. Loll, Phys. Rev. Lett. 100, 091304 (2008), arXiv:0712.2485;

[51] R.D. Sorkin, arXiv:gr-qc/0503057v1 (2005); R.D. Sorkin, Proceedings of the PASCOS-07 Conference, July 2007, Imperial College London; arXiv:0710.1675 (2007;)

[52] A. Strominger, C. Vafa, Phys. Lett. B379:99-104 (1996), arXiv:hep-th/9601029v2;

[53] G. Parisi, Statistical Field Theory, Addison-Wesley, Reading, Mass. (1988) ;

[54] I. Prémont-Schwarz, A. Hamma, I. Klich, F. Markopoulou, arXiv:0912.4544v1(2009); A. Hamma, F. Markopoulou, I. Premont-Schwarz, S. Severini, Phys. Rev. Lett.102 017204, arXiv:0808.2495v2 [quant-ph];

[55] N. Seiberg, Emergent Spacetime, Rapporteur talk at the 23rd Solvay Conference in Physics (2005), arXiv:hep-th/0601234.

[56] K.S. Stelle, Phys.Rev. D16 (1977) 953-969; L. Modesto, arXiv:1107.2403 (2011); T. Biswas, E. Gerwick, T. Koivist, A. Mazumdar, arXiv:1110.5249 (2011);

[57] J. M. Maldacena, Adv. Theor. Math. Phys. 2, 231 (1998); Int. J. Theor. Phys. 38, 1113 (1999)

[58] A. R. Liddle, Proceedings of 'From Quantum Fluctuations to Cosmological Structures', Casablanca, Morocco, (1996) arXiv:astro-ph/9612093

[59] V. Sahni, Lect. Notes Phys. 653:141-180 (2004) arXiv:astro-ph/0403324

[60] C. Will, Physics 4, 43 (2011) arXiv:1106.1198; Living Rev. Relativity 9 3 (2006);

[61] M. Reuter, F. Saueressig, Lectures delivered at Zakopane 2007, arXiv:0708.1317v1 (2007)

[62] P. Horava, Phys. Rev. D79:084008 (2009), arXiv:0901.3775

[63] T. Jacobson, Phys. Rev. Lett. 75, 1260 (1995)

[64] F. Caravelli, F. Markopoulou, Phys. Rev. D84 024002 (2011), arXiv:1008.1340

[65] J. Q. Quach, C.-H. Su, A. M. Martin, A. D. Greentree, arXiv:1203.5367 (2012)

[66] G. De las Cuevas, W. Dur, H. J. Briegel, M. A. Martin-Delgado, New J. Phys. 12, 043014 (2010), arXiv:0911.2096

[67] J. Haegeman, J. I. Cirac, T. J. Osborne, I. Pizorn, H. Verschelde, F. Verstraete, (2011), arXiv:1103.0936

[68] R. J. Adler, D. I. Santiago , Mod.Phys.Lett. A14 1371 (1999)

[69] Leonhardt, Nature 415 (2002); Phys. Rev. A 65,043818 (2002);W.G. Unruh, R. Schützhold, arXiv: gr-qc/0303028 (2003); W.G. Unruh, R. Schützhold, quant-ph/0408145 (2004);

[70] E.H. Lieb, D.W. Robinson, Commun. Math. Phys.28 :251-257 (1972); B. Nachtergaele, R. Sims, contribution to "Entropy and the Quantum", R. Sims and D. Ueltschi (Eds), Contemporary Mathematics, volume 529, American Mathematical Society (2010) pp 141-176

[71] P. Hayden and J. Preskill, JHEP 0709:120 (2007) arXiv:0708.4025

[72] Y. Sekino, L. Susskind, Fast Scramblers, JHEP 0810:065 (2008) arXiv:0808.2096; L. Susskind, Addendum to Fast Scramblers, arXiv:1101.6048

[73] S. Kalyana Rama, Phys. Lett. B 645, 365 (2007), arXiv:hep-th/0610071

[74] A. Hamma, work in progress.

[75] M. Lewenstein, A. Sanpera, V. Ahufinger, B. Damski, A. Sen De, U. Sen, Adv. in Phys. Vol. 56 Nos. 1-2, 243-379 (2007) arXiv:cond-mat/0606771

[76] W. G. Unruh, Phys. Rev. Lett. 46, 1351 (1981).

[77] E. A. Calzettam B. L. Hu, arXiv:cond-mat/0207289v3 (2002)

[78] T. Banks, "TASI lectures on matrix theory," arXiv:hep-th/9911068 (1999)

[79] S. B. Giddings, Phys. Rev. D 74, 106005 (2006), arXiv:hep-th/0605196; S. B. Giddings, D. Marolf and J. B. Hartle, Phys. Rev. D 74, 064018 (2006), arXiv:hep-th/0512200

[80] T. Konopka, F. Markopoulou and L. Smolin, arXiv:hep-th/0611197 (2006)

[81] F.Markopoulou, Class. Quant. Grav. 17, 2059 (2000), arXiv:hep-th/9904009

[82] S. Lloyd, quant-ph/0501135 (2005)

[83] J. Stachel, in "Structural Foundations of Quantum Gravity," edited by D.P. Rickles, S.R.D. French and J. Saatsi Oxford University Press (2006).

[84] M.R.Garey and D. S. Johnson, Computers and Intractability: A Guide to the Theory of NP-Completeness, New York: W. H. Freeman (1983)

[85] J. B. Kogut and L. Susskind, Phys. Rev. D 11, 395 (1975).

[86] G. L. Sewell, Quantum Theory of Collective Phenomena, Oxford University Press (1986)

[87] B. Simon, A. D. Sokal, J. Stat. Phys. 25 4, p.679 (1981)

[88] M. Karonski, Random graphs, Handbook of Combinatorics, Vol. 1 (R. L. Graham, M. Grötschel, L. Lovász, eds.), pp. 351-380. Elsevier, Amsterdam (1995)

[89] M. Requardt, arXiv:gr-qc/0308089 (2003)

[90] M. Requardt, Class. Quant. Grav. 17 2029 (2000), arXiv:gr-qc/9912059

[91] A. N. Jourjine, Phys. Rev. D 31 1443 (1985)

[92] N.Wormald, Models of random regular graphs, Surveys in combinatorics, 1999 (Canterbury), (J. D. Lamb and D. A. Preece, eds.), pp. 239-298, London Math. Soc. Lecture Note Ser., 267, Cambridge Univ. Press, Cambridge (1999)

[93] A. Terrasm H. Stark, Advances in Mathematics 121 (1996), 124-165.

[94] O.Dreyer, arXiv:gr-qc/0710.4350 (2007)

[95] S. Bravyi, M. B. Hastings, and F. Verstraete, Phys. Rev. Lett. 97, 050401 (2006)

[96] E. H. Lieb, and D. W. Robinson, Comm. Math. Phys. 28, 251 (1972)

[97] B. Nachtergaele, Y. Ogata, and R. Sims, J. Stat. Phys. 124, 1 (2006)

[98] M. B. Hastings, and T. Koma, Comm. Math. Phys. 265, 781 (2006); B. Nachtergaele and R. Sims, Comm. Math. Phys. 265, 119 (2006)

[99] J. Eisert, T. J. Osborne, Phys. Rev. Lett. 97, 150404 (2006)

[100] X.G. Wen, Quantum Field Theory of Many-Body Systems, (Oxford Univ. Press, Oxford, 2004); Phys. Rev. B 40, 7387 (1989); Int. J. Mod. Phys. B 4, 239 (1990); Adv. Phys. 44, 405 (1995).

[101] X. G. Wen, Q. Niu, Phys. Rev. B 41, 9377 (1990)

[102] A. Y. Kitaev Annals Phys. 303, 2 (2003).

[103] A. H. Guth, Phys. Rev. D 23, 347 (1981); A. Linde, Phys. Lett. B **108**, 389 (1982).

[104] J. Magueijo, Rep. Prog. Phys. 66, 2025 (2003).

[105] J. Moffat, Int. J. Mod. Phys. A20 (2005) 1155-1162.

[106] J. Moffat, Reinventing Gravity. HarperCollins (2008)

[107] T. Konopka, F. Markopoulou, S. Severini, Phys. Rev. D 77, 104029 (2008)

[108] J.A. Wheeler, K. Ford, Geons, black holes and quantum foam: a life in physics, W.W. Norton Company, Inc., New York (1998)

[109] J.A. Wheeler, Annals of Physics 2, 604-614 (1957)

[110] M. Visser, Lorentzian Wormholes: from Einstein to Hawking, American Institute of Physics Press, Woodbury, New York (1992)

[111] A. Hamma, F. Markopoulou, S. Lloyd, F. Caravelli, S. Severini, K. Markstrom, Phys. Rev. D 81, 104032 (2010), arXiv:0911.5075

[112] F. Caravelli, A. Hamma, F. Markopoulou, A. Riera, Phys. Rev. D 85 044046 (2012), arXiv:1108.2013

[113] F. Caravelli, F. Markopoulou, arXiv:1201.3206 (Accepted in PRD, 2012)

[114] K.S. Stelle, Phys.Rev. D16 (1977) 953-969;

[115] http://edge.org/response-detail/2797/what-is-your-favorite-deep-elegant-or-beautiful-explanation

[116] G. Dvali, S. Folkerts, C. Germani, Phys. Rev. D84: 024039 (2011)

[117] C. Wuethrich, Philosophy of Science, 72 (2006) pp. 777-788

[118] L. Modesto, arXiv:1107.2403 (2011); T. Biswas, E. Gerwick, T. Koivist, A. Mazumdar, arXiv:1110.5249 (2011);

[119] M. Mecklenburg, B. C. Regan, Phys. Rev. Lett. 106 (2011) 116803

[120] R. Sorkin, Proceedings of the Valdivia Summer School, edited by A. Gomberoff, D. Marolf, arXiv:gr-qc/0309009 (2003)

[121] F. Markopoulou, A. Hamma, New J. Phys. 13:095006 (2011), arXiv:1011.5754;

[122] C. Prescod-Weinstein, L. Smolin, Phys. Rev. D80 063505 (2009), arXiv:0903.5303.

[123] F. Conrady, J.Statist.Phys.142:898 (2011), arXiv:1009.3195

[124] S. Krasnikov , Phys. Rev. D 67 (10): 104013 (2003). arXiv:gr-qc/0207057

[125] P. F. Gonzalez-Diaz, Phys. Rev. D 54 (10): 6122–6131 (1996). arXiv:gr-qc/9608059.

[126] M. Morris , K.S. Thorne,U. Yurtsever, Phys. Rev. Lett. 61 (13): 1446 (1988)

[127] M. S. Morris, K. S. Thorne, Am. J. of Phys. 56 (5): 395–412 (1988)

[128] A. R. Thomas, arXiv:gr-qc/0409090 (2004)

[129] M. Visser, contribution to "The future of theoretical physics and cosmology", Cambridge University Press, Cambridge (2002), arXiv:gr-qc/0204022

[130] M. Visser, Phys. Rev. D 39 (10): 3182–3184 (1989)

[131] R. Garattini, Mod. Phy. L. A 19 (36): 2673–2682 (2004). arXiv:gr-qc/0409015

[132] Planck collaboration, Nature 462, 331-334 (2009)

[133] G. 't Hooft, M. Veltman, Ann. Inst. Henri Poincaré, Vol. XX, n 1, p. 69-94 (1974)

[134] M.H. Goroff, A. Sagnotti, Nucl. Phys. B160, 123 (1985)

[135] M.H. Goroff, A. Sagnotti, Nucl. Phys. B266, 799 (1986)

[136] S. W. Hawking, Nature 248 (5443): 30 (1972)

[137] W.G. Unruh,Phys. Rev. D 14, 870 (1976)

[138] B. DeWitt, Phys. Rev. vol 160 n 5 (1967)

[139] B. DeWitt,Phys. Rev. vol 162 n 5 (1967)

[140] K. Goedel, Rev.Mod.Phys, 21 3 (1949)

[141] J. L. Bell, Transcendent Philosophy 3 (2002)

[142] H. Everett, Rev. Mod. Phy.29 454-462, (1957)

[143] J. Mattingly, The Universe of General Relativity: Einstein Studies, volume 11. Ed. Jean Eisenstaedt, Anne Kox. Boston: Birkhauser (2006)

[144] B. Carter, Gen. Rel. and Grav., Vol. 1 N. 4", 349-391 (1971)

[145] A. D. Sakharov, Gen. Rel. Grav. 32: 365-367

[146] M. Visser, Mod.Phys.Lett. A17 (2002) 977-992

[147] C. Isham, NATO Summer School 1992, arXiv:gr-qc/9210011v1

[148] A. M. Polyakov, Gauge fields and Strings, Contemporary Concepts in Physics, Vol 3, Camberwell (1987); J. Polchinski, String Theory, Cambridge University Press, Cambridge (1984); C. Johnson, D-Branes, Cambridge University Press, Cambridge (2007);

[149] F. Tipler, Phys. Rev. D 9 (1974)

[150] D. R. Terno, Foundations of Physics 36:102-111 (2005)

[151] T. W. B. Kibble, In: Quantum Gravity 2, A second Oxford Symposium, C.J. Isham, R. Penrose and D. W. Sciama, eds. Oxford: Clarendon, 63-80. (1981)

[152] L. Rosenfeld, Nucl. Phys. 40, 353-356 (1963)

[153] G. Vitagliano, Cilindri rotanti e la possibilita di curve chiuse di tipo tempo in Relativita Generale, Bachelor of Science thesis, Pisa (2008)

[154] L. D. Landau, E. M. Lifsfits, The classical theory of fields, Butterworth Heinemann, 7th edition (1987)

[155] J. Natario, arXiv:math/0603190v2 (2006)

[156] R. Penrose,Society for Industrial and Applied Mathematics (1972)

[157] S. Hawking, G. F. R. Ellis, The Large Scale Structure of Spacetime, Cambridge University Press (1989)

[158] G. F. R. Ellis, arXiv:astro-ph/0703751 (2007)

[159] M. Veltman, Les Houches Lectures (1976)

[160] V. R. Shaginyan, A. Z. Msezane, K. G. Popov, G. S. Japaridze, V. A. Stephanovich, Europhysics Letters 97, 56001 (2012)

[161] N. Schuch, S. K. Harrison, T. J. Osborne, J. Eisert, Phys. Rev. A 84, 032309 (2011)

[162] J. F. Donoghue, Advanced School on Effective Field Theory Proceedings, arXiv:gr-qc/9512024v1 (1995)

[163] C. Barcelo, S. Liberati, M. Visser, Liv. Rev. Rel. 8 12 (2005) arXiv:gr-qc/0505065

[164] J. W. Moffat, arXiv:hep-th/0208122 (2002)